University of Szeged

Faculty of Pharmacy

Institute of Pharmaceutical Technology and Regulatory Affairs

Head: Prof. Dr. Ildikó Csóka

Development of modern drug identification technologies using laser technology, against drug counterfeiting

Ph.D. Thesis

By

Krisztina Ludasi

Supervisor:

Dr. Géza Regdon jr.

Szeged

2021

LIST OF ORIGINAL PUBLICATIONS

1) **Ludasi K.**, Oláh I., ifj. Regdon G., Gyógyszerhamisítás elleni védelem, modern gyógyszerazonosítási technológiák alkalmazása – I. rész, Gyógyszerészet, 2018, 62, 80-87

2) **Ludasi K.**, Oláh I., ifj. Regdon G., Gyógyszerhamisítás elleni védelem, modern gyógyszerazonosítási technológiák alkalmazása – II. rész, Gyógyszerészet, 2018, 62, 140-147

3) **K. Ludasi**, T. Sovány, O. Laczkovich, B. Hopp, T. Smausz, G. Regdon Jr., Unique laser coding technology to fight falsified medicines, European Journal of Pharmaceutical Sciences, 2018, 123, 1-9, doi.org/10.1016/j.ejps.2018.07.023,

Q1 IF.: 3.532

4) **K. Ludasi**, T. Sovány, O. Laczkovich, B. Hopp, T. Smausz, G. Regdon Jr., Comparison of conventionally and naturally coloured coatings marked by laser technology for unique 2D coding of pharmaceuticals, International Journal of Pharmaceutics, 2019, 570, 118665, doi.org/10.1016/j.ijpharm.2019.118665,

Q1 IF.: 4.845

5) **K. Ludasi**, O. Jójárt-Laczkovich, T. Sovány, B. Hopp, T. Smausz, A. Andrásik, T. Gera, Z. Kovács, G. Regdon Jr., Anti-counterfeiting protection, personalized medicines − development of 2D identification methods using laser technology, International Journal of Pharmaceutics, 2021, 605, 120793, doi.org/10.1016/j.ijpharm.2021.120793,

Q1 IF.: 5,875 (2020)

PRESENTATIONS RELATED TO THE THESIS

1) **K. Ludasi,** T. Sovány, O. Laczkovich, B. Hopp, T. Smausz, G. Regdon jr.: Unique laser coding technology to fight falsified medicines, 7th BBBB International Conference on Pharmaceutical Sciences, Balatonfüred, Hungary, 5-7 October 2017 (Poster presentation)

2) **K. Ludasi**, O. Laczkovich, T. Sovány, B. Hopp, T. Smausz, G. Regdon jr.: Fighting Against Falsified Pharmaceuticals by 2D Laser Coding Technology in Case of Using Naturally Colored Polymer Film Coating, 12th Central European Symposium on Pharmaceutical Technology and Regulatory Affairs, Szeged, Hungary, 20-22 September 2018 (Poster presentation)

3) **K. Ludasi**: Lézeres technológiával a gyógyszerhamisítás ellen, SZTE Orvos- és Gyógyszerésztudományok doktori iskolák II. Ph.D. Szimpóziuma, Szeged, Hungary, 30 November 2018. (Verbal presentation)

4) **K. Ludasi**, G. Regdon Jr.: Anti-counterfeiting protection, development of modern drug identification technologies using laser technology, I. Symposium of Young Researchers on Pharmaceutical Technology, Biotechnology and Regulatory Science, Szeged, Hungary, 31 January 2019 (Verbal presentation)

5) **K. Ludasi**, G. Regdon jr.: Development of QR coded tablets for anti-counterfeiting of drugs by laser technology, II. Symposium of Young Researchers on Pharmaceutical Technology, Biotechnology and Regulatory Science, Szeged, Hungary, 23-24 January 2020 (Verbal presentation)

6) **K. Ludasi**, G. Regdon jr.: Gyógyszerhamisítás elleni védelem, modern gyógyszerazonosítási technológiák alkalmazása, „Hét Csillagos Gyógyszerész", Kötelező Továbbképző Tanfolyam, SZTE, Szeged, 19. November 2016, 27. May 2017, 18. November 2017, 26. May 2018, updated (Verbal presentation)

7) **K. Ludasi**, O. Laczkovich, T. Sovány, B. Hopp, T. Smausz, G. Regdon jr.: Védelem a gyógyszerhamisítás ellen, bevont tabletták egyedi kódolása lézerrel, II. Fiatal Technológusok Fóruma, MGYT Gyógyszertechnológiai Szakosztály, Budapest, Hungary, 10. April 2019 (Verbal presentation)

8) **K. Ludasi**: Medical training Course for resident physicians at Neurological Clinic , Szeged, Gyógyszerhamisítás, 03. September 2019 (Verbal presentation)

9) **K. Ludasi**, A gyógyszerhamisítás aktuális kérdései, „Hét Csillagos Gyógyszerész", Kötelező Továbbképző Tanfolyam, Szeged, Hungary, 20.-22. November 2020, 30. May 2021. (Online presentation)

TABLE OF CONTENTS

ABBREVIATIONS

2D	two-dimensional
API	Active pharmaceutical ingredient
ArF laser	ArF 193nm UV excimer laser
blue	patent blau 85
cherry	azorubin
DSC	Differential Scanning Calorimetry
E-L30 D55	Eudragit L30 D55
EU	European Union
EudrC	Eudraguard® control
femto laser	Titan-Sapphire Femtosecond Laser
GMP	Good manufacturing practice
HPMC	Hydroxypropyl methylcellulose
Ibu	Ibuprofen DC 85
KrF laser	KrF 248 nm UV excimer laser
MS	Mass spectrometry
orange	gelborange
PCIDs	Physical-chemical identifiers
red	iron oxide red
RFID	Radio frequency identification
SC laser	semiconductor laser
SEM	Scanning electron microscopy
SNC-G	SEPIFILM™ NATurally COLoured Green
SNC-P	SEPIFILM™ NATurally COLoured Pink
SPW-G	SEPIFILM™ PW Green
SPW-R	SEPIFILM™ PW Red
SPW-W	SEPIFILM™ PW White
SF	Substandard and falsified
TG	Thermogravimetry
TGA	Thermal gravimetric analysis
TiO_2	Titanium dioxide
WHO	World Health Organization

1. INTRODUCTION

Medicines have always been high value-added products, have a high intellectual, scientific and technical value, and are expensive to manufacture. It is understood that the production and distribution of such special products are subject to strict quality assurance, thus ensuring the safety of medicines for users and prescribers and recommenders (doctors, pharmacists) [1].

The production of drugs is officially regulated by law, it requires a Manufacturing Drug License, and these processes are controlled by the authorities. Good manufacturing practice (GMP) gives the minimum standard that a medicines manufacturer must meet during production. It has the force of law, requiring that manufacturers, processors, and packagers of drugs ensure that their products are effective and safe with adequate purity [2]. This protects the consumer from purchasing a product that is not effective or even dangerous.

Unfortunately, it is not surprising that counterfeiters have entered the market for such high-value-added products in the hope of making a quick profit.

Substandard and falsified (SF) medicines pose a serious threat to global public health. According to the World Health Organization (WHO), it is estimated that 1 in 10 medical products is substandard or falsified in low- and middle-income countries where health systems are weak or non-existent [3]. It is threatening that over 50% of medicines purchased over the Internet are counterfeit in the cases when sites conceal their actual physical address [4,5].

With the spread of the Internet, patients are increasingly self-diagnosing and medicating themselves. This has led to the emergence of thousands of unregulated websites that provide unattended access to inappropriate and SF medical products. Unregulated websites, social media platforms, and smartphone applications may also be direct channels for counterfeit medical products [6]. Globally, there are around 30,000-35000 online pharmacies. 96% of these operate illegally. They do not comply with regulatory and safety requirements, and they can even sell prescription drugs without a valid prescription. [7]. Patients around the world endanger their health and even their lives by unknowingly consuming SF medicines that have been badly stored or that have expired [8]. SF medical products can lead to a loss of confidence in medicines, healthcare providers, and health systems. All regions of the world are affected. Responsible governments prohibit SF medicine under national law but remain vulnerable to organized criminals doing business in countries where laws or enforcement are lax, 30% of countries have little or no medicine regulation according to the WHO [9].

It has to be emphasized that, in addition to all kinds of protection and coding, the most important strategy that can be adopted for the patients' safety is to organize communication and education campaigns to educate the public on the safe use of Internet pharmacies. People must be taught to be able to differentiate between legal and illegal medication suppliers [10].

The European Union (EU) has a strong legal framework for medicines. At the end of the distribution chain, only licensed pharmacies and approved retailers are allowed to sell medicines, including legitimate sale via the Internet [11]. For EU Member States, since February 2019, it has been mandatory to satisfy the requirements of Commission Delegated Regulation EU 2016/161 [12] and Directive 2011/62/EU [13] of June 2011. Serialisation prevents SF medicinal products from entering the legal distribution chain. It involves tracing an each product from the manufacturer through the wholesaler and the pharmacy to the patient, by a two-dimensional (2D) identification that is put on each box of prescription drugs. The 2D code should include the product code, the batch number, the serial number, the expiry date, and the national identification number if required by the Member State where the product is placed on the market [12]. In order to combat drug counterfeiting, pharmaceutical manufacturers and suppliers are working on adopting a worldwide standardized identification system [14].

2. AIMS

The aim of this research is to support the regulation by developing a technology for marking an individual traceable code directly on the surface of the medicine, besides the obligatory identification code that has been on each box of drugs in the EU since 2019. Anyone with a camera-enabled phone and a suitable application should be able to authenticate these uniquely marked drugs, thus helping in the fight against counterfeiters.

The main steps in the experiments were as follows:

- Selection of the dosage form to be coded
- Choosing the instrument for marking
- Selection of lasers
- Determination of coatings required for lasering
- Selection of tablet coating materials
- Laser ablation with different lasers
- Comparison of the effects of different lasers on the coated tablet sample (physicochemical tests, analytical evaluation)

3. THEORETICAL BACKGROUND

3.1. Social and economic effects of SF medicines

WHO adopted the name SF medicinal products for the medicines that fail to meet either national or international quality standards or specifications[15,16]. The failure rate of SF medical products is approximately 10.5% [17,18]. It means that each year 72,000-169,000 children may die of pneumonia, or 64,000-158,000 additional deaths of malaria could be caused according to the estimations of the University of Edinburgh and London School of Hygiene and Tropical Medicine, respectively [19]. In 2013 an estimated 91,577-154,736 under-five deaths were associated with the consumption of poor-quality antimalarials only in 39 sub-Saharan African countries, which suggests that these poor-quality medicines are important contributors to child mortality [20] and may help the spread of growing resistance geographically. The number of drugs is also growing in the global marketplace, especially sales on the Internet [21], which has become an accepted, and more and more popular way to purchase medications in high-income countries [22,23]. The culture of self-diagnosis and self-determination is on the rise. The Pew Research Center's Internet & American Life Project explored in the health survey, that in the year 2012, 35% of U.S. adults had gone online to figure out their medical condition, and after that only half of them visited a medical professional. Also, within a year's time, 72% of adult Internet users looked for some medical information online, and around 1/3rd engage in self-diagnosing of their health problems [24,25]. So, the increase of illicit online pharmacies makes ordering drugs through the Internet, which is very dangerous, whereas legal internet pharmacies provide lots of advantages [26].

The motivation of patients to use illicit online pharmacy services can be, that it is beneficial to the consumers as it is convenient to order, they are available 24 hours a day, do not require in-person interview and medical examination of the patient, and they provide privacy for those people who have embarrassing personal questions. Furthermore, it is globally reachable, doesn't need prescription from a physician, and gives anonymity. In some instances, they even sale medications not yet approved for distribution in certain countries, or vaccines, essential medicines [22,25–30].

A report of EU Intellectual Property Office (EUIPO) shows that fake medicines cost the EU pharmaceutical sector EUR 10.2 billion (4.4% of sales) each year. This is a direct estimate of sales lost by legitimate manufacturers and wholesalers of medicines in the EU due to counterfeiting. Moreover, 37,700 jobs and EUR 1.7 billion of government revenue are lost annually (taxes and social contributions) [31].

The links between drug counterfeiting and other forms of crime are proven both by the methods used and the nature of the products that are regularly seized. Traffickers have a single motivation: extreme profitability. To give an example: for $1,000 invested, the trafficking of counterfeit currency or of heroin would bring a return of $20,000, of counterfeit cigarettes $43,000, and in the case of SF medicines, the return would be between $200,000 and $450,000. SF medicine would therefore be 10 to 25 times more profitable than the trafficking of narcotics [32], [33]. Illegal activities increase as they can easily circumvent regulatory oversight [34], and globalization makes it harder to regulate the medical products that are sold in this way [35]. Managing illicit drug trafficking and limiting access to potentially counterfeit medicines should be a priority for governments and drug delivery systems [36]. Recently, global pharmaceutical supply chains have been developing stricter regulatory requirements. The FDA's Drug Supply Chain Security Act sets out the necessary steps to implement an electronic, interoperable system to identify and trace prescription drugs distributed in the US [37]. To prevent SF medicines from entering the legal supply chain, the EU adopted Directive 2011/62/EU [13,38].

3.2. Anti-counterfeiting technologies

To protect medical products, a large number of security technologies can be used for authentication. The choice of technology depends on the available financial resources, security level, feasibility, etc. It is recommended to use more than one technology at the same time to provide effective protection against counterfeiting. The technologies that can be used include, but are not limited to the following: printing technologies (offset lithography, flexography, gravure, screen printing, laser printing, pad printing, embossing and debossing, laser engraving, inkjet printing), security labels (adhesive, frangible, security cuts and perforation, void labels, holograms) and tracking technologies (serial numbers, linear bar codes, matrix codes, radio frequency identification (RFID)) may be used on the packaging of the medicines [39]. Furthermore, various methods such as unique coating colours, shapes, tooling, texture, sizes, physical feature, unique tablet designs, logos, texts, pearlescent film, printing etc. may be used for on-dose visual identification. Physical-chemical identifiers (PCIDs) include inks, pigments, flavours, and molecular taggants, for example, TruTag′s on-dose authentication [40], or Microtag [41] may be incorporated into solid oral dosage forms as in-dose features. Some PCIDs could require the use of instrumental detection. The ideal mark for medical applications is indelible, easy to read, difficult to copy or alter, contains unique serialization information, and does not change product functionality in any way [42].

Other research groups are also investigating alternative techniques for the direct marking of dosage forms. You et al., applied a fluorescent 3D QR code consisting of three different colour layers directly printed on the surface of the drug capsules. [43]. Another study reports the interface between 3D printing and 2D inkjet printing technologies in order to fabricate a drug-loaded 3D printed tablet with a unique track-and-trace measure in a single step process. 2D codes were printed onto the surface of polymeric based printlets. [14]. In one case, CO_2 laser engraving was used to achieve roughness over different surfaces causing a difference in the grey levels on translucent materials. This effect and the micro mold process was used to achieve micro pattern of the QR code and to obtain drug-laden biodegradable label [44]. In the literature, there are several studies on mobile phones as a device capturing image and processing data for the authentication of fake drugs [28,45–48].

Oral drug delivery is the most preferred and convenient route of pharmaceutical drug administration [49], and tablets are chosen 90% of the time of the solid dosage forms. They are physically and chemically stable during storage, simple-to-use, have sustainable production, and generally have excellent content uniformity [50].

Film coating is used in the pharmaceutical industry for solid dosage form because of taste masking, visual identifying, improved product stability, controlled release of the API, etc. [51], [52], [53]. Unique and distinctive colored coatings can improve identification and make counterfeiting more difficult [54]. Coloring is not enough to distinguish each tablet from one to another. Further marking is necessary.

There is a wide range of options for labelling medicines, and several aspects have to be taken into account when making the choice. From among many different options, printing is one of the most attractive methods for marking (like offset, inkjet and pad printing) as the capital equipment cost is relatively low [14]. However, the clear printing pattern may easily be affected by the environmental conditions of the process room, uniformity, temperature, and drying of the ink [55]. The printing process necessitates contact between the substrate and some form of ink carrier, toner reservoir, or stamp, so it could be a source of contamination. High printing speed is required for some of the fastest production lines and that can result in a loss of image quality and the risk of unreadable codes [39,56]. Furthermore, the ink formulation has to be designed with respect to its viscosity and surface tension to guarantee continuous printing and high reproducibility of the forming droplets [57]. Printability is also affected by the surface roughness of tablets, which may cause problems such as mottled appearance, blur, or dirt of the

inks. Also, organic solvents which are harmful to the employees' health and the environment are often used for the inks [58].

3.3. Laser technology in anti-counterfeiting applications

Lasers are a tool to be used every day in the laboratory or factory for a wide variety of advanced applications in precision manufacturing and R&D. The word laser stands for Light Amplification by Stimulated Emission of Radiation [59].

The mystical part of a laser is that it works at all. This is entirely due to the stimulated emission phenomenon. Through Einstein's analysis of radiation from hot objects, he postulated that there must be a radiant term based on a photon of radiation striking an excited species and causing it to release the energy of excitation.[60].

Spontaneous emission occurs when transition from the excited state to the lower energy level is not stimulated by any incident radiation but occurs more or less naturally. This happens because the excited atoms want to go back down to their ground state, and if left alone, it is just a matter of time before they do. If the atom was completely stable in its excited state, there would be no spontaneous emission [61]. Stimulated emission is when the atom gives up its excess energy, to the field, adding coherently to the intensity. A photon originates from the energy change between an excited state and a lower state. Many materials can be made to show this stimulated emission phenomenon, but only a few have significant power capability, since a further condition is that a population inversion is necessary, whereby there are more atoms or molecules in the excited state than in the lower-energy state, so as to allow amplification as opposed to absorption. To achieve this, the lifetime of the excited species has to be longer than that of the lower-energy state. [60].

A laser consists of three important components: the laser medium (it can be solid, liquid, gas or plasma, e.g. CO_2 or crystals), whose atoms are put into an energetically more favorable state by the pump, the second important component of a laser (flash lamps, electron beam). The third component of every laser is the resonator, which ultimately ensures that the high-energy photons generated in the laser medium leave the material, which is the actual laser beam.

With the laser, the applied energy can be placed precisely on the surface only where it is needed. Thus, it is a unique tool for surface engineering. Short pulses from a Nd:YAG laser, excimer or a transversely excited atmospheric pressure (TEA) laser can make a mark by removing a layer, modifying the surface morphology, causing a local reaction. The mark thus made is then shaped into a pattern by direct writing, projecting through a mask or scan-writing a dot matrix.

Laser ablation overcomes the drawbacks of ink printing technologies. The laser coding technology is a non-contact, chemically clean method that avoids the problems of contamination and eliminates the cost of consumables. [60,61].

When marking individual tablets by laser, the following cases should be considered: if the tablets do not have a coating, at least one colored layer should be applied to the drug so that the laser coding process can be performed on the surface. In cases when tablets have a colored coating (for example, for improved swallowability or identification purposes), that layer could be marked. When a functional coating is needed because of the therapy, an extra coating is required on top of it to enable marking without the loss of coating functionality.

This coding process could have benefits for tracking drugs across the distribution chain and for adding information for personalized medicines, too with codes tailored for each patient on each tablet.This information is increasingly necessary, when dose flexibility is needed for specific patient groups depending on age, gender, weight and genetic background [45,62].

4. MATERIALS

4.1. Tablet core materials

4.1.1. In preformulation

Tablet samples for laser marking preformulation were original tablets from the legal supply chain: Sinecod (GSK), Telfast (Sanofi), Klacid (Abbott), furthermore Eudraguard® control (EudrC) and HPMC coated placebo tablets.

4.1.2. During selection of the lasers

In the further research to select the lasers, EudrC and HPMC coated round placebo tablets were used, with no break line (diameter: 7 mm, crown height: 4 mm).

4.1.3. During QR code ablation

QR codes were ablated on the model tablets with active ingredient Ibuprofen DC 85 (Ibu), BASF, Germany): 16.66% (w/w), and excipients were: talc 3% (w/w), crospovidone (Kollidon CL-M, BASF, Germany) 5% (w/w), magnesium stearate 1% (w/w), microcrystalline cellulose (Vivapur 102, JRS Pharma, Germany) 74.33% (w/w), used as received.

Placebo tablets were also used for coating to save time and material. Placebo tablets were round with biconvex surface and had no break line on it (diameter: 10 mm, crown height: 4.2 mm, average weight: 350 mg).

The shape of the tablets was: Nr. 1 type: round with flat surface and no break line on it (diameter: 12 mm, crown height: 4.1 mm, average weight: 600 mg). Nr. 2 type: round with flat

surface and no break line on it (diameter: 10 mm, crown height: 3.1 mm, average weight: 300 mg). Nr. 3 type: round with flat surface and no break line on it (diameter: 10 mm, crown height: 4.8 mm, average weight: 500 mg).

4.2. Coating materials

In the experiment to select the lasers, an aqueous-based enteric coating solution was prepared. It consisted of 52% w/w dry substance of a neutral copolymer based on ethyl acrylate and methyl methacrylate with a ratio of 2:1 (EudrC dispersion 30% w/w (Evonik Nutrition & Care GmbH, Germany)), 16% w/w talc, 28% w/w alginic acid sodium salt, 4% w/w glycerol, and distilled water. Coatings were colored with 1% w/w patent blau 85 (blue), 3% w/w gelborange (orange), 1.5% w/w azorubin (cherry) or 1.5% w/w iron oxide red (red).

To test free films, aqueous HPMC coating solutions were used and applied to plastic balls. They consisted of 15%w/w dry substance in the case of SEPIFILM™ NATurally COLoured coatings agents, and 20%w/w dry substance in the case of Sepifilm™ PW coating systems. According to the supplier′s recommendation, they were prepared by dispersing them in distilled water. The total mixing time lasted for 45 min, followed by passing the dispersion through a 0.5 mm sieve. For the comparison of lasering conventionally colored coatings with naturally colored coatings, HPMC-based ready-to-use coating formulas were used: Sepifilm PW Red (SPW-R), Sepifilm PW Green (SPW-G), Sepifilm PW White (SPW-W) and naturally coloured Sepifilm NAT Pink (SNC-P) and Sepifilm NAT Green (SNC-G, Seppic S.A., Paris La Defense, France). They were dispersed in distilled water.

For the QR code ablation, an API containing tablet with two coatings was used: the first, (functional) film-forming agent was the aqueous-based enteric coating dispersion: an anionic polymethacrylate, Eudragit L30 D55®, (E- L30 D55, Evonik Nutrition & Care GmbH). The polymer dispersion was diluted with distilled water to a 56 % w/w polymer content and plasticizer/anti-tacking agent PlasAcryl® HTP 20 was added to a 14 % w/w content, based on the polymer, 1 h before coating. The second film-forming substance was a HPMC-based coating formula, SPW-R.

The aqueous HPMC coating solutions consisted of 20% w/w dry substance in the case of the SPW-R coating system. According to the supplier′s recommendation, they were dispersed in purified water. The total mixing time took 45 min, followed by sieving the dispersion through a 0.5 mm sieve.

5. METHODS

5.1. Preparation of API content tablets

For the Ibu containing tablet (see the composition in Chapter 3.1.3), the pressing procedure was the following: the ingredients of the tablet were homogenized with a Turbula mixer (Willy A. Bachofen Maschienenfabrik, Switzerland) for 8 minutes, and for 2 minutes after the addition of the lubricant. The homogenous powder mixture was compressed with a Korsch EK0 (E. Korsch Maschienenfabrik, Germany) single punch eccentric tablet press.

5.2. Tablet coating procedure

The spray coating process was performed using a 4M8 Pancoat (Pro-C-epT, Belgium) perforated coating pan.

5.2.1. Coating with EudrC dispersion

The spray coating process was performed on a batch of 500 g tablets. The process was divided into three stages. The coating parameters are shown in *Table 1*.

Table 1. Coating parameters of placebo tablets with EudrC.

Step	Inlet air temp. (°C)	Exhaust air temp. (°C)	Tablet bed temp. (°C)	Drum speed (rpm)	Air flow rate (m^3/min)
Warm-up	50		until 30	5	0.50
Coating	49±2	32±2	30±2	18	0.50
Drying & cooling	40	27	25	5	0.50

For the application of the atomized spray coating solution, 0.8 mm spray nozzle was used for 140 min, with an atomizing air pressure of 1.5 bars and an air flow rate of 0.50 m^3/min. The drying and cooling processes together lasted for 30 min.

5.2.2. Preparation of free films

Experiments were carried out on free films that were sprayed on the surface of 2.5 cm in diameter polyethylene balls (Primary Balls Kft., Hungary). After drying the film was removed. The coating parameters are shown in *Table 2*.

Table 2. Coating parameters of balls with Sepifilm.

Step	Inlet air temperature (°C)	Exhaust air Temperature (°C)	Ball temperature (°C)	Drum speed (rpm)
Warm-up	60	N/A	Until 50	3
Coating	50-55	40-42	45	9
Drying	40	30	27	3
Cooling	25	25	25	3

A 0.8 mm spray nozzle was used for 55 min, with an atomizing air pressure of 2.0 bars and an air flow rate of 0.70 m^3/min. The drying and cooling process lasted for 15 min each.

5.2.3. Coating procedure of tablets with API content

330 g of placebo tablets and 70 g of Ibu containing tablets were coated together at the same time in order to save material and time. During spray coating, 2 layers of coating were put on the tablets. The first layer was E-L30 D55. A 0.8 mm spray nozzle was used for the application of the atomized spray coating solution for 75 min, with an atomizing air pressure of 1.0 bar, a spray rate of 3 g/min and an air flow rate of 0.70 m^3/min. The drying and cooling process lasted for 15 min. The other coating parameters are shown in *Table 3*.

Table 3. Coating parameters of E-L30 D55.

Step	Inlet air temperature (°C)	Exhaust air Temperature (°C)	Tablet temperature (°C)	Drum speed (rpm)
Warm-up	60		Until 50	3
Coating	45-55	40-45	30-35	15
Drying	50	38-40	35-37	3
Cooling	25	25	25	3

The second layer was the HPMC-based ready-to-use coating formula. A 0.8 mm spray nozzle was used for the application of the atomized spray coating solution for 45 min in the case of Sepifilm PW coating, with an atomizing air pressure of 2.0 bars, a spray rate of 2 g/min and an air flow rate of 0.70 m^3/min. The drying and cooling process lasted for 15 min. The other coating parameters for the second layer are shown in *Table 4*.

Table 4. Coating parameters of Sepifilm films.

Step	Inlet air temperature (°C)	Exhaust air Temperature (°C)	Tablet temperature (°C)	Drum speed (rpm)
Warm-up	60		Until 50	3
Coating	55	40-42	35	9
Drying	40	30	27	3
Cooling	25	25	25	3

5.3. Measurement of final coating thickness

It was determined by light microscopy using a LEICA Image Processing and Analysis System (LEICA Q500MC, LEICA Cambridge Ltd., United Kingdom).

In the case of EudrC coating, after calibration, 4–4 halved tablets of different colors were examined, each at 10 places and averaged.

In the case of the API containing tablets, which had two coatings, after calibration, 4–4 tablets were examined, which were cut in half along the middle of the tablet band, and each was measured at 10 places and averaged.

5.4. Irradiation by laser

5 different types of lasers were used for the irradiation of the films and the tablets.

5.4.1. Neodymium-doped Yttrium Aluminum (Nd:YAG) laser

The laser that was first tested is the pulsed Nd:YAG laser, which is shown in *Fig. 1A*, wavelength: 1064 nm, power: 1–2.6 W, frequency: 1 kHz.

5.4.2. Semiconductor laser (SC laser)

Secondly, the continuous wave SC laser was used, wavelength: 405 nm, spot size: 73 μm, power: 1000 mW, irradiation time: 15–20 ms, which is shown in *Fig. 1B*.

5.4.3. ArF 193nm, UV excimer laser (ArF laser)

The next laser was the pulsed LLG TWINAMP type ArF laser, which is shown in *Fig. 1C*. Parameters of the laser: wavelength: 193 nm, energy: 3±0.2 mJ, fluence: 444 mJ/cm^2, FWHM: 20 ns, spot size: 375 μm, using a simple square-shaped mask, which has resulted in a 1 mm^2 square-shaped ablation hole, to study the effect of the laser on the coating film.

5.4.4. KrF 248 nm, UV excimer laser (KrF laser)

KrF laser, which is shown in *Fig. 1D*, was used for the next UV-regime ablation, a twin-tube hybrid dye-excimer laser-system [63,64]. The current laser-setup produced 60 mJ laser pulses with a pulse length of 700 fs. The central part of unfocused 4 cm x 4 cm pulses was cut out by an aperture with a diameter of 2 cm. Parameters of irradiation using KrF laser: wavelength: 248 nm, energy: 0.5 mJ, number of impulses: 10, spot size: 100 μm, FWHM: 700 fs, fluence: 6.37 J/cm^2.

5.4.5. Titan-Sapphire Femtosecond Laser (femto laser)

The femto laser (*Fig. 1E)* operates in the TeWaTi laser lab at the University of Szeged [65] and provided amplified pulses with a repetition rate of 200 Hz and maximum pulse energy of 1 mJ.

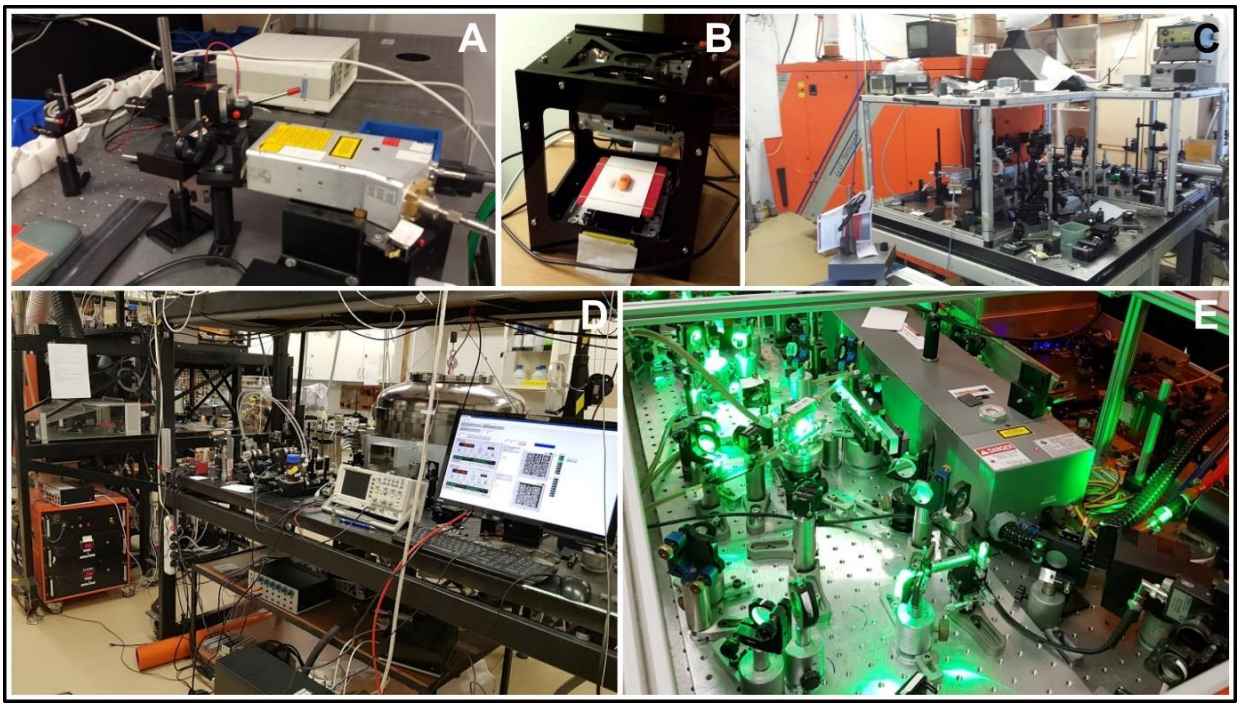

Fig. 1. Lasers used in the study. A: Nd:YAG laser, B: SC laser, C: ArF laser, D: KrF laser, E: femto laser.

An achromatic lens with a focal length of 150 mm focused the beam onto the target placed into the focal plane, allowing a beam imaging of f/19 (F-number) and processing of the target surface with 135 fs pulses. Irradiation of tablets using femto laser: wavelength: 800 nm, energy: 0.62 mJ, number of impulses: 20, spot size: 110 μm, FWHM: 135 fs, repetition rate: 200Hz, fluence: 6.52 J/cm^2.The experimental setup for the laser processing is outlined in *Fig. 2*.

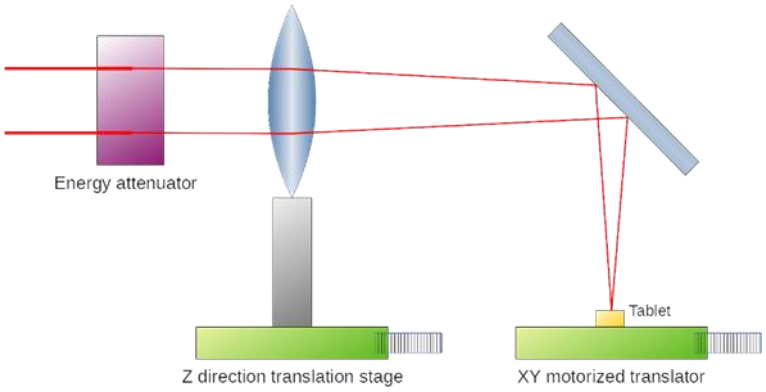

Fig. 2. Experimental setup for laser processing. The tablet position was adjusted with a motorized XY translator during the QR code engraving. The Z direction translator stage was used to set the focus plane precisely at the surface of the tablet.

A computer-controlled movable desktop, a motorized translator was created for the tablet to be able to change its position during lasering, in the case of the SC laser, KrF laser, and femto laser. The QR code was ablated hole by hole.

5.5. Digital microscope

The surface morphology of the ablated film was observed by using a Digital Microscope (KEYENCE, VHX-6000). This instrument is equipped with a newly developed REMAX VI High-Performance Graphics Engine and D.F.D. 2.0 image processing engine. This enables the creation of a precise 3D image by analyzing small changes in texture after capturing numerous images at different heights and different angle positions, HDR and image-stitching. Through line roughness and surface roughness measurements, reliable evaluation of surfaces can be performed and converted to a figure. Data were evaluated by HDR playback / measurement / stitched image playback software developed by KEYENCE.

5.6. Surface profilometer

Profilometry measurements were performed using a Veeco, Dektak 8 Advanced Development Profiler®. The tips employed had a radius of curvature ~2.5 μm, and the force applied to the surface during scanning was ~30 μN. The horizontal resolution was 0.1–0.13 μm. The vertical resolution was 40 Å. Data were evaluated by Dektak software (Microsoft® Windows XP®: interactive data acquisition) and Vision® 32 software (data processing, 2-D and 3-D image analysis) (Veeco Instruments Inc., NY, USA).

5.7. Determination of the ablation threshold

The ablation threshold indicates the minimal laser energy required to remove the material from the substrate (i.e., tablet surface). The threshold value is a fundamental parameter for laser fine-tuning. In most of the cases, the laser operates close to the threshold but slightly higher to be effective, and to avoid unwanted side effects, such as the thermal distortion of the material. The final etching depth is controlled by the number of laser impulses and not by fluence [66].

The characteristics of the ablation holes were examined with a surface profilometer. The laser parameters required for ablation were determined from the data obtained using a profilometer. The calculation method of the ablation threshold value for each laser that is required to generate QR codes is described below at the particular instruments.

5.8. Scanning electron microscope (SEM)

The ablated tablets were observed by using S4700 SEM (Hitachi, Japan). The tablets were mounted rigidly on a specimen holder with a double-sided carbon adhesive tape and a conductive ultrathin golden layer was deployed on them with a sputter device (Polaron, UK). The measurements were performed at a magnification of 30–5000, applying 10.0 kV electron energy and 1.3–13 MPa air pressure.

5.9. Raman spectroscopy

Raman spectroscopy was used for the examination of the samples treated by lasers. Spectra were acquired with a Thermo Fisher DXR Dispersive Raman spectrometer (Thermo Fisher Scientific Inc., MA, USA), a diode laser operating at a wavelength of 780 nm and equipped with a CCD camera. Raman measurements were carried out with a laser power of 4 mW (Ibu), 6 mW (EudrC), 12 mW (E-L30 D55, SNC-P, SPW-R, SPW-W, SPW-G) and 24 mW (SNC-G) at a slit aperture size of 25 µm. OMNIC 8 software was used for data collection, with cosmic ray and fluorescence corrections.

The spectra of the individual substances of EudrC film were collected using an exposure time of 6 s, a total of 48 scans in the spectral range of 1700-200 cm^{-1}. The individual films Sepifilm and Sepifilm films treated by lasers spectra were collected using an exposure time of 6 sec. The data were collected in the spectral range of 3407-24 cm^{-1}. The API containing tablets treated by lasers spectra were collected using an exposure time of 6 sec, and 10 spectra were averaged in the spectral range of 3200-200 cm^{-1}.

Raman chemical mapping was also performed with the same equipment to confirm the chemical degradation of the EudrC film. It was profiled to the special changed area of the spectra which was treated by SC laser (1800 cm^{-1}-500 cm^{-1}). Then the chemical map was profiled to the untreated Raman spectra of the film coating.

For the API containing tablets, spectral data were collected on the surface of the lasered tablet, and on the fracture surface of the halved tablet, including the treated and intact region, too. The spectra were determined at certain points in a defined area, while the sample had a translational motion between each discrete measurement. The point scan system measures each spectrum individually at a series of predefined points. The chemical map was profiled to the spectra of E-L30 D55 and to the spectra of SPW-R. In the case of Ibu, profiling was done to the peak 1604 cm^{-1} because it was found to be the most typical for the API, and it was the most separated from the spectra of the other investigated components.

Furthermore, sample analyses were performed on the cross-section surface of KrF laser and femto laser treated tablets (in 10 points directly below the lasered coated surface and in 10 points in the core of the lasered tablets). The mean of these 10 spectra was compared with the mean of the 10 spectra taken from the core of the untreated tablet and the spectrum of Ibu. These averaged spectra were normalized to peak 1604 cm^{-1} of the Ibu spectrum.

Data were evaluated by Spectragryph - optical spectroscopy software [67].

5.10. Thermal gravimetric analysis (TGA)

The TGA of the samples was carried out with a Mettler-Toledo TGA/DSC1 instrument (Mettler-Toledo GmbH, Switzerland). The start temperature was 25 °C, the end temperature was 500 °C, the applied heating rate was 10 °C/minute. Nitrogen atmosphere was used (Cell gas: 50 ml/min, method gas: 70 ml/min). 5 ± 1 mg samples were measured into aluminum pans (40 µl). The TG curves were evaluated with Mettler-Toledo STAR^e Software.

5.11. Mass spectrometry (MS)

The gas analysis of the tablet coating material was carried out with the Thermo Star (Pfeiffer Vacuum, model ThermostarTM GSD 320, Germany) quadrupole mass spectrometer (maximum 300 amu) for gas analysis, which was coupled to the TG instrument. The measurements were carried out in a flow of nitrogen atmosphere. The connection between the TG and the mass spectrometer was made by means of a heated silica capillary, which was maintained at 120 °C. Ions with various mass numbers were determined with the SEM MID measurement module of the Quadera software. Continuous recordings of sample temperature and sample mass were performed. The obtained results were exported and then plotted in one coordinate system with the TG curves using the Mettler-Toledo STAR^e software.

5.12. In vitro drug disintegration

In the disintegration studies, the tablets were tested according to the standard method of the European Pharmacopoeia with an Erweka model ZT71 apparatus (Erweka, Germany). First, 900 ml of artificial enzyme-free gastric juice (pH = 1.22) was preheated and maintained at a temperature of 37 ± 0.5 °C. According to the guideline, enteric coating should be intact for 2 hours in acidic media. After 2 hours, the medium was changed to a phosphate buffered saline solution (pH = 6.82). The time necessary for each tablet to disintegrate in acidic and intestinal solution was recorded automatically by the apparatus.

5.13. In vitro drug dissolution

In the present study, the investigation of drug release kinetics from marked tablets was carried out with an Erweka DT 700 (Erweka GmbH, Germany) dissolution tester according to the standards of the European Pharmacopoeia. A rotating basket method was used for the dissolution tests, where the rotation speed was 100 rpm, the dissolution medium was 900 ml of artificial enzyme-free gastric juice (pH = 1.22) for 2 hours, and then it was replaced with 900 ml of phosphate buffered saline solution (pH = 6.82) for 1 hour. The pH value was checked with a pH meter. The temperature was maintained at 37± 0.5 °C. As a sample, 5 ml of the

dissolution medium was taken manually at predetermined intervals without being replaced. Medium loss was not taken into account during the calculations. Samples were filtered through a 10 μm Poroplast filter (Erweka, Germany). The absorbance of ibuprofen DC85 was analyzed at 222 nm, using a spectrophotometer (Genesys 10S UV-VIS, Thermo Fisher Scientific Inc., MA, USA). Four tablets were tested, and samples were taken at the following time intervals: at 120 min in the case of gastric juice, and after changing to intestinal fluid at 5, 10, 15, 30, 45 and 60 min.

6. RESULTS AND DISCUSSION

In this experiment, the final plan is to put two coatings on the tablet surface in different colors, a functional one and a second one for marking. After the laser ablation of the upper film layer, the differently colored code could be read even by the patient using a mobile phone with the appropriate application. When selecting lasers, the aim was to compare as many different types of instruments as possible to give a broad overview of the effects of different lasers on drugs.
In the following, I would like to present the experiments and tests performed with different lasers.

6.1. Nd:YAG laser

The preformulation study began using an inexpensive, more widely used pulsed Nd:YAG laser on original tablets. It was found that the intervention burned the tablet's coating during testing, so the device was not part of our further research. The result of the treatment is presented in *Fig. 3*. The phenomenon can be explained by the fact that due to its longer wavelength (1064 nm), it has a higher heat effect, which can lead to thermal decomposition.

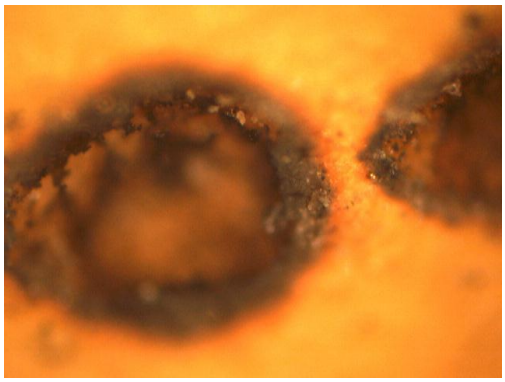

Fig. 3. Coated tablet treated by Nd:YAG laser.

6.2. Semiconductor laser

A SC laser was chosen next. The continuous mode laser ablates with a photothermal effect and has the advantages of being compact, efficient, with a quick modulation response and reliability. It is relatively small in size, and it is easy to fabricate by mass production, thus it has a low cost. In addition, it operates at different wavelengths.

With this instrument, a 2D QR code could be marked on the tablets. In this case, a full QR code was generated using online ZXing ("Zebra Crossing") code generator software, an open-source, multi-format 1D/2D barcode image processing and a code generator library implemented in Java. The standard QR code was generated (ISO/IEC 18004:2015) with 8 numerical characters using a resolution of 300 dpi and the lowest error correction (Level L). To read the QR code, the same software application was used by a mobile phone. The 3D geometric correction has not yet been applied to the 2D images, since it was projected to the tablet, which has negligible curvature compared to the real tablet surface. The effect of a SC laser on the quality of the coating films was also tested.

6.2.1. Semiconductor laser treated EudrC coating

The photograph of the SC laser treated tablet is shown in *Fig. 4A*. This indicates that the laser beam blackened the coating. Factors that change the color of the coating with SC laser irradiation needed to be clarified. In *Fig. 4B* the microscopic image also shows signs of black burns.

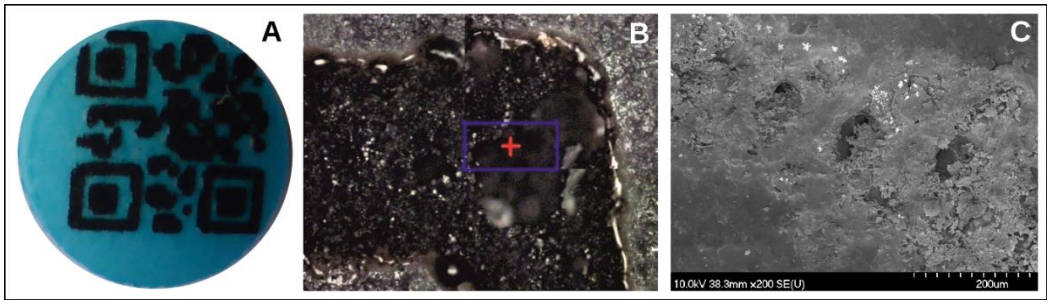

Fig. 4. SC laser treated EudrC coated tablet. A: Photograph, B: microscopic picture, C: SEM micrograph (magnification of 200×).

6.2.1.1. Investigations of the lasered coating

6.2.1.1.1. Scanning electron microscopy

The SEM micrograph (*Fig. 4C*) shows the SC laser caused considerable damage in the coating structure during the treatment. Holes are seen in every 200 μm on the film, surrounded by a wide range of burn traces. There are blistering, snowflake like crystals around the holes,

probably due to melting and recrystallization. It is unclear whether these are the results of a consequential loss of water or the melting of the coating material.

6.2.1.1.2. Coating film thickness

The final coating thickness averages measured on 4 different tablets are: yellow: 60.79 ± 9.11 µm, blue: 59.31 ± 11.82 µm, cherry: 49.19 ± 10.18 µm and red: 88.02 ± 18.98 µm.
In the following, the chemical structure degradation described above was analyzed by Raman and TG-MS analytical tests.

6.2.1.1.3. Raman investigations

Raman spectroscopy is becoming one of the most widely used and applicative approaches to analyze pharmaceutical materials. To investigate the effect of the SC laser on film coating, Raman spectroscopy was used. The fingerprint region of EudrC is 1800 cm^{-1} – 500 cm^{-1}. In the summary Figure (*Fig. 5*), the spectra of raw dispersion, raw free film and film treated by SC laser are seen. The spectra of the film treated by the laser changed completely compared to the untreated film; it smoothed. It is assumed that this is the result of the combustion shown in the image above in *Fig. 4*.

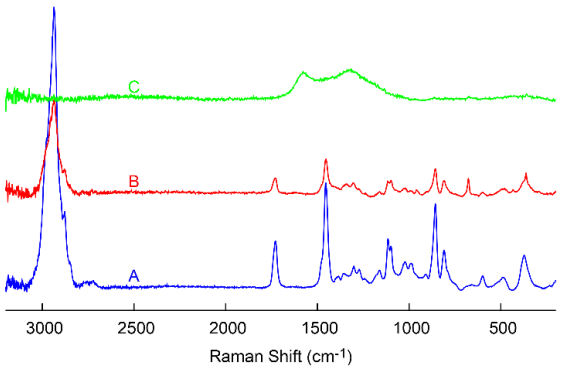

Fig. 5. Raman spectra. A: EudrC dispersion, B: free film of EudrC, C: SCr laser ablated EudrC film.

To confirm the chemical degradation of the film polymer, Raman chemical mapping was performed. The area treated by SC laser which contained burst and intact film, too, was selected. The microscopic mosaic photograph is presented in *Fig. 6A*. The area framed with blue lines is the chemically mapped part. The spectra were determined in the blue points. Then this chemical map was profiled to the special changed area of the spectra treated by SC laser (1800 cm^{-1} – 500 cm^{-1}).

The warm colors show the area which contains these spectra (*Fig. 6B*). Then the chemical map was profiled to the untreated Raman spectra of the film coating (*Fig. 6C*). In this picture the warm colors show the original (raw) intact film. This picture is the inverse of *Fig. 6B*. Thus, it

was concluded that chemical changes had been caused by the SC laser source. The warm colors show the area which contains these spectra (Fig. 6B). Then the chemical map was profiled to the untreated Raman spectra of the film coating (Fig. 6C). In this picture the warm colors show the original (raw) intact film. This picture is the inverse of *Fig. 6B*. Thus, it was concluded that chemical changes had been caused by the SC laser source.

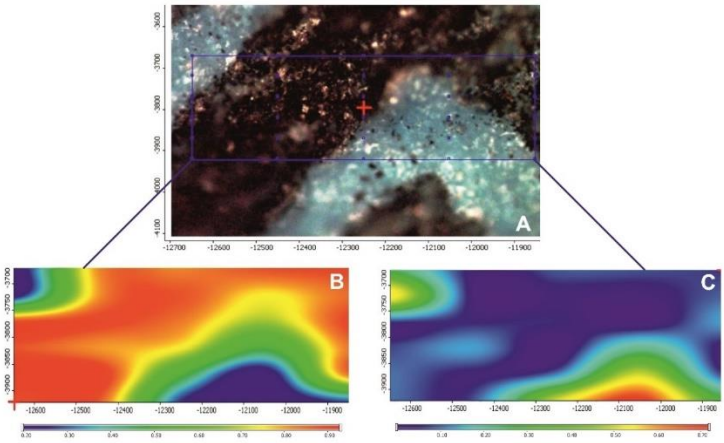

Fig. 6. A: Microscopic picture of blue EudrC film treated by SC laser, B: chemical map profiled to the special changed area of the spectra treated by SC laser, C: chemical map profiled to untreated Raman spectra of film coating.

6.2.1.1.4. TGA and evolved gas analysis with MS

TGA is a method of thermal analysis which provides curves corresponding to mass loss characteristics. As the measured substance degrades, basic information is given about its behavior during temperature rise. Data from mass reduction through this system alone do not allow the classification of the molecules.

Table 5. shows TG temperature ranges, mass loss, DTG normalized integral of the examined materials and peak temperatures. The main characteristics of the samples derived from the TG curves as corresponding mass loss values were used to define the thermal behavior and combustion characteristics of the films. It is seen that mass loss in the coating films comes in three stages. The first mass loss occurred between 30 and 120 °C, the second stage between 120 and 290 °C, and the third between 290 and 500 °C.

In order to clarify the decomposition mechanism of the films, mass loss should be characterized during each decomposition process by the identified evolution of gas components. The mass spectra were interpreted on the basis of the degassing profiles of the molecule ions and ion fragments of various gases. The evolution of released gas species was followed in situ by the

coupled system of TG-MS instruments. The evolution curves are shown as current ion versus time curves. The characterization of water release by means of MS is possible with the molecule H_2O, m/z=18 (peak at 50 °C). It can be safely concluded from (Annex 1)*Fig. 32* that water is given out from the samples at about 50 °C, which is consistent with the mass loss observed from the TG curves. The dehydration of the film takes place at around this temperature.

Table 5. Decomposition behavior of the raw EudrC film and the film treated by SC laser.

TG-DTG data	EudrC film	Laser treated EudrC film
First step		
Thermal range (°C)	30-120	30-120
Mass loss (%)	4.31	4.12
Normalized integral (s/°C)	-0.11	-0.13
Peak (°C)	72.83	64.65
Second step		
Thermal range (°C)	120-290	120-290
Mass loss (%)	15.03	18.75
Normalized integral (s/°C)	-0.57	-0.60
Peak (°C)	232.99	230.66
Third step		
Thermal range (°C)	290-500	290-500
Mass loss (%)	50.59	69.96
Normalized integral (s/°C)	-2.12	-2.79
Peak (°C)	362.78	358.40

An important increase in the concentration of methyl methacrylate is recorded for m/z=41 and for m/z=69 due to the decomposition of the polymer at temperatures at around 360 °C. The abundance of the m/ z=41 and m/z=69 signals vs. temperature can be seen in Annex1, *Fig. 32*. The evolution of CO_2 gas, m/z=44 signal, was detected in two steps at slightly higher temperatures around 240 °C and 365–370 °C, as it is seen in the MS curves in Annex1, *Fig. 32.* The release of ethanol, m/z=31, by means of the MS curves seen in Annex1, *Fig. 32*, happened at a temperature around 355 °C. The results of mass spectroscopy are consistent with the mass loss observed from the TG curves, as the decomposition of the material occurred slightly sooner in the film treated with SC laser in the case of m/z=44 and m/z=69, where decomposition started sooner as deacylation had taken place earlier during the laser treatment.

Raman distinguished the raw film and the film treated by the SC laser. It was concluded that chemical changes had been caused by the SC laser source compared to the original film. The main finding of the TG measurement showed that the decomposition of the material occurred sooner in films marked by laser, in higher temperature ranges, which is probably due to the decomposition process that had already started during the laser marking intervention.

6.2.2. SC laser treated Sepifilm coating

Since the SC laser is a cheap and easy-to-use, it was found worthwhile to test the laser on materials of other compositions. In view of the growing demand for natural materials and for titanium dioxide-free (TiO_2) alternatives for consumers and manufacturers of dietary supplements, HPMC-based, ready-to-use coating formulas were chosen, which had been colored with natural colors (Sepifilm ™ Naturally Colored coatings), and for comparison, conventionally colored coating formulas were also examined (SPW-R, SPW-G, and SPW-W). The experiments were carried out on free films that were sprayed on the surface of polyethylene balls, and thereafter the film was removed from the ball, marked by laser and examined. The result of the treatment by SC laser is black burst signals *(Fig. 7ABC*) or fading of the color of coatings, which may be seen in *Fig. 7D* and *E*, respectively. Further investigations were made to clarify the nature of the changes on the treated surface.

Fig. 7. Photographs of HPMC-based coating films treated by SC laser. A: SPW-W, B: SPW-R, C: SPW-G, D: SNC-P, E: SNC-G.

6.2.2.1. Investigations of the lasered coating

6.2.2.1.1. Microscopic analysis of the coated surface

The microscopic images confirm what is visible to the naked eye: laser treated films changed color, blackened, or possibly burned. Holes are seen, especially on the SPW-W film (*Fig. 8F*)

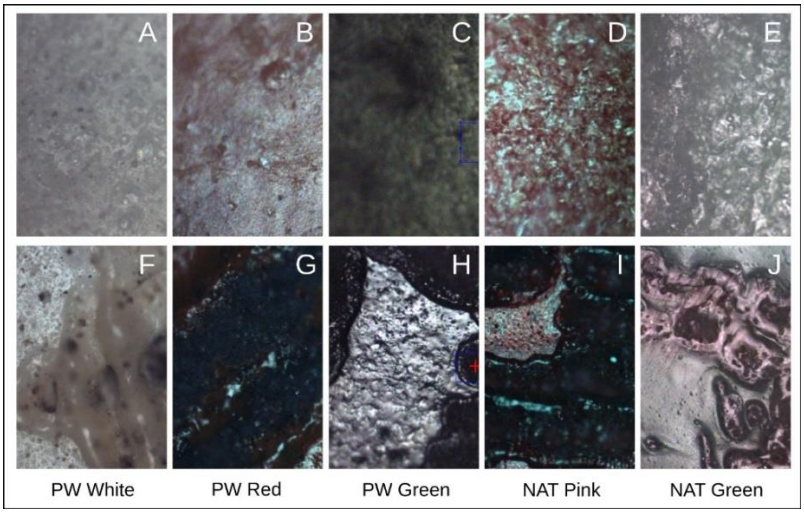

Fig. 8. Sepifilm coatings. First row: untreated films, second row: films treated by SC laser.

SC lasers ablate material with a photothermal effect. Heat flows by thermal conduction and material evaporates by boiling after prior melting or burning. [60,61].

6.2.2.1.2. Raman investigations

The SC laser seemingly burned or faded the films. To find out what kind of chemical changes happened, Raman investigations were carried out in this case, too. Nevertheless, the complex composition of the coatings, especially the ones that contain natural colorings (e.g., extracts of fruits, vegetables, plants or algae), where the exact composition is not known, makes analysis difficult. The components and the related relevant literature for Raman spectroscopic examinations are listed in *Table 6*. The fingerprint region of Sepifilm is 1800 cm^{-1}– 500 cm^{-1}. The spectra of raw free films and films treated by the laser are summarized in *Fig. 9.*

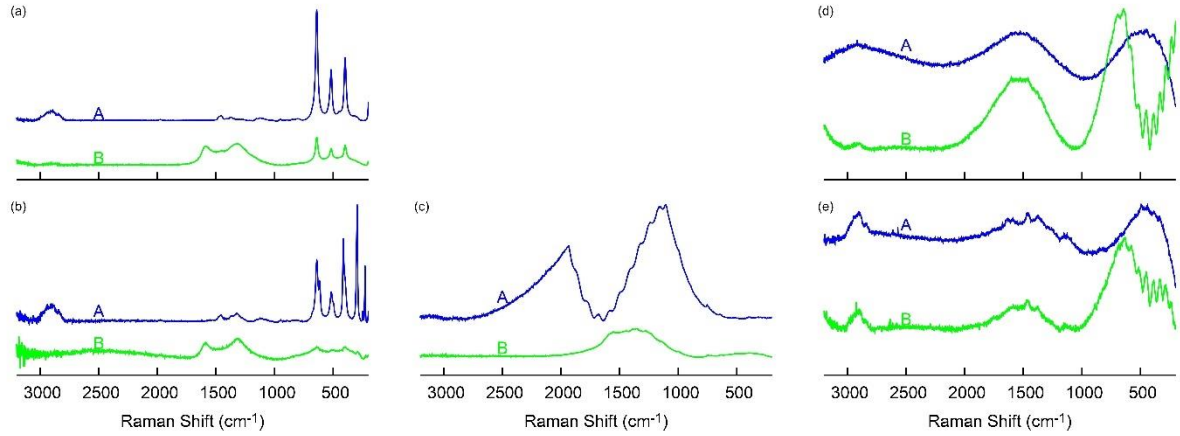

Fig. 9. Raman spectra of Sepifilm coatings treated with SC laser. (a): SPW-W, (b): SPW-R, (c): SPW-G, (d): SNC-P, (e): SNC-G (A: original, B: SC laser treated film).

In all cases, the spectra of the films treated by the SC laser changed. Firstly, it should be emphasized that the polymer films containing the extract of coloring foodstuffs, SPW-G, SNC-P and SNC-G (*Table 6*) exhibited severe fluorescence during the measurement (*Fig. 9(c)(d)(e)*). This effect could not be corrected by photobleaching, and it made the analysis difficult or impossible. In the case of SPW-G (*Fig. 9(*c*))*, fluorescence disappeared after marking it by the SC laser, presumably because of a change in the structure of chlorophyll, which resulted in the change of the color of the coating (*Fig. 7E*).

In the spectra of *Fig. 9(d)(e)* considerable fluorescence was detectable in the region of 1700 cm^{-1} to 1200 cm^{-1} in the case of the SC laser treated films, which is probably due to the product degradation that had occurred during the laser treatment. It was concluded that chemical changes had been caused by the SC laser source in the ablated films colored by natural and by conventional colorings too, just as it had happened in the previous experiment with EudrC film.

Table 6. Compositions and Raman spectroscopic references of conventionally (PW) and naturally (NAT) colored coatings.

PW colored films	**Literature background Raman activity of components**		**NAT colored films**	**Literature background Raman activity of components**	
HPMC	[68]		HPMC	[68]	
PEG	[68]		Glycerin	[68]	
Talc	[69]		MCC	[70]	
TiO_2	[58]				
Coloring agents	white: -		Coloring food agents		
	red: iron oxide	[71]		pink: beetroot extract	[72]
	green: chlorophyll	[73]		green: algae extract	[74]

6.2.2.1.3. Thermal gravimetric analysis (TGA)

TGA measurements were performed to reveal the effect of the assumed chemical changes on the structure of the films. The main characteristics of the samples derived from the TG curves as corresponding mass loss values were used to define the thermal behavior and combustion characteristics of the films. To represent all different types of coatings, the unstained white sample and one from naturally and one from conventionally colored coating samples were chosen to be examined by TG (*Table 7*). It is seen that mass loss in SNC-P and SPW-R coating comes in two stages. The first mass loss occurred between 25 and 120 °C with both coatings, the second stage between 290 and 430 °C in the case of SNC-P film, and between 290 and 440°C in the case of SPW-R. The mass loss of SPW-W film was observed between 25 and 500 °C.

The TG curves revealed that the decomposition occurred sooner in all 3 sample coatings if they were marked by a SC laser, as can be seen in Annex1, *Fig. 33*. These results correlate with the results of the previous research material EudrC film treated with SC laser (Annex1 *Fig. 32* TG curves). It can be seen from the microscopic mosaic picture of the pre- and post-lasered films that in contrast with the untreated intact films (*Fig. 8* first row), the SC laser treated films (Fig. Fig. 8 second row) exhibit damaged structures. It can be concluded that the weight loss seen in the first step of the TG curve may show the water loss of the films *(*Annex1, *Fig. 33* (a)(c)), as it might escape through the holes as a result of the heat effect. The visual signs of the damage (*Fig. 8*. second row) and the corresponding TG curves of SC laser treated films, - where these curves reveal that decomposition occurred sooner -, all indicate that the decomposition process had already started during the laser marking process. Overall, the earlier the mass loss of the TG curves began, the more damaged the surface of SC laser-coded coatings were.

An important conclusion is that, despite the chemical modifications obtained, SC lasers could be a useful and less expensive alternative to tablet coding if a non-functional coating is marked. The coating has to be thick enough to avoid heat transfer to the tablet core and it has to be proven that no harmful by-products are formed under the influence of heat.

Table 7. Decomposition behavior of the raw film and the film treated by SC laser.

TG data	**SNC-P film**	**Laser treated SNC-P film**
First step		
Thermal range (°C)	25-120	25-120
Mass loss (%)	2.85	4.91
Second step		
Thermal range (°C)	290-430	290-430
Mass loss (%)	58.26	68.94
	SPW-R film	**Laser treated SPW-R film**
First step		
Thermal range (°C)	25-120	25-120
Mass loss (%)	1.07	1.80
Second step		
Thermal range (°C)	290-440	290-440
Mass loss (%)	51.88	55.12
	SPW-W film	**Laser treated SPW-W film**
Thermal range (°C)	25-500	25-500
Mass loss (%)	56.06	65.63

In the further research, the lasers that do not produce a heat effect during ablation were tested.

6.3. ArF 193 nm UV excimer laser

Based on the literature data, the UV excimer laser was chosen for the next experiment as it works by photochemical ablation, so it has a negligible heat effect, which minimizes the chemical degradation of the material during the process.

6.3.1. ArF laser treated EudrC coating

6.3.1.1. Microscopic analysis of the laser treated surface

The experiment started with the EudrC film, as in the previous case. A simple square-shaped mask was used during the treatment, which resulted in a 1 mm^2 square-shaped ablation hole. First, the effect of laser ablation on the coating film was studied at 10, 20, 30, 40, 50, 60, 70, and 80 pulses. The result is shown in *Fig. 10A*, where the square holes are seen (the number of pulses increases from the bottom line left to the top line left), visibly separated from the environment. In *Fig. 10B* the square-shaped 'print' is seen on the surface with a microscope, too.

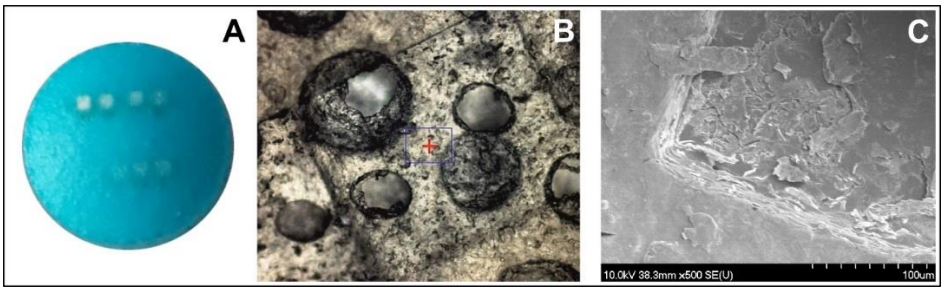

Fig. 10. ArF laser treated EudrC coated blue tablet. A: Photograph, square-shaped holes from bottom line left: 10, 20, 30, 40, from upper line right: 50, 60, 70, 80 impulses, B: microscopic picture of one ablated square, C: SEM micrograph of the ablated square (magnification of 500×).

6.3.1.2. Profilometric analysis of the lasered surface

The ablated holes of the ArF laser were studied by a surface profilometer, their extent was measured. On the surface of the red tablet series of the ablated holes were examined with a full profilometer scan (*Fig. 11*). The tablet coating was treated by ArF laser using 10, 20, 30, 40, 50, 60, 70, 80, 90 impulses. The curves on the left figure show the depth of the holes made by different number of pulses. The ablation depths were calculated by extracting the affected regions from the data set, and a near linear line can be fitted to them, which is seen in the right figure. The aggregated data show a similar linear relation between the applied number of impulses and ablation depth.

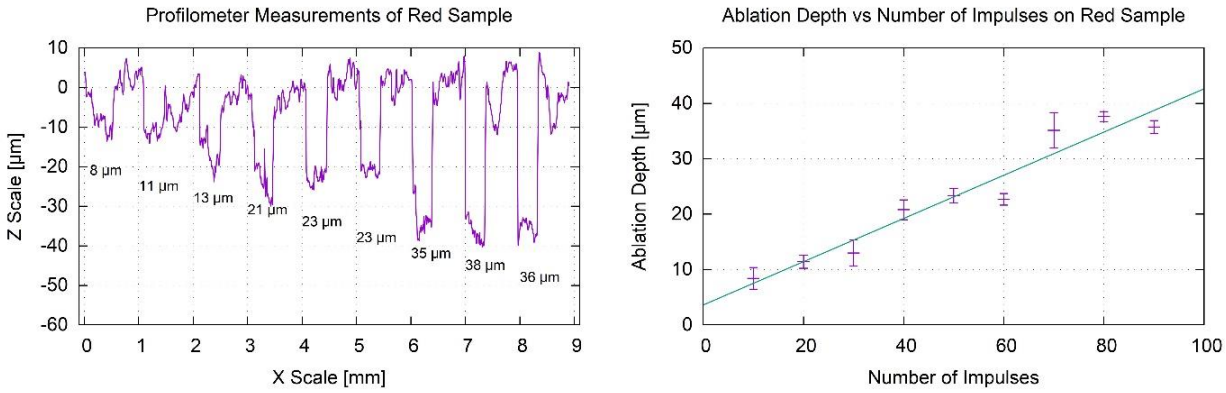

Fig. 11. Profilometer analysis of the series of the ablated holes on the EudrC coated red tablet surface. Left: the curve shows the depth of the ablated holes made by growing numbers of ArF laser pulses, right: the figure shows a near linear relation between the applied number of impulses and ablation depth.

The influence of the colour of differently coloured coatings on ablative depth was examined. The results are shown in *Fig. 12* for blue, cherry and orange samples. Some influence of the

different colors on ablation depth was found. The weighted average of ablation performance is 0.411 ± 0.025 μm/impulse using 2.8–3.2 mJ impulses in EudrC films.

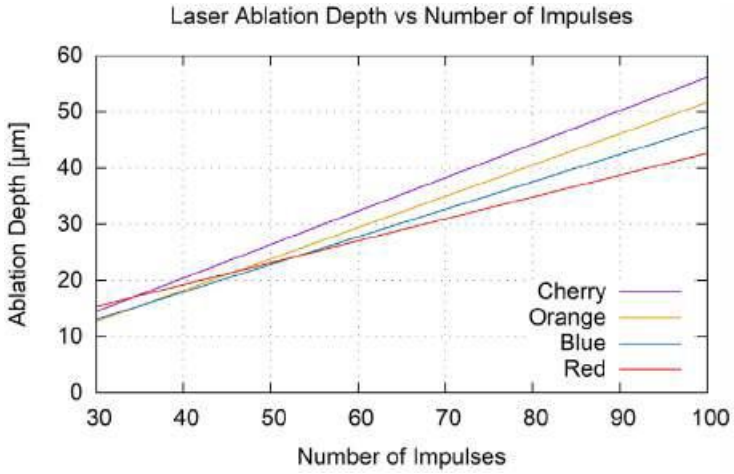

Fig. 12. Comparison of the measurements of the ablated hole depth of tablets with different colours.

6.3.1.3. Scanning electron microscope

The pre- and post-laser structure was examined by SEM as well. In *Fig. 10C*, the micrograph of the blue EudrC film treated with ArF laser is seen. It shows the ablation square at a magnification of 500x. The ablated surface of the sample exhibits no large destructions, the structure of the film is relatively intact. The shape of the hole is a well-distinguished regular square, returning the shape of the mask used. It is clearly visible at the edge of the ablative pit that the film has a layered texture due to the drying of droplets during the coating procedure. It looks as if these layers came off one after another in accordance with the number of laser impulses used. Despite the lack of bigger destructions, there are some cracks in the affected area, which may be the result of loss of water caused by local temperature elevation or by a photocatalytic reaction.

To determine how ablation affected the structure of the film, analytical analyses were performed.

6.3.1.4. Raman investigations

In the following, investigations were performed by Raman spectroscopy to find out if the ArF laser had any effect on the coating film. The spectra of the raw film dispersion, the raw free film and the films treated by ArF laser are summarized in *Fig. 13.* In the fingerprint region of EudrC, there was no significant difference between the spectra taken from the raw film and from the ArF lasered EudrC film.

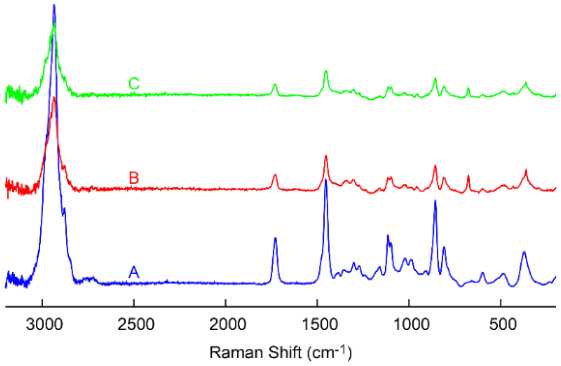

Fig. 13. Raman spectra. A: EudrC dispersion, B: EudrC free film, C: ArF laser ablated EudrC film.

6.3.1.5. Thermal gravimetric analysis (TGA)

The TG and DTG curves of the raw polymer film and the film treated by ArF laser run together, which indicates that the material did not change during lasering, as seen in Annex1, *Fig. 34*. *Table 8* shows the TG temperature ranges, mass loss, DTG normalized integral of the examined materials and peak temperatures.

It is seen that mass loss in the coating films comes in three stages. The first mass loss occurred between 30 and 120 °C, the second stage between 120 and 290 °C, and the third between 290 and 500 °C. Thermogravimetry showed that similar degradation occurred in the raw material and in films marked by ArF laser. Taking into the account the results discussed above, it can be concluded that no chemical changes were observed on the EudrC coating treated by ArF laser.

Table 8. Decomposition behavior of the raw EudrC film and the film treated by ArF laser.

TG-DTG data	**EudrC film**	**Laser treated EudrC film**
First step		
Thermal range (°C)	30-120	30-120
Mass loss (%)	4.31	3.90
Normalized integral (s/°C)	-0.11	-90.41e-03
Peak (°C)	72.83	57.03
Second step		
Thermal range (°C)	120-290	120-290
Mass loss (%)	15.03	14.28
Normalized integral (s/°C)	-0.57	-0.59
Peak (°C)	232.99	233.74
Third step		
Thermal range (°C)	290-500	290-500
Mass loss (%)	50.59	51.88
Normalized integral (s/°C)	-2.12	-2.12
Peak (°C)	362.78	360.07

6.3.2. ArF excimer laser treated Sepifilm coating

After the promising results, it was time to test the laser on other types of coatings as well. HPMC-based ready-to-use coating formulas were studied next, the same films that were used for the SC laser. After marking the polymer films, a detailed quality analysis was performed.

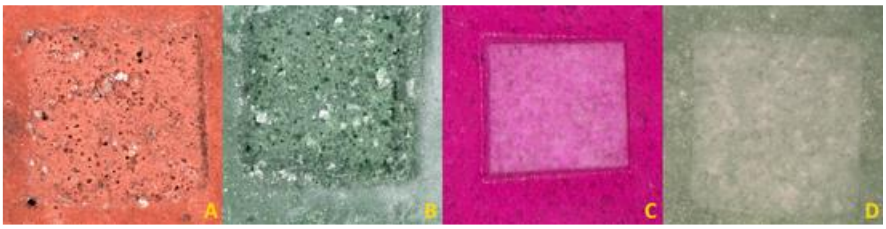

Fig. 14. 3D digital microscope images of coating films treated by ArF laser. A: SPW-R, B: SPW-G, C: SNC-P and D: SNC-G.

The square-shape mask was used, as before for the EudrC film. The ablations of the differently colored coatings were considerably different: in coatings SPW-R and SPW-G white and black particles appeared, which are seen in *Fig. 14A* and *B*. This phenomenon had been seen previously neither on the SC laser treated surface *(Fig. 7)*, nor on the naturally colored SNC-P and SNC-G coatings (*Fig. 14C* and *D*). The difference in the composition of the coatings is shown in *Table 6*. Conventionally colored coatings, SPW-R, SPW-W and SPW-G contain TiO_2 and talc. TiO_2 is a white pigment used in most conventional coatings to make films opaque or increase their opacity. The opacifying effect is due to its high refractive index, which results in the scattering of visible light, and it also has excellent heat and light stability [75]. But unfortunately, TiO_2 makes precision laser coding more difficult as the white particles stay in place and they change the overall surface color, which can affect drug identification. On the other hand, new naturally colored film formulations do not contain the excipients in question.

6.3.2.1. Microscopic analysis of the coated surface

The next step in the present study had to focus on clarifying how TiO_2 particles interfere with laser ablation. The microscopic pictures of the untreated and the ArF laser treated films is seen in *Fig. 15*. The first row shows the raw material, while the second row shows the lasered ones. Black and white particles (arrows point to them in *Fig. 15FGH*) are seen here as well in the square-shaped ‘print’ in conventionally coloured films. This phenomenon may be connected to the three existing crystal structures of TiO_2, rutile, anatase, and brookite [55,75]. During the laser treatment of TiO_2, apart from ablation, three main events are expected to occur: reduction, phase transition and melting.

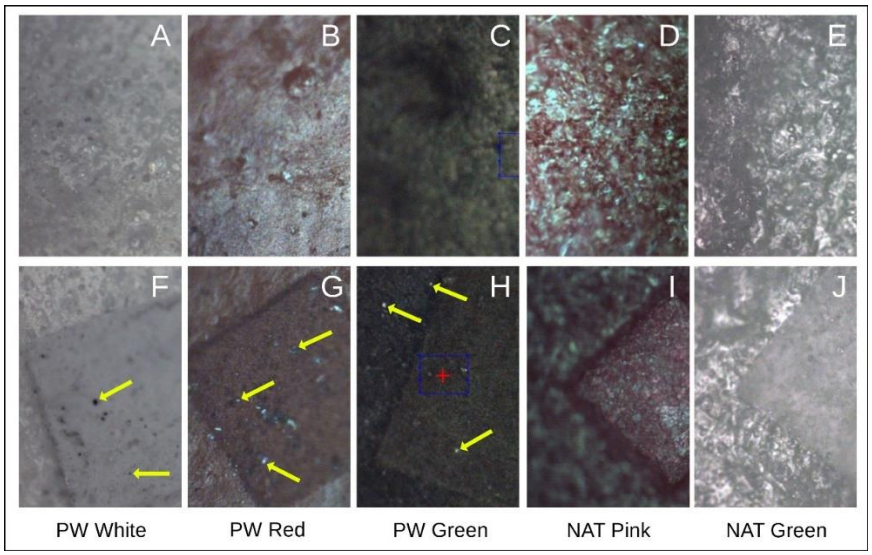

Fig. 15. Microscopic pictures of Sepifilm films. First row: untreated films, second row: films treated by ArF laser.

These can be qualitatively graded according to the respective characteristic temperatures of 500°C, 750 °C, and 1870 °C. It was reported by Robert et al. that the irradiation of TiO_2 by pulsed, UV, KrF laser at a wavelength of 248 nm induced a colour change from white to dark blue, which was the phase transition of anatase to rutile, indicating surface reduction [76]. Furthermore, Kato et al. studied the mechanism of printing film-coated tablets containing TiO_2 by using a tripled Nd: YVO4 UV laser printing machine (wavelength of 355 nm). They marked clear numbers and letters on the surface of the tablet by turning the colour of the TiO_2 particles in the film from white to black, causing the film to turn gray on the lasered surface. This is the result of the appearance of many black particles in the white film. The black particles are formed by the agglomeration of the grayed oxygen-defective TiO_2 by UV laser irradiation [58]. It was assumed that in the present case the white and black points in *Fig. 15* are also associated with the laser irradiated TiO_2, since the reactions of TiO_2 to laser ablation differ significantly from the other ingredients of the coating material. Each material has its characteristic ablation threshold. This value is specific to the material, the type of laser, the ablation method, the wavelength and the fluence [60,61]. In the studies of Laude et al., the ablation of talc started at 250 mJ/cm^2 fluence, at 248 nm wavelength [77], so it is likely that talc was ablated during the laser treatment in this study.

The ablation of TiO_2 requires higher fluence or wavelength, than the other ingredients of the coating material need, and it is likely to require higher fluence than ArF laser can provide. In the present case, the laser was used at 193 nm wavelength and 444 mJ/cm^2 fluence, whereas literature data about the ablation threshold of TiO_2 are available only at 248 nm wavelength and

1.44 J/cm^2 [78] or 910 mJ/cm^2 fluence [76]. The threshold value for the current investigation was still below the ablation threshold of TiO_2 and was not enough for its removal, but it was enough for the removal of the rest of the coating. Therefore, the presence of these excipients can disturb the 2D code recognition.

In the case of TiO_2 -free, SNC-P and SNC-G coatings *(Fig. 15IJ)* those black and white particles are not visible.

6.3.2.2. Analysis by 3D microscope

The previously discussed TiO_2 enrichment can disturb 2D code recognition by increasing surface roughness. The remaining particle size can be about half of the ablation depth, as shown by the results of the ArF laser treated SPW-R film as an example (*Fig. 16*). The designated line where the measurement was taken passes through the ablation hole (*Fig. 16B*) and the corresponding profile of the ablation hole is shown in *Fig. 16C.*

The metal oxide and pigment ratio also changed during the ablation procedure. This effect modifies the colour of the treated coating and consequently degrades the contrast of the 2D code.

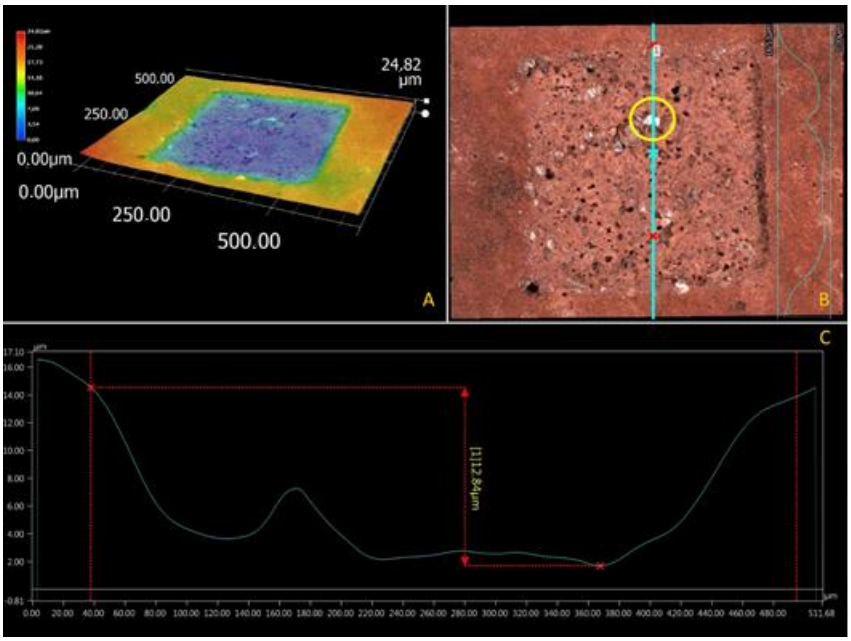

Fig. 16. Surface analysis by 3D microscope of the ArF laser treated region of SPW-R coating. A: 3D surface graph, B: top view with the original colours of the ablation hole, the white TiO_2 particle is marked with a yellow circle, C: profile analysis

According to the literature, it was supposed that the thermal effect of pulsed UV radiation of 193 nm is negligible, only rapid photochemical reactions take place in the irradiated volume, "exploding" the molecules from the surface (photoablation), and there is no time for any heat

transfer. This hypothesis was supported by the microscopic pictures where no sign of thermal degradation or modification of the film structure was visible (*Fig. 14* and *Fig. 15*).

6.3.2.3. Raman investigations

As in the case of a SC laser, Raman examination was done to find out whether a chemical change had occurred during lasering. Fluorescence interfered with the measurement in this case, too. Among the listed components (*Table 6*), TiO_2 is one of the most important ones that influenced the ArF laser ablation results, as already discussed above. In the corresponding articles, the peaks of the Raman spectra of TiO_2 dioxide may be found at 396, 516, and 638 cm^{-1}, which characteristic peaks were found in the Raman spectra of Seppic PW films, too, see *Fig. 17(a)(b).* These peaks exhibited a minor decrease in films treated by the ArF laser, and a more considerable decrease in intensity when they were lasered by the SC laser, as seen above in *Fig. 9*, in the same way as Kato et al. reported [58], confirming the fact that TiO_2 is indeed the substance in question. In the case of SPW-G film, which also contains TiO_2, it is hard to analyze the spectra because of the fluorescence of chlorophyll. In all cases, the spectra of the raw films and the lasered films run together (*Fig. 17*), so it can be concluded that the ArF laser did not cause considerable alteration in the coatings.

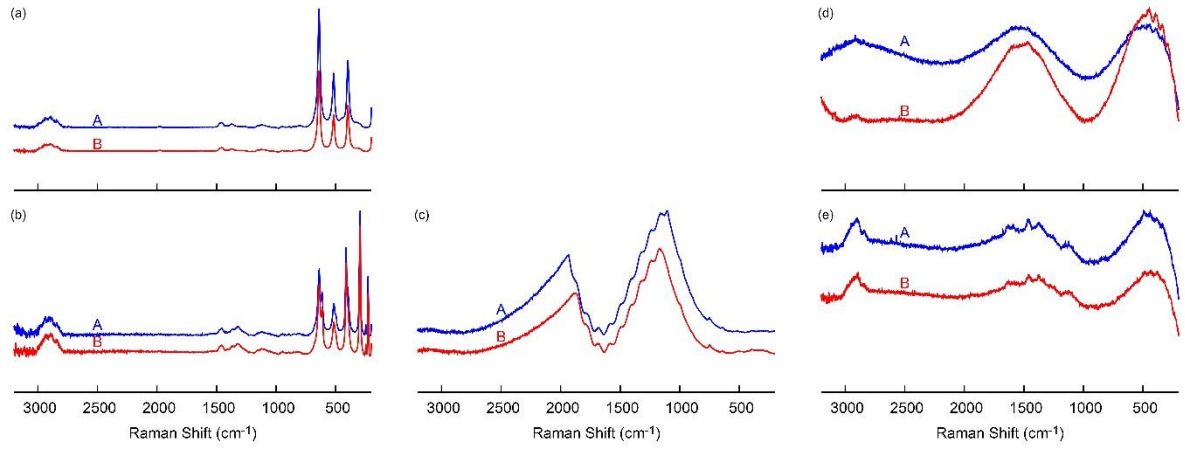

Fig. 17. Raman spectra of a raw film and a coating treated with ArF laser. (a): SPW-W, (b): SPW-R, (c): SPW-G, (d): SNC-P, (e): SNC-G (A: original, B: ArF laser).

6.3.2.4. Thermal gravimetric analysis (TGA)

In the micrographs of the ArF laser treated films (*Fig. 15*, bottom line), it is seen that the ablated surface of the sample exhibits no considerable destruction, the structure of the film is relatively intact. TG results are shown in *Table 9* and Annex 1, *Fig. 35*, were the TG curves of the laser marked films run together with the curves of the raw films which means that the film has not

been damaged, during coding. The ArF laser treatment of tablets could be a promising solution for limited type of coatings.

Table 9. Decomposition behavior of raw Sepifilm films and films treated by ArF laser.

TG-DTG data	**SNC-P film**	**Laser treated SNC-P film**
First step		
Thermal range (°C)	25-120	25-120
Mass loss (%)	2.85	4.05
Second step		
Thermal range (°C)	290-430	290-430
Mass loss (%)	58.26	59.98
	SPW-R film	**Lasered SPW-R film**
First step		
Thermal range (°C)	25-120	25-120
Mass loss (%)	1.07	1.15
Second step		
Thermal range (°C)	290-440	290-440
Mass loss (%)	51.88	52.11
	SPW-W film	**Lasered SPW-W film**
Thermal range (°C)	25-500	25-500
Mass loss (%)	56.06	54.80

6.4. KrF laser

To eliminate the problem of the remained particles further solution had to be found to be able to ablate those particles. Each material has an ablation threshold, and for successful marking, the threshold value of the material has to be exceeded [61]. The ablation threshold of a substance is determined by several parameters, which are mostly related to the laser beam. These include the repetition rate of the laser (Hz), wavelength, pulse energy, and duration, energy density and the absorption properties of the substrate. By selecting the proper laser parameters, the desired ablation depth can be achieved [79]. To solve the previous difficulties, KrF laser was chosen with a higher wavelength (248 nm). From what have been seen so far, it is known the excimer laser is safe, and the literature data confirmed that the ablation threshold of TiO_2 is below the wavelength of 248 nm [78].

In the following experiment, API containing tablets (white) were coated with 2 layers of differently coloured coatings. The transparent bottom layer was the functional one, while the red-coloured top layer was applied to enable marking. The 2D codes were drawn by ablating specific parts of the upper coating layer.

The focus is also on demonstrating the effectiveness of a QR code-based authentication process, presented from the formulation of the QR-coded tablets by laser ablation to the decoding step using a QR code reader application on a smartphone.

6.4.1. Microscopic analysis of the coated surface

The QR code *(Fig. 18A*) that was lasered on the tablets was generated by the QR code generator library libqrencode [80]. A simple code (with content: 12345678) was made, as the aim was to find out if it was possible to ablate a decodable QR code on the surface of the tablet by this laser.

Fig. 18. The QR code sample. A: The common form of the QR code, B: the inverse of the QR code ablated onto the coloured tablet, C: the same QR code but made of dots, prepared for laser and desktop control.

The results of the KrF laser treatments, and the decoding result are seen in *Fig. 19*.

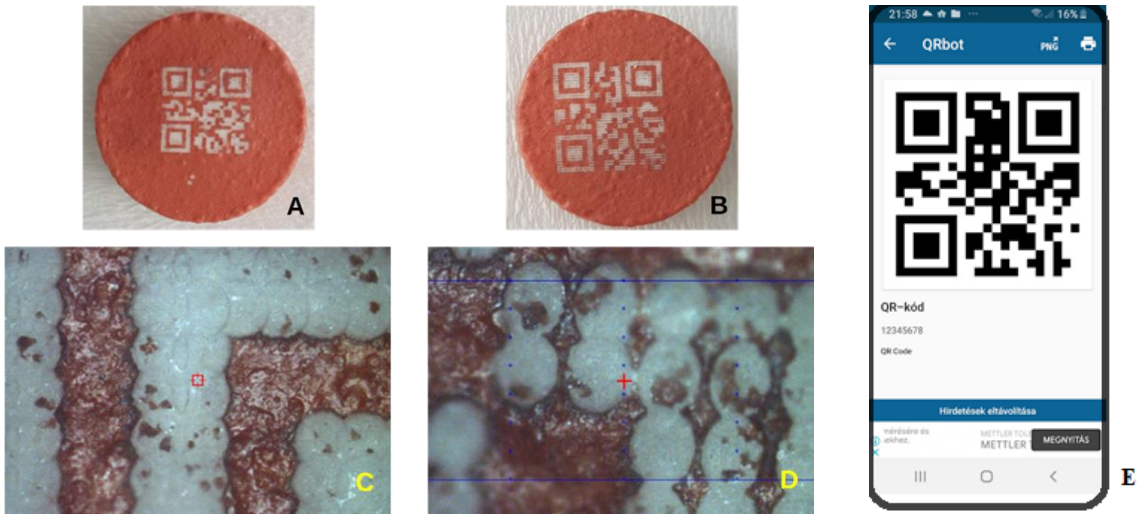

Fig. 19. Tablet encoded by KrF laser. A: The size of the QR code is 4x4 mm, B: the size of the QR code is 5x5 mm, C: microscopic picture of the 4x4 mm QR code, D: microscopic picture of the 5x5 mm QR code, E: QR code authenticated by a mobile phone (by QRbot app).

The QR codes applied on the tablets are readable by a smartphone with QR code scanner applications downloaded from the Internet for example, with QRbot (https://qrbot.net/) or with the photo mode of the mobile phone. The only requirement is that the application must be able to read the "inverse" QR code (*Fig. 18B)*, as in this case the tablet surface is coloured and the ablated part is white, just the opposite of the usual QR codes.

TiO_2 particles had been totally ablated and did not interfere with decoding. It is known that a usable QR code can also be created by not overlapping parts, such as dots. The oval-shaped holes in the film ablated with the KrF laser were in accordance with the shape of the beam. It was possible to generate a readable code from oval-shaped holes, too, even when laser irradiation was not perfect, as the code has error correction capability that can restore the missing data, as seen on the ablated QR code that is made up of individual points (*Fig. 19BD*). Better coverage can be obtained by overlapping the holes, which results in a more readable code. Nevertheless, care must be taken not to punch through the E-L30 D55 layer. The depth of ablation can be controlled by changing the number of the pulses on the sample place or the fluence, which allows the accurate setting of the penetration depth to the coating layer.

It took 1.5 and 2 hours to create such a code by the KrF laser, depending on whether there was an overlap between the holes or not. Fewer shots mean faster but still effective marking.

Fig. 20 displays the SEM micrographs of the 4x4 mm QR code on the tablet treated by KrF laser.

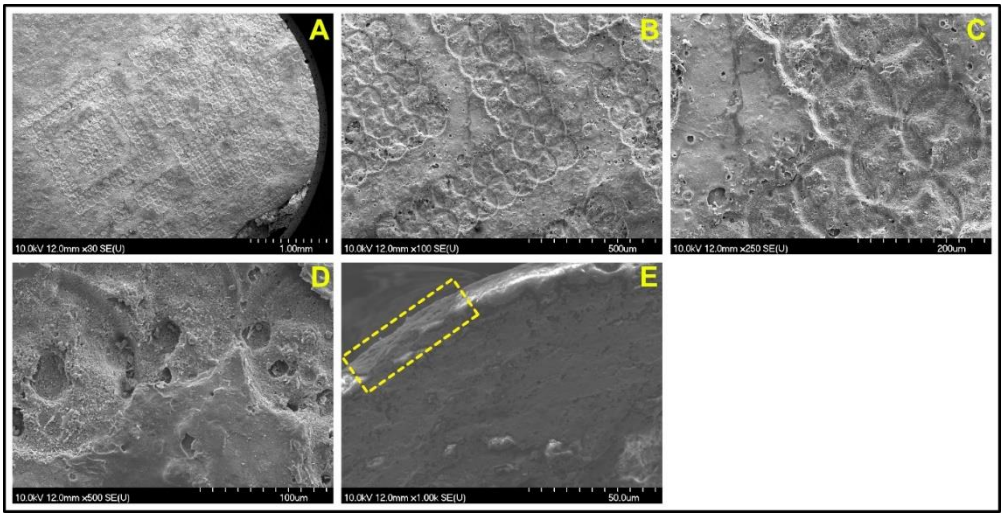

Fig. 20. SEM micrographs of KrF laser treated tablets. A: Tablet surface at a magnification of 30x, B: Tablet surface at a magnification of 100x, C: Tablet surface at a magnification of 200x, D: Tablet surface at a magnification of 500x, E: The tablet's cross-section surface at a magnification of 1000x. The place of lasering is shown in the framed section.

Fig. 20A shows the lasered tablet's surface. In *Fig. 20B* it is clearly visible that the QR code is made of overlapping dots, as described above. It can be seen in *Fig. 20C* that the holes are deeper at the overlapping parts and also that the surface of the untreated coating is uneven. The cavities visible on the untreated surface may have remained from the bubbles formed during the coating process due to too quick drying since the air did not have time to diffuse out.

Fig. 20D displays the lasered tablet's surface at greater magnification. The holes in the ablated surfaces could also have resulted from bubble formation. *Fig. 20E* shows the cross-section surface of the tablet, where the place of lasering is seen in the framed part. The glossy part on the top of the tablet is the SPW-R coating, which is about 5-10 μm thick. The bottom coating, which is 60-70 μm thick, seems to be intact. The ablated surface of the sample has no large damage. Only a physical change is observed in the structure as a result of the removal of the coating by the KrF laser, and no obvious sign of chemical change is detected.

6.4.2. Disintegration test

In the disintegration studies, six pieces of coated and KrF laser ablated tablets were tested from tablet type Nr 3. The tablets remained intact during the 2-hour disintegration process in the artificial enzyme-free gastric juice, which corresponds to the result expected according to the European Pharmacopoeia, as they had a gastro-resistant coating. After changing to the intestinal fluid, the disintegration test was complete in 30 minutes for all tablets. This result confirmed our preliminary conclusion based on SEM analysis, according to which the lasering of the upper coating left the functional coating in the bottom intact, so it is possible to mark functionally coated tablets, too.

6.4.3. Coating film thickness

In the case of double coated tablets, microscopic film thickness measurement was applied to confirm the assumption that not only the inter-tablet but also the intra-tablet variability of final coating thickness is spread over a wide range. Coating thickness averages measured on different tablets, determined on the basis of the measurements at 10 places of 4-4 half tablets, are presented in *Table 10*. It is seen even visually how the thickness of the coatings on the tablet varies in different places.

Table 10. Thickness of the two different coatings of the API containing tablet.

	12 mm diameter round flat tablet (600 mg)	10 mm diameter round flat tablet (300 mg)	10 mm diameter round flat tablet (500 mg)
SPW-R coating thickness (μm)	49.43 ± 9.23	16.19 ± 9.19	88.02 ± 18.98
	63.12 ± 14.72	61.78 ± 14.67	95.42 ± 13.45
	59.31 ± 11.82	34.81 ± 11.76	73.26 ± 22.65
	76.75 ± 13.98	45.78 ± 14.56	69.76 ± 16.54
E-L30 D55 coating thickness (μm)	182.34 ± 22.44	79.62 ± 17.79	155.45 ± 19.57
	145.93 ± 29.54	123.65 ± 29.67	98.02 ± 23.77
	204.54 ± 17.57	97.43 ± 23.65	136.23 ± 29.76
	163.78 ± 32.23	134.75 ± 36.76	102.43 ± 13.65

6.4.4. Raman investigations

The dispersive Raman spectrometer was used to detect possible changes in the double coated tablets, and chemical mapping was chosen to determine if there was a laser-induced modification in the coating layers or in the API. The examination was done on the surface of the lasered tablet and on the fracture surface of the halved tablet. The chemical map was profiled based on the spectra that are summarized in. *Fig. 21*. The full spectrum was applied for raw free films (E-L30 D55, SPW-R) and a single peak (1604 cm^{-1}) for the API Ibu. *Fig. 22* and *Fig. 23* present the data of the obtained chemical maps. Part A of the figures shows the microscopic mosaic photograph of the KrF laser treated region; the chemically mapped area is framed with a blue line. The spectra were collected from places marked by blue points. The other parts of the figures show chemical maps, where BC and D show the profiling result of the E- L30-D55, Ibu and SPW-R film, respectively. In these maps, the warm colours show a higher concentration of the profiled materials. Profiling of the SPW-R spectrum was performed only for tablet cross-sections.

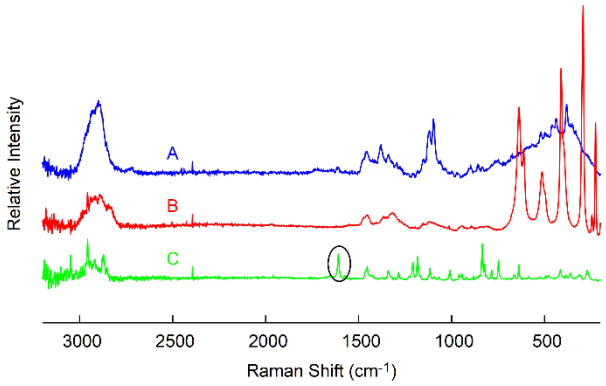

Fig. 21. Raman spectra of the film coatings and of the API. (A) E- L30-D55, (B) SPW-R, (C) API Ibu. Chemical map profiling was performed on spectra A,B and a single peak which is circled on spectrum C (1604 cm^{-1}).

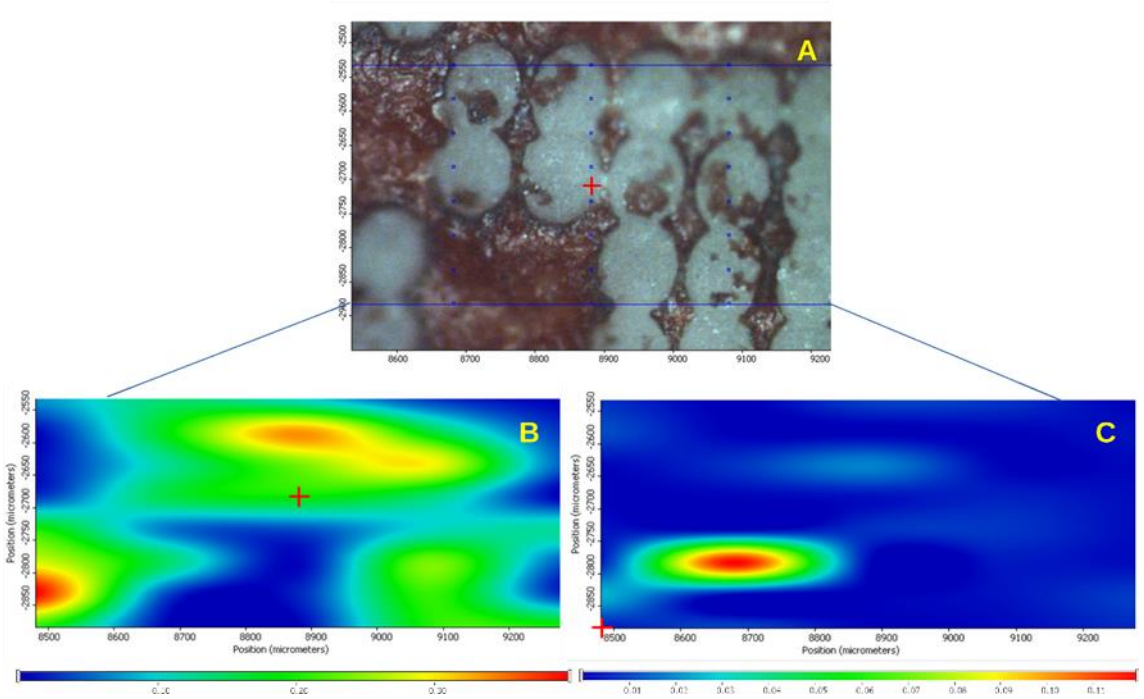

Fig. 22. Surface of the tablet treated by KrF laser. A: Microscopic picture of the surface of the lasered tablet, B: chemical map profiled to E-L30-D55, C: chemical map profiled to Ibu.

The results confirm that the SPW-R upper layer *(Fig. 23D*) was completely ablated in the places that were lasered. Based on *Fig. 22C*, it can be assumed that the laser had reached the API. It could happen because the thickness of the coating was not consistently even, and furthermore because the API might have penetrated into the E-L30 D55 coating, which appears in green color (*Fig. 23C).* To determine if there was a laser-induced change in the API, Raman measurements were performed on the fracture surface of the tablets, too. Sample analyses were made at 10 points directly below the lasered coating surface and at 10 points in the core of the lasered tablets. As described in the "Methods" section, 10 spectra were averaged at each point. The mean of these spectra was compared with the average of 10 spectra taken from the core of an untreated tablet and with the spectrum of Ibu. These spectra were normalized to peak 1604 cm^{-1} of the Ibu spectrum and are shown in *Fig. 24*. There was no significant difference between the spectra taken from the KrF laser treated area and the spectra taken from the non-lasered area. The most characteristic peaks of Ibu are present in all the spectra, with no slip visible. The observed peak intensities can be attributed to the relative inhomogeneity of the materials in the tablet, depending on how rich or poor Ibu was in the studied region.

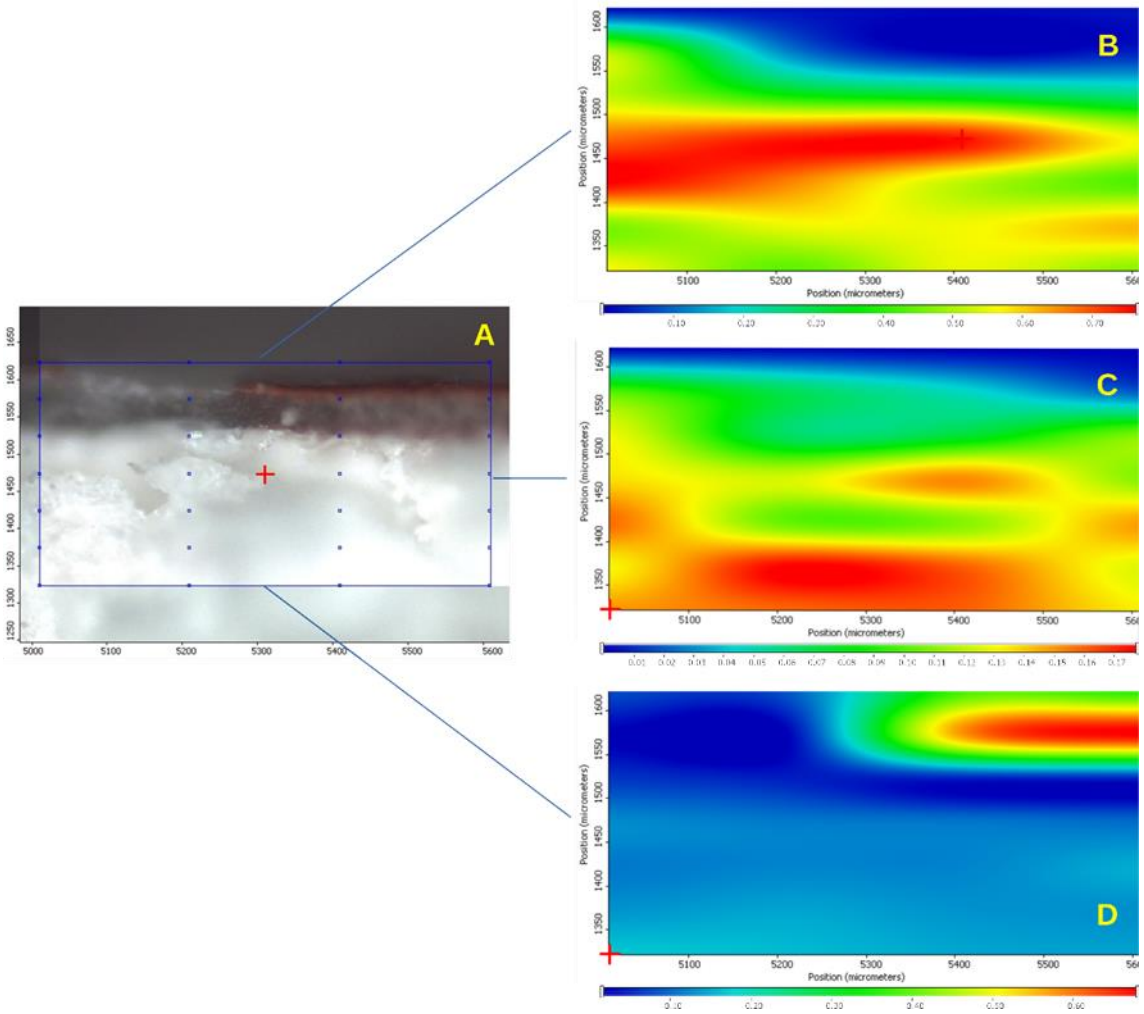

Fig. 23. Fracture surface of a tablet treated by KrF laser after halving. A: Microscopic picture of the fracture surface of the lasered tablet, B: chemical map profiled to E-L30-D55, C: chemical map profiled to Ibu peak, D: chemical map profiled to SPW-R.

Sampling with a small laser spot may also result in different intensities due to the inhomogeneous composition of the tablet. It can be stated that no chemical structural change was observed after the labelling. Overall, despite the fact that, mainly due to the uneven thickness of the coating, the laser can occasionally reach the functional coating during the removal of the PW red layer, and that Ibu can penetrate from the tablet core into the functional coating, no chemical structural changes were observed in the coatings during the coding process, and thus the laser is found to be suitable for drug labelling.

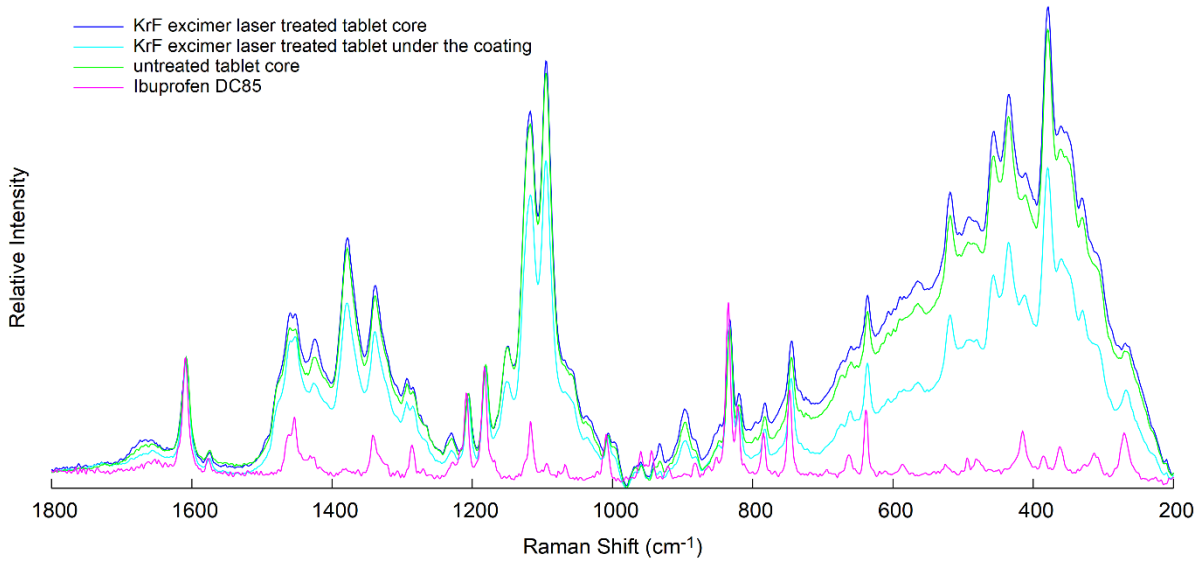

Fig. 24. Averaged and normalised (to peak Ibu 1604 cm^{-1}) spectra taken from the KrF laser treated and non-treated places, spectra of untreated tablet core and Ibu spectrum.

6.5. Ti:sapphire femtosecond laser

Finally, a near-infrared (800 nm), short-pulse femto laser was tested. The assumption was if the pulse is ultrashort, the heat effect is insignificant, and no or just little chemical or thermal damage occurs during the removal of the material. As it works at a high wavelength, it has to be suitable for the elimination of TiO_2 [60].

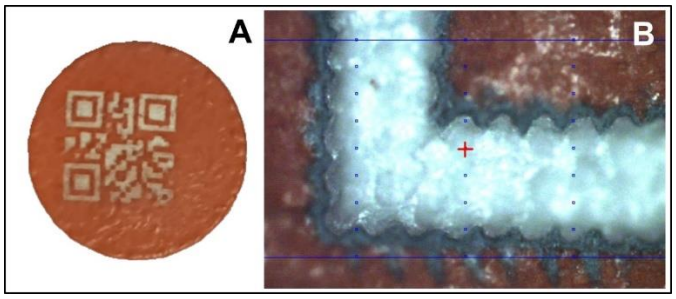

Fig. 25. Tablet encoded by femto laser. A: Visible to the naked eye, B: microscopic picture.

6.5.1. Microscopic analysis of the coated surface

The same computer-controlled movable desktop was coupled with femto laser as in the case of KrF laser to mark the tablet. This time, the shape of the beam was round, thus the ablated holes were too, and they overlapped, as shown in *Fig. 25B*. The ablation of the QR code took around 10 minutes, as the most important limiting factor of overall ablation is the repetition rate of the laser. Therefore, the higher frequency (200 Hz) of the femto laser dramatically shortens the marking procedure.

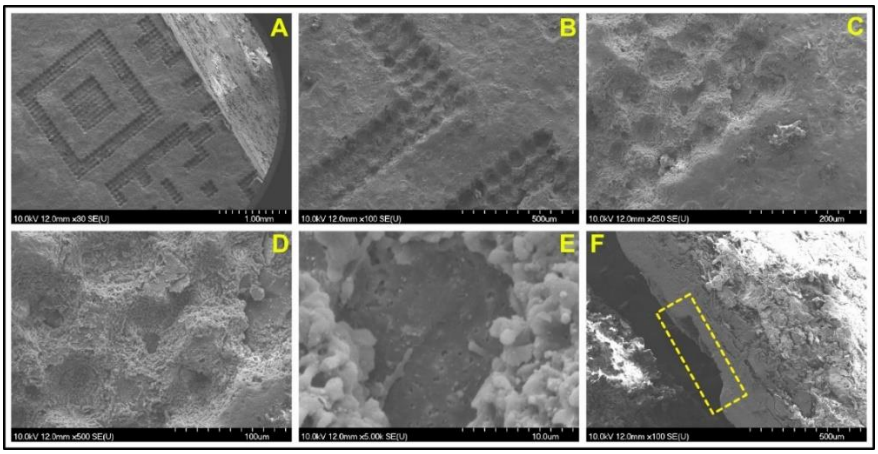

Fig. 26. SEM micrographs of femto laser treated tablets. A: Tablet surface at a magnification of 30×, B: tablet surface at a magnification of 100x, C: tablet surface at a magnification of 250x, D: ablation hole at a magnification of 500×, E: ablation hole at a magnification of 5000x, F: the tablet's cross-section surface at a magnification of 100×. The place of lasering is shown in the framed section.

6.5.2. Scanning electron microscope

Fig. 26. displays the SEM micrographs of the femto lasered tablet. Apart from element F where the tablet's cross-section surface is seen, others show the tablet's lasered top surface with a section of a QR code, at increasing magnifications. The dots which compose the QR code are clearly visible. In *Fig. 26ABCD*, intact regions can be identified between the holes. *Fig. 26E* shows one hole at a higher magnification. At the bottom of the ablation cavity, a different material is detected, which is thought to be the functional coating because of its different, more porous structure. The laser penetration here seems to have taken place right up to the bottom of the coating. The tablet was fixed to the holder upside down *(Fig. 26F)*. The ablation area is visible in the framed part. The femto laser removed the upper coating, which is about 50 μm thick, and in some places, the laser also penetrated into the functional E-L30 D55 coating. Nevertheless, because its thickness is about 150 μm, the functionality may still be intact despite its partial absence.

Similarly to excimer lasers, it can be stated that the femto laser did not cause considerable damage in the coating structure during the treatment, either. Only a physical change can be detected in the ablated area, fragments of the coating film are visible where the coating was removed. No visible sign of chemical changes was detected in the upper or in the bottom layer.

6.5.3. Disintegration test

As with the disintegration study of KrF laser-treated tablets, 6 femto lasered tablets (type Nr 3) were tested, too, and the result was the same, i.e., the tablets did not dissolve in the acid within 2 hours, only after transfer to the base, in accordance with the European Pharmacopoeia.

6.5.4. In vitro Drug Dissolution test

Excimer lasers are known to be intended for laboratory use, while femto lasers are much more widely used in industry. Although reducing the ablation time to 10 minutes is considered as a great result, but it is still a long time to produce tablets on an industrial scale. Nevertheless, it was considered important to measure the dissolution parameters of lasered tablets, as a continuation of the experiment to confirm that it is possible to mark tablets with functional coating without damaging them during the procedure.

For in vitro drug dissolution tests, tablets of different shapes were used: A: Type Nr. 1, B: Type Nr. 2, C, and D: Type Nr. 3. Three of the investigated tablets remained intact after 120 minutes in the gastric medium. The amount of the dissolved API was 0.15%, 2.12%, and 0.92%, for A, C and D, respectively, while the dissolved API was 35.2 % for Tablet B, which partially disintegrated during this period. The dissolution profile of the tablets in the gastric medium is shown in Fig. 28.

To save time and material, the differently shaped API containing tablets were coated together with placebo tablets. Presumably, due to their different geometry, they were mixed inappropriately during coating, therefore they might have different coating thicknesses. Tablet coating thickness may also vary in the case of identical tablets, as observed by M. Wolfgang et.al., where it varied between 56.3 μm and 86.9 μm [81]. The literature also confirms that the shape of the tablet directly influences intra-tablet coating uniformity. The most likely reason for intra-tablet coating variability is the preferred orientation of tablets when passing through the spray zone of the coater [82]. There was another investigation of inter-tablet coating layer thickness, where a comparison of both sides of the tablet surface was made. It shows that the thickness of the coating layer of some tablets is up to 10μm thicker on one side of the tablet than on the other side [83]. Achieving a high level of intra-tablet uniformity is especially important for functional film coatings [84], where uniform thickness is required to guarantee the desired drug release rate to the patient [81].

The film layers of a halved, dual-coated tablet are shown in the micrograph in Fig. 27, which shows that the coating thickness varies over a wide range within a tablet. There is seen the

difference in the thickness of the coating on the top and on the side of the medicine. Also, in Chapter 6.4.3. above, *Table 10* has the summary of the thickness of the different coatings.

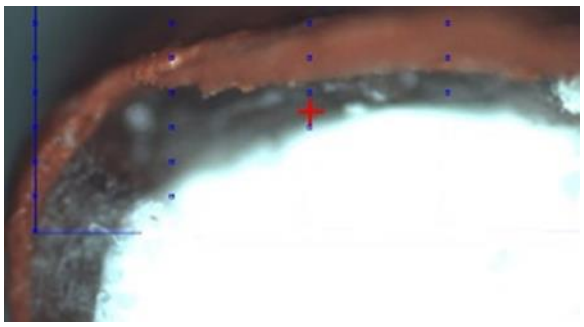

Fig. 27. Uneven thickness of the double coated tablet's coatings

In the present study, it can be assumed that in the case of Tablet B, the coating was thinner for the reasons indicated above and might have been damaged during the marking. It is likely that if only tablets of the same shape are coated at a time, the layer thickness will be more uniform and the inner, functional layer can be protected from damage.

The dissolution profile of the tablets in phosphate buffered saline solution is also seen in *Fig. 28*.

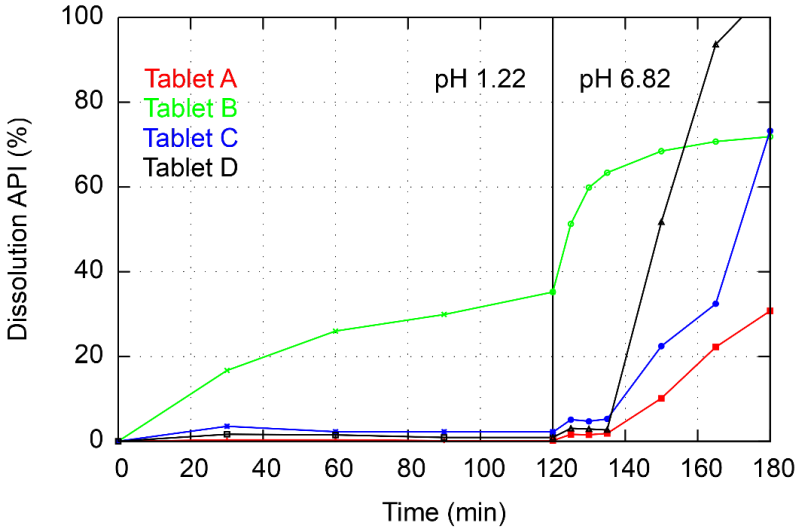

Fig. 28. Drug dissolution curves of the 4 coated and lasered tablets

It can be concluded that during the one-hour in vitro studies, the tablets acted in accordance with pharmacopoeial standards, and the disintegration and dissolution process started. It is seen that the dissolution of Tablet B started earlier than that of the others, and the final concentration was lower. The explanation for this phenomenon is that the dissolution of Tablet B had already started in the gastric medium.

6.5.5. Raman spectroscopy

As in previous studies, Raman measurements were performed to check if the tablet material had changed during lasering. *Fig. 29* and *Fig. 30* display the tablet surface and the cross-section of femto laser treated tablets, respectively. In *Fig. 29B* E-L30 D55 is seen in the laser treated areas, while in *Fig. 29C* the warm colours show the API Ibu, which suggests that the coating thickness was not consistently even, and the laser might have reached the API or it penetrated into the coating in this case as well. In *Fig. 30A* the arrow points to the missing SPW-R coating, and the mapping (*Fig. 30D*) confirms that it was ablated by the laser. The profiling shows that the API is mostly in the tablet core (*Fig. 30C*), but in the same picture, the area of the inner coating is green, which means that the API partly migrated from the tablet core to the E-L30 D55 film. According to the literature, such migration during the coating process can happen if the coating is aqueous based. Migration is enhanced if a component is soluble in the coating solution, and it also depends on the spray conditions used during the coating operation [85,86].

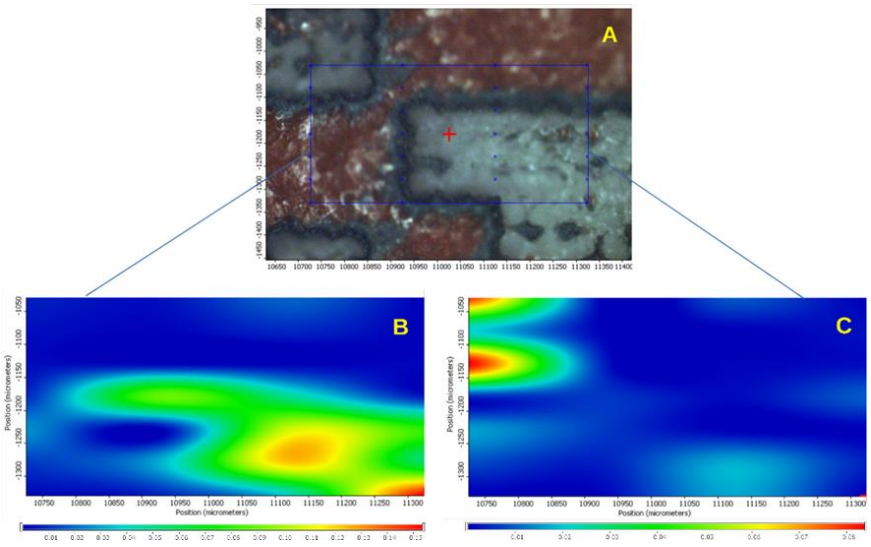

Fig. 29. The surface of the tablet treated by femto laser. A: Microscopic picture of the lasered tablet, B: chemical map profiled to E-L30-D55, C: chemical map profiled to Ibu.

Similarly to the previous case, Raman measurements were performed on the fracture surface of the femto laser treated tablets, too, to determine if there was a change in the API, as described in the "Methods" section. These spectra were normalized to peak 1604 cm^{-1} of the Ibu spectrum and are shown in *Fig. 31*. As with the KrF laser results, there was no significant difference between the spectra taken from the laser treated region and the spectra taken from the non-lasered region.

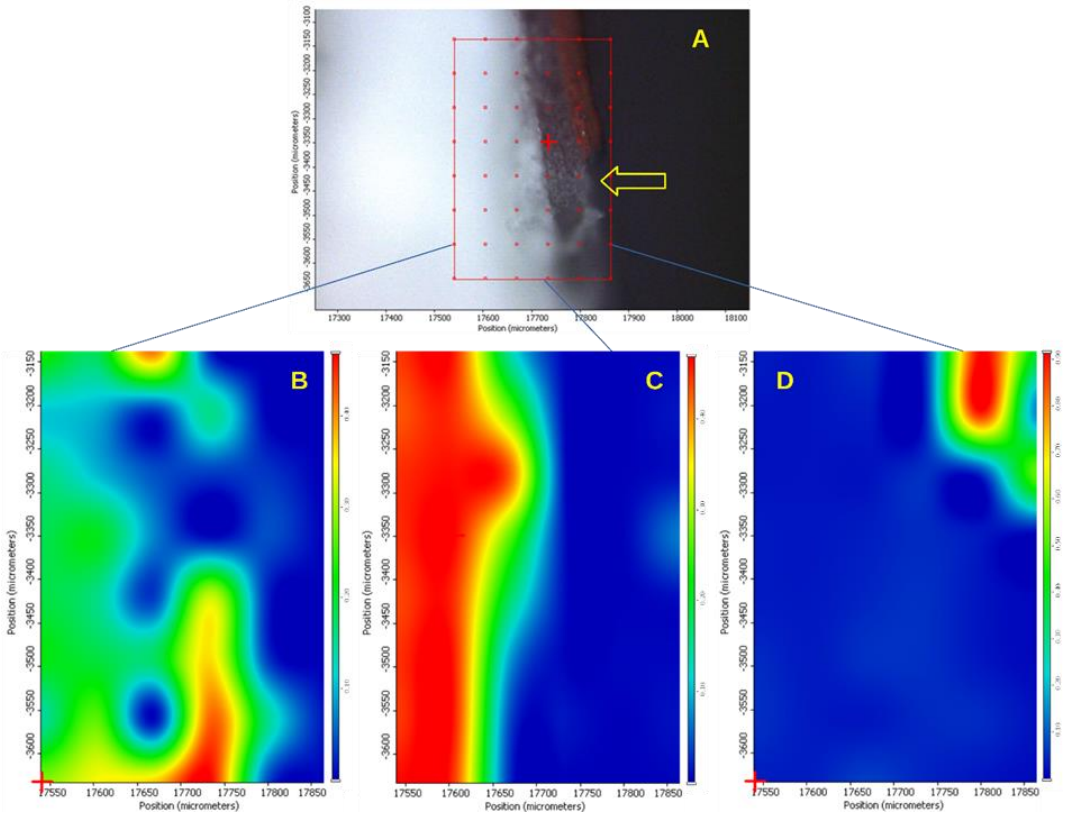

Fig. 30. Cross-section surface of the femto laser treated tablet. A: Microscopic picture of the halved tablet, the arrow pointing to the missing SPW-R coating, B: chemical map of the tablet surface profiled to E-L30 D55, C: chemical map of the tablet surface profiled to Ibu, D: chemical map of the tablet surface profiled to SPW-R.

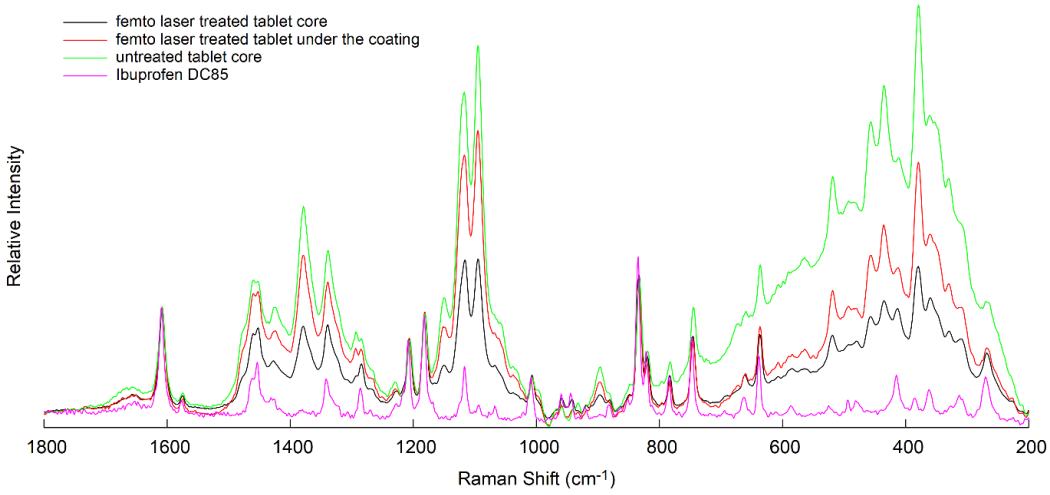

Fig. 31. Averaged and normalised (to Ibu peak 1604 cm^{-1}) spectra taken from the femto lasered and non-lasered places, spectra of untreated tablet core and Ibu spectrum.

Again, the different peak intensities here can be attributed to the relative inhomogeneity of the material in the tablet, depending on how rich or poor the Ibu was in the area of interest.

It can be stated that no chemical structural change was observed because of the ablation process.

7. SUMMARY

The aim of the experiment was to develop a new, efficient way of a unique marking method to combat drug counterfeiting. For five different lasers, investigations were made to find out how the drug changes in response to the laser beam.

Tablets were selected for coding as they are widely used and are physicochemically stable.

- Laser was chosen as a coding tool as it is a non-contact method, thus minimizing the problems of contact contamination.
- In selecting lasers, the goal was to compare different types of instruments during ablation and to obtain a general overview of their effects on the drug. As the study progressed, it was found out that certain lasers had a detrimental effect on the sample, so it was necessary to look for devices that would not cause changes in the material.
- When laser coding is applied, it should be considered that the tablet must be coated. At least one colored layer should be applied to the drug, even if it already has a functional coating on, as the 2D code is created by ablating the coating.
- It is clear from the preliminary experiments [87] that great care must be taken when choosing coating materials to ensure that they are compatible with the laser of choice, for example, that the laser is able to remove all components of the coating, such as TiO_2, that the remained white particles do not interfere with 2D code recognition.
- The choice of the optimal instrument and its parameterization is essential for coding.

8. CONCLUSION AND PRACTICAL USEFULNESS

The results presented in this thesis provide useful information for laser drug coding. The present research led to the following findings:

- The aimed anti-counterfeit coding technology was accomplished with three potential lasers, excimer laser (ArF and KrF) and femto laser, which did not cause a qualitative change in the material during laser marking.
- It was found that the ArF laser requires higher fluence, or wavelength, to be able to exceed the ablation threshold of TiO_2, so the usability of this type of laser is limited to TiO_2 -free coatings.
- The higher repetition rate of the femto laser allows faster and more efficient coding, which has key importance in mass production.

- Further results show that due to the high performance in the femtosecond region, the wavelength is no longer the critical parameter as it is for a nanosecond or longer pulses. Thermal effects are negligibly low in the fs region even at high peak powers. The thermal effects of laser ablation can be avoided by reducing the wavelength or the impulse length based on the current study.
- The excimer laser is a laser for laboratory use, while femto lasers are commonly used in the industry. It is known that the efficient use of this technology requires further development in speed. Other near-infrared pulsed lasers that operate at multi-kHz versions (with a repetition frequency of multi ten-kHz and also MHz) could potentially further shorten ablation time. Those devices could even be used for line speed marking in pharmaceutical companies.
- Various coating materials were tested, Eudraguard® control, SEPIFILM™ NATurally COLoured coatings agents, Sepifilm™ PW coating systems, Eudragit L30 D55®. Experience showed that the ability to laser the coatings is determined not only by the type of coating, but also by the quality and parameters of the laser.

New findings/practical relevance of the work

- Based on the study, a novel, non-contact, functionally advanced marking technology was developed by using the lasers mentioned in this study, highlighting the femto laser as a potential solution for pharmaceutical companies that would like to have additional protection against drug counterfeiters or to label personalized medicines.
- It should be noted that the method needs further development and scaling-up to enable this technology to serve the high volumes of industrial production.

9. REFERENCES

[1] D. Csupor *et al.*, *Gyogyszereszet*, vol. 54, pp. 387-399., 2010.

[2] B. Jarvis, *Encycl. Food Microbiol. Second Ed.*, pp. 106–115, 2014.

[3] WHO, 2018. https://www.who.int/en/news-room/fact-sheets/detail/substandard-and-falsified-medical-products. [Accessed: 04-July-2021].

[4] WHO IMPACT, 2006, http://www.who.int/medicines/services/counterfeit/impact/TheNewEstimatesCounterfeit.pdf. [Accessed: 04-July-2021]

[5] UNICRI, 2012. http://www.unicri.it/topics/counterfeiting/medicines/report/Ctf_medicines_and_oc_advance_unedited2013.pdf. [Accessed: 08-May-2019].

[6] WHO, 2018. http://www.who.int/mediacentre/factsheets/fs275/en/. [Accessed: 04-July-

2018].

[7] CSIP, “2016. https://safemedsonline.org/resource/the-internet-pharmacy-market-in-2016-trends-challenges-and-opportunities/. [Accessed: 14-Sep-2020].

[8] Interpol, 2013. http://www.interpol.int/Crime-areas/Pharmaceutical-crime/Operations/Operation-Pangea. [Accessed: 28-Feb-2018].

[9] S.J. Trenfield *et al.*, “*Int. J. Pharm.*, vol. 567, no. June, 2019.

[10] A. Attaran *et al.*, “*BMJ*, vol. 345, no. 7884, pp. 1–6, 2012.

[11] A. Fittler *et al*., *J. Med. Internet Res.*, vol. 20, no. 8, pp. 1–11, 2018.

[12] European Medicines Agency, http://www.ema.europa.eu/ema/index.jsp?curl=pages/special_topics/general/general_content_000186.jsp&mid=WC0b01ac058002d4e8. [Accessed: 08-May-2019].

[13] European Commission, *Off. J. Eur. Union*, 2015.

[14] The European Parlament and the Council of the European Union, *Off. J. Eur. Union*, vol. L 174/74, pp. 74–87, 2011.

[15] WHO, http://www.who.int/mediacentre/news/releases/2017/dementia-immunization-refuguees/en/. [Accessed: 09-Jan-2021].

[16] World Health Assembly, *Seventieth World Heal. Assem.*, p. A70/23: 33-36, 2017.

[17] WHO, http://www.who.int/medicines/regulation/ssffc/publications/gsms-report-sf/en/. [Accessed: 09-Jan-2021].

[18] WHO, 2017. http://www.who.int/medicines/regulation/ssffc/publications/gsms-report-sf/en/. [Accessed: 09-Jan-2021].

[19] WHO, http://www.who.int/mediacentre/news/releases/2017/substandard-falsified-products/en/. [Accessed: 07-Nov-2018].

[20] J.P. Renschler, *et al*., *Am. J. Trop. Med. Hyg.*, vol. 92, no. Suppl 6, pp. 119–126, 2015.

[21] G.M.L. Nayyar *et al., Am. J. Trop. Med. Hyg.*, vol. 00, no. July 2019, pp. 1–8, 2019.

[22] J.C. Gallagher, *et al.*, vol. 34, no. 12, pp. 1483–1485, 2000.

[23] G. Ghinea, *et al.*, *IEEE Trans. Inf. Technol. Biomed.*, vol. 10, no. 4, pp. 794–802, 2006.

[24] S. Fox and M. Duggan, “Pew Internet Project: Health Online 2013,” 2013.

[25] T.K. Mackey and B.A. Liang, University of Liverpool Library,” 2013.

[26] T.K. MacKey and G. Nayyar, *Br. Med. Bull.*, vol. 118, no. 1, pp. 115–131, 2016.

[27] BBC, “BBC News _ HEALTH _ UK’s first online pharmacy opens,” 1999. http://news.bbc.co.uk/2/hi/health/537928.stm. [Accessed: 4-July-2020].

[28] T.K.Mackey and G. Nayyar, *Expert Opin. Drug Saf.*, vol. 16, no. 5, pp. 587–602, 2017.

[29] A.B. Jena and D. Goldman, *Health (Irvine. Calif).*, vol. 30, no. 6, pp. 1192–1199, 2011.

[30] A. Fittler, *et al. Med. Internet Res.*, vol. 15, no. 9, pp. 1–18, 2013.

[31] N. Wajsman, C. Arias Burgos, and C. Davies, no. September, 2016.

[32] IRACM, http://www.iracm.com/en/thematic-observatory/organized-crime. [Accessed: 28-Feb-2018].

[33] A Royal Pharmaceutical Society Publication, *Pharm. J.*, vol. 292, no. 7805, p. 392, 2014.

[34] N. Siva, *Lancet*, vol. 376, no. 9754, pp. 1725–1726, 2010.

[35] R.E. Bichell, "Fake Drugs Are A Major Global Problem , WHO Reports," 2017.

[36] R.G. Vida *et al.*, *Int. J. Clin. Pharm.*, vol. 39, no. 1, pp. 78–87, 2017.

[37] FDA, http://www.fda.gov/Drugs/DrugSafety/DrugIntegrityandSupplyChainSecurity/DrugSupplyChainSecurityAct/. [Accessed: 04-Mar-2019].

[38] European Commission SWD supplementing Directive 2001/83/EC of the European Parliament and of the Council by laying down detailed rules for the safety features appearing on the packaging of medicinal product for human use, SWD(2015) 188 final

[39] M. Davison, *et al.*, Publication, 2011, pp. 103–140.

[40] TruTag Technologies, https://trutags.com/pharmaceutical-nutraceutical/.

[41] J.S. Nogaja, *Int. J. Pharm. Sci. Res.*, vol. 4, no. 1, pp. 29–33, 2013.

[42] J. Heller, https://www.industrial-lasers.com/articles/print/volume-30/issue-6/features/precision-laser-marking-for-medical-applications.html. [Accessed: 28-Feb-2018].

[43] M. You *et al.*, *Nanoscale*, vol. 8, no. 19, pp. 10096–10104, 2016.

[44] J. Fei and R. Liu, *Mater. Sci. Eng. C*, vol. 63, pp. 657–662, 2016.

[45] M. Edinger, *et al.*, *Int. J. Pharm.*, vol. 536, no. 1, pp. 138–145, 2018.

[46] J. Fei and R. Liu, *Mater. Sci. Eng. C*, vol. 63, pp. 657–662, 2016.

[47] K. Langhauser, *Phamaceutical Manuf.*, 2013.https://www.pharmamanufacturing.com/articles/2013/oct-digital-insights/ [Accessed: 04-July-2018].

[48] S. Ur Rehman *et al.*, *8th Int. Conf. High-Capacity Opt. Networks Emerg. Technol. HONET 2011*, pp. 273–279, 2011.

[49] P. Viswanathan, *et al.*, *Nanostructures Oral Med.*, pp. 173–201, 2017.

[50] M. Haaser, K.C. Gordon, C.J. Strachan, and T. Rades, *Int. J. Pharm.*, vol. 457, no. 2, pp. 510–520, 2013.

[51] D.M. Koller, *et al.*, *Eur. J. Pharm. Sci.*, vol. 44, no. 1–2, pp. 142–148, 2011.

[52] K. Korasa, *et al.* , *Eur. J. Pharm. Sci.*, vol. 93, pp. 484–492, 2016.

[53] D. Markl, *et al.*, *Eur. J. Pharm. Sci.*, vol. 55, no. 1, pp. 58–67, 2014.

[54] L. Pérez-Ibarbia, *et al.* , *Eur. J. Pharm. Sci.*, vol. 93, pp. 264–273, 2016.

[55] A. Hosokawa and Y. Kato, *Drug Dev. Ind. Pharm.*, vol. 37, no. 8, pp. 901–906, 2011.

[56] J. Daehwan, *et al.*, vol. 25, no. 14, pp. 2629–2635, 2009.

[57] N. Genina *et al.*, *Eur. J. Pharm. Sci.*, vol. 47, no. 3, pp. 615–623, 2012.

[58] Y. Kato, *et al.*, *Drug Dev. Ind. Pharm.*, vol. 36, no. 4, pp. 405–412, 2010.

[59] A.L. Schawlow and C.H. Townes, *Phys. Rev.*, vol. 112, no. 6, pp. 1940–1949, 1958.

[60] W. Steen and J. Mazumder, *Laser Material Processing*, 4th ed. Springer, 2010.

[61] E.Kannatey-Asibu,*Principles of Laser Material Processing*2009 ISBN 9780470177983

[62] H. Vakili *et al.*, *Int. J. Pharm.*, vol. 483, no. 1–2, pp. 244–249, 2015.

[63] S. Szatmári, *Appl. Phys. B Laser Opt.*, vol. 58, no. 3, pp. 211–223, 1994.

[64] S. Szatmári and F.P. Schäfer, *Opt. Commun.*, vol. 68, no. 3, pp. 196–202, 1988.

[65] TeWaTi, www.tewati.eu. [Accessed: 11-Jun-2020].

[66] J. Lawrence, Ed., *Advances in Laser Materials Processing Technology, Research and Application*, no. 1–2. Woodhead Publishing, 2010.

[67] F. Menges, "Spectragryph - optical spectroscopy software, Version1.2.15 2020, http://www.effemm2.de/spectragryph/." 2020.

[68] J. Romann, *et al,. Chem. C*, vol. 114, no. 24, pp. 10677–10682, 2010.

[69] R. Szostak and S. Mazurek, *Analyst*, vol. 127, no. 1, pp. 144–148, 2002.

[70] P.M. Fechner, *et al.*, *AAPS J.*, vol. 5, no. 4, pp. 1–13, 2003.

[71] Y.S. Li, *et al.*, vol. 324, no. 8, pp. 1543–1550, 2012.

[72] V.E. de Oliveira, *et al.*, *Raman Spectrosc.*, vol. 41, no. 6, pp. 642–650, 2010.

[73] Y. Koyama, Y. Umemoto, A. Akamatsu, K. Uehara, and M. Tanaka, *J. Mol. Struct.*, vol. 146, no. C, pp. 273–287, 1986.

[74] T. L. Weiss *et al.*, *J. Biol. Chem.*, vol. 285, no. 42, pp. 32458–32466, 2010.

[75] M. J. B. James, *et al.*, *Aqueous Polymeric Coatings for Pharmaceutical Dosage Forms*, Third Edit. CRC Press, 2008.

[76] T. D. Robert, *et al.*, *Thin Solid Films*, vol. 440, no. 1–2, pp. 268–277, Sep. 2003.

[77] L. D. Laude, *et al.*, *Nucl. Instruments Methods Phys. Res. Sect. B Beam Interact. with Mater. Atoms*, vol. 131, no. 1–4, pp. 211–218, 1997.

[78] O. Van Overschelde, *et al.*, *Appl. Surf. Sci.*, vol. 252, no. 13 SPEC. ISS., pp. 4722–4727, 2006.

[79] D. J. Elliott, *Ultraviolet Laser Technology and Applications*. 1995.

[80] K. Fukuchi, https://github.com/fukuchi/libqrencode. [Accessed: 11-Jan-2021].

[81] S. Sacher *et al.*, *Int. J. Pharm.*, vol. 566, no. May, pp. 57–66, 2019.

[82] K.E.Wilson and E.Crossman,*Drug Dev.Ind. Pharm.*,vol.23, no.12,pp.1239–1243, 1997.

[83] L. Ho *et al.*, *J. Control. Release*, vol. 119, no. 3, pp. 253–261, 2007.

[84] Y. Dong, *et al.*, *J. Pharm. Sci.*, vol. 106, no. 2, pp. 546–553, 2017.

[85] R. Dansereau, *et al.*, *Drug Dev. Ind. Pharm.*, vol. 19, no. 7, pp. 793–808, 1993.

[86] H. X. Guo, *et al.*, *AAPS PharmSciTech*, vol. 3, no. 2, p. 8, 2002.

[87] K. Ludasi, *et al.*, *Eur. J. Pharm. Sci.*, vol. 123, no. July, pp. 1–9, 2018.

ACKNOWLEDGEMENTS

I would like to express my grateful thanks to **Prof. Dr. Piroska Szabó-Révész** the former Head of the Institute of Pharmaceutical Technology**,** for providing me with the opportunity to work in this Department after long years of absence, and for giving me useful advice during my Ph.D. work.

I am thankful to the Head of the Institute of Pharmaceutical Technology and Regulatory Affairs, **Prof. Dr. Ildikó Csóka,** for ensuring that I could continue the work I had started.

I would like to express my gratitude to my supervisor, **Dr. Géza Regdon Jr.**, who invited me to come back to the university, for his guidance, for patience, and for support I received from him during the research.

I wish to thank **Dr. Tamás Sovány** for his immense help in the measurements and evaluations especially for SEM, and for critically reviewing my manuscripts, and also **Dr. Katalin Kristó** for her inspiring help in my studies.

I would like to express my warmest thanks to **Dr. Orsolya Jójártné Laczkovich** for her generous help, for her abundant advice in my scientific work, especially in Raman measurements and evaluations, but mostly for the encouragement I received and the continuous support of my research.

I express my kindest gratitude to **Prof. Dr. Béla Hopp, Dr. Tamás Smausz, Attila Andrásik, Tamás Gera**, Department of Optics and Quantum Electronics, University of Szeged, and **Dr. Zsolt Kovács**, Department of High Energy Experimental Particle and Heavy Ion Physics, Wigner Research Centre for Physics for their huge help in lasering the coated tablets, for co-operation, for their useful advice during my Ph.D. work, and for the encouragement.

I wish to thank **the members** of the first research group, and **all the members** of the Institute of Pharmaceutical Technology and Regulatory Affairs, for their help and support.

I would like to thank Evonik Industries AG and Seppic S.A. for for their support in supplying the polymers, and Keyence Corporation for 3D microscope measurements.

This research was supported by the EU-funded Hungarian grant EFOP-3.6.1-16-2016-00008

Finally, I am especially thankful to **my husband**, for his support and tremendous help, his patience, and for ensuring a peaceful background. I would like to thank **my children**, **my family**, and **my friends** for their love and tireless support, encouragement, understanding and help during my studies.

ANNEXES

1. Supplementary materials (TG-MS curves of the various samples)
2. **K. Ludasi**, T. Sovány, O. Laczkovich, B. Hopp, T. Smausz, G. Regdon Jr., Unique laser coding technology to fight falsified medicines, European Journal of Pharmaceutical Sciences, 2018, 123, 1-9, doi.org/10.1016/j.ejps.2018.07.023,
3. **K. Ludasi**, T. Sovány, O. Laczkovich, B. Hopp, T. Smausz, G. Regdon Jr., Comparison of conventionally and naturally coloured coatings marked by laser technology for unique 2D coding of pharmaceuticals, International Journal of Pharmaceutics, 2019, 570, 118665, doi.org/10.1016/j.ijpharm.2019.118665,
4. **K. Ludasi**, O. Jójárt-Laczkovich, T. Sovány, B. Hopp, T. Smausz, A. Andrásik, T. Gera, Z. Kovács, G. Regdon Jr., Anti-counterfeiting protection, personalized medicines − development of 2D identification methods using laser technology, International Journal of Pharmaceutics, 2021, 605, 120793, doi.org/10.1016/j.ijpharm.2021.120793,

ANNEX 1.

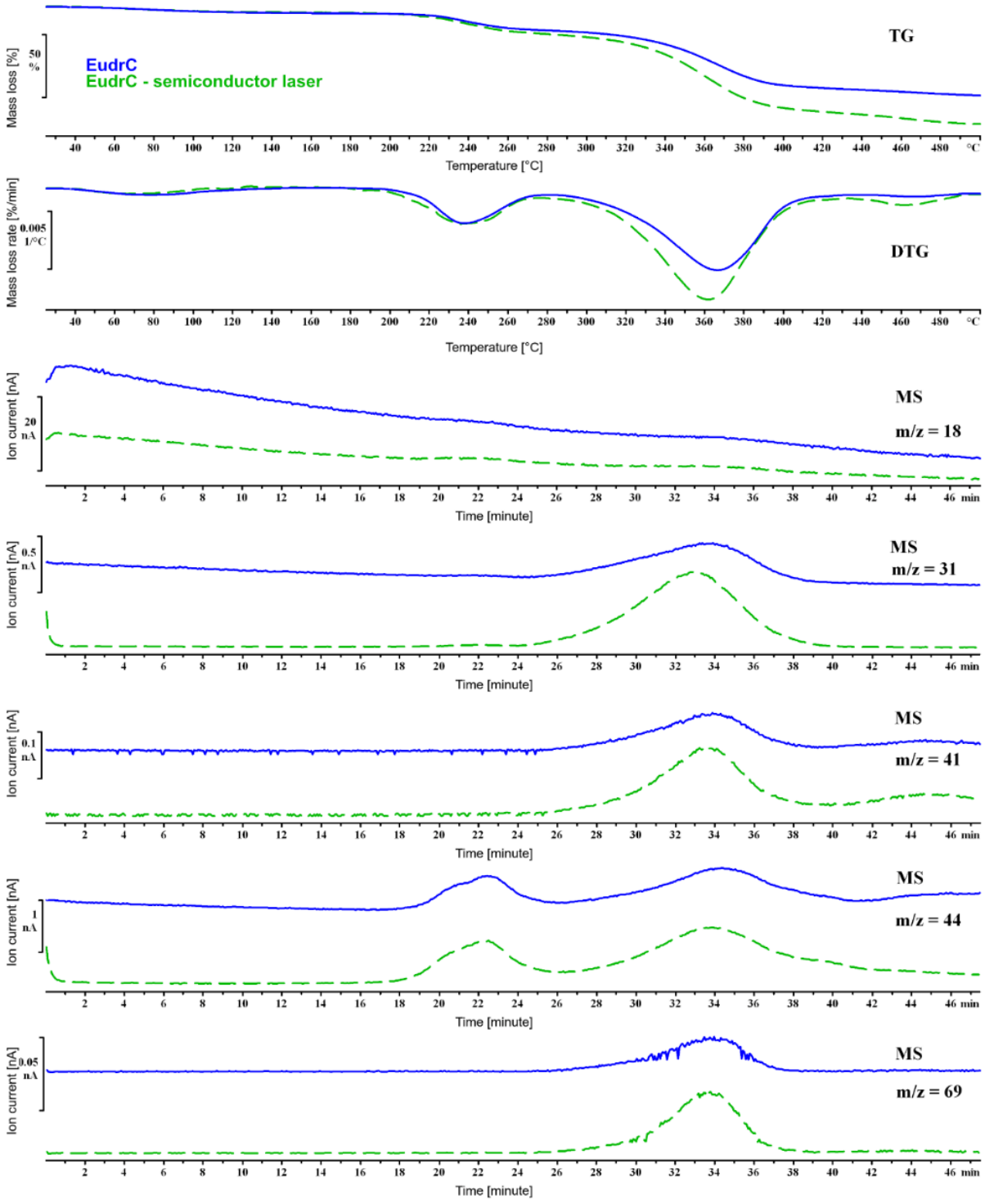

Fig. 32. TG, DTG and MS curves of EudrC film , and EudrC film treated with SC laser.

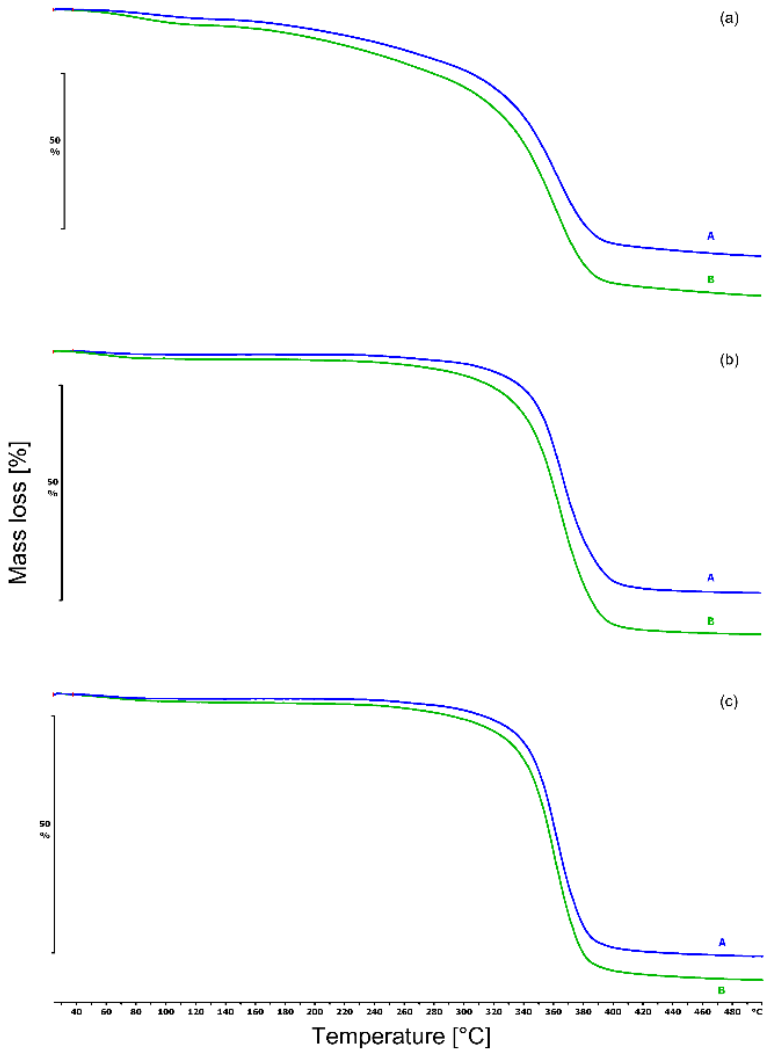

Fig. 33. TG curves of Sepifilm films treated with SC laser. (a): SNC-P, (b): SPW-W, (c): SPW-R (A – original, B – SC laser treated).

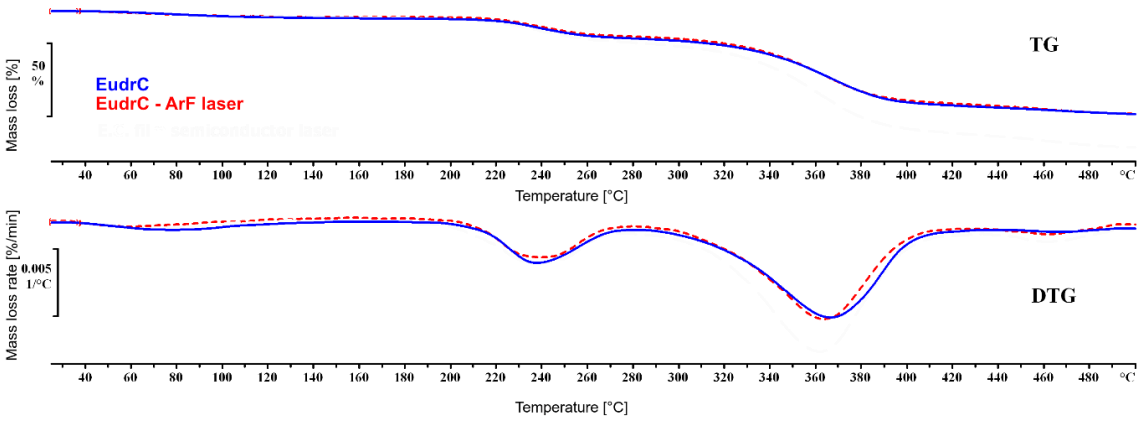

Fig. 34. TG and DTG curves of EudrC film , and EudrC film treated with ArF laser.

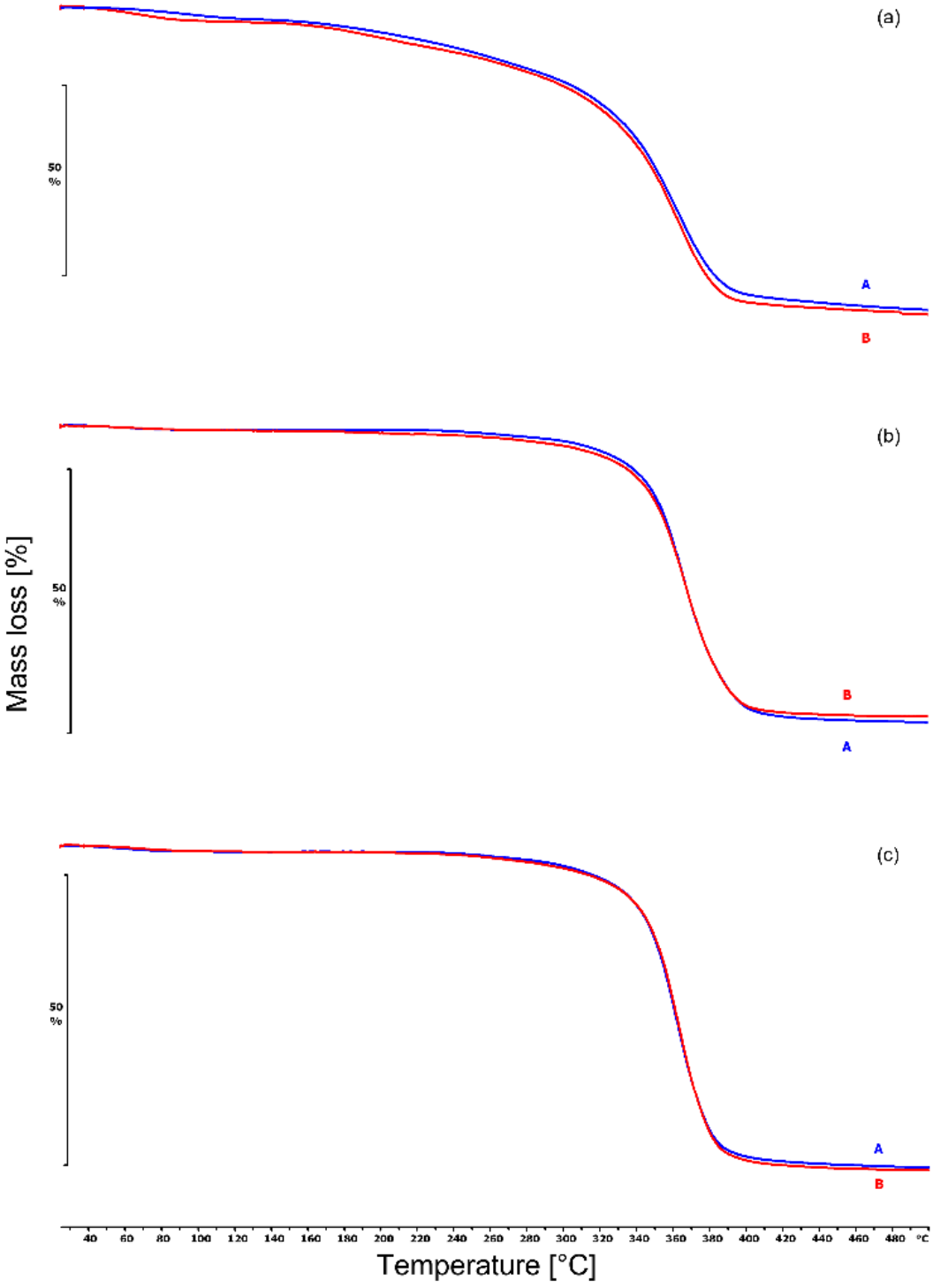

Fig. 35. TG curves of a raw Sepifilm coating, and the films treated with ArF laser. (a): SNC-P, (b): SPW-W, (c): SPW-R (A: original, B: ArF laser treated).

European Journal of Pharmaceutical Sciences 123 (2018) 1–9

Contents lists available at ScienceDirect

European Journal of Pharmaceutical Sciences

journal homepage: www.elsevier.com/locate/ejps

Unique laser coding technology to fight falsified medicines

K. Ludasi[a], T. Sovány[a], O. Laczkovich[a], B. Hopp[c], T. Smausz[b,c], G. Regdon Jr.[a,*]

[a] Institute of Pharmaceutical Technology and Regulatory Affairs, University of Szeged, Eötvös utca 6, 6720 Szeged, Hungary
[b] MTA-SZTE Research Group on Photoacoustic Spectroscopy, University of Szeged, Dóm tér 9, 6720 Szeged, Hungary
[c] Department of Optics and Quantum Electronics, University of Szeged, Dóm tér 9, 6720 Szeged, Hungary

ARTICLE INFO

Keywords:
Falsified medicines
Identification
Anti-counterfeiting
Laser marking
Unique laser coding
Safety

ABSTRACT

Based on WHO statistics, counterfeit medicines represent 10% of the global drug trade. According to Directive 2011/62/EU as regards the prevention of falsified medicines from entering into the legal supply chain, a unique identification should be put on each box of drugs to be able to track and trace them. The objective of this study is to develop a technology to mark an individual traceability code directly on the surface of the tablet. By using this technique, anyone with a camera-enabled phone and a suitable application installed should be able to authenticate these drugs. By marking the medicine's surface, patients could be protected from fake drugs.

The aim of the present work was to study how different types of lasers affect the film coating of the tablet during the laser marking intervention.

To sum up, the present findings may contribute to efficient and reliable laser marking solutions in the unique identification procedure. Based on our measurement results, it can be stated that the excimer UV laser is clearly the most suitable marking instrument for anti-counterfeiting coding on solid coated tablet form as this caused the least amount of chemical degradation of the polymer film.

1. Introduction

In the interest of avoiding misunderstanding, it is important to remark that the expression counterfeit medicine used in this article comprises the WHO's definitions for **substandard** (authorized medical products that fail to meet either their quality standards or specifications, or both), **unregistered** (that have not undergone approval by the National or Regional Regulatory Authority for the market in which they are distributed), and **falsified** (that deliberately misrepresent their identity, composition or source) medical products (WHO, 2018).

Counterfeit drugs pose a great threat for health and they cause serious social and economic damage. Based on WHO statistics, it is estimated that 1 in 10 medical products is substandard or falsified in low- and middle-income countries where health systems are weak or non-existent (WHO, 2018). The most frequently falsified medicines in wealthy countries were lifestyle medicines, such as hormones, steroids and antihistamines. In developing countries, they included medicines used to treat life-threatening conditions such as malaria, tuberculosis and HIV/AIDS (European Medicines Agency, 2018).

It is threatening that medicines purchased over the Internet from sites that conceal their actual physical address are counterfeit in over 50% of cases (UNICRI, 2012; WHO IMPACT, 2006).

A culture of self-diagnosis and self-prescribing has led to the emergence of thousands of unregulated websites providing unsupervised access to substandard and falsified medical products. Unregulated websites, social media platforms, and smartphone applications can also be direct conduits of counterfeit medical products (WHO, 2018). Patients across the world put their health, even life, at risk by unknowingly consuming fake drugs or genuine drugs that have been badly stored or that have expired (Interpol, 2013).

Responsible governments prohibit falsified medicines under national law but remain vulnerable to organized criminals doing business in countries where laws or enforcement are lax—30% of countries have little or no medicine regulation according to WHO (Attaran et al., 2012).

Globally, there are around 30,000–35,000 online pharmacies. 96% of these operate illegally. They do not comply with regulatory and safety requirements and they may sell prescription drugs without a valid prescription. On average, 20 online pharmacy websites are created each day (CSIP, 2016).

Falsified medicines in the legal supply chain are less prevalent in the EU, but this trend seems to be on the rise. 2 cases reported in 2012 vs. 12 in 2013 and 15 in 2014 (European Commission Staff Working Document, 2015). For example, in 2014 falsified vials of the cancer treatment Herceptin (trastuzumab) were stolen in Italy, manipulated and later reintroduced illegally into the legal supply chain in some

* Corresponding author.
E-mail address: geza.regdon@pharm.u-szeged.hu (G. Regdon).

https://doi.org/10.1016/j.ejps.2018.07.023
Received 15 March 2018; Received in revised form 18 June 2018; Accepted 9 July 2018
Available online 12 July 2018
0928-0987/

countries (European Medicines Agency, 2014; Sukkar, 2014).

A European Union Intellectual Property Office (EUIPO) report shows that fake medicines cost the EU pharmaceutical sector EUR 10.2 billion (4.4% of sales) each year. This is a direct estimate of sales lost by legitimate manufacturers and wholesalers of medicines in the EU due to counterfeiting. Moreover, 37,700 jobs and EUR 1.7 billion of government revenue are lost annually (household income taxes, social security contributions and corporate income taxes) (Wajsman et al., 2016).

The links between drug counterfeiting and other forms of crime are proven both by the methods used and the nature of the products that are regularly seized. Counterfeiting is a world-wide problem. Traffickers have a single motivation: extreme profitability. In the study report written by Eric Przyswa he has given an example: according to the International Federation of Pharmaceutical Manufacturers and Associations (IFPMA), for $1000 invested, the trafficking of counterfeit currency or of heroin would bring a return of $20,000, of counterfeit cigarettes $43,000, and in the case of counterfeit drugs, the return would be between $200,000 and $450,000. Counterfeit drugs would therefore be 10 to 25 times more profitable than the trafficking of narcotics. The major distribution vehicle is the Internet, which is decentralized and anonymous. The malleability and permanent interconnection of networks seem to offer genuine opportunities for illicit trafficking. (A Royal Pharmaceutical Society Publication, 2014; IRACM, 2013; Przyswa, 2013).

According to Directive 2011/62/EU as regards the prevention of falsified medicines from entering into the legal supply chain, a unique identification should be put on each box of drugs (The European Parliament and the Council of the European Union, 2011). The new Delegated Regulation 161/2016/EU shall enter into force from 9 February 2019, which, besides serialization requirements, demands additional anti-tampering devices for drug packaging. In Europe pharmaceutical manufacturers who distribute their products must, in the future, assign prescription medications with a serial code as a unique identification feature, save this serial number and transfer it to a Europe-wide database under the tightest security requirements. The security code specified by the EU is a 2D data matrix code that ensures traceability along the entire supply chain (European Comission, 2016).

Our team would like to extend this process by working on the development of a technology to mark an individual traceability code directly on the surface of the tablet. Anyone with a camera-enabled phone and a suitable application installed on it should be able to authenticate these drugs. Also, as in certain Member States the persons authorized or entitled to supply medicinal products to the public are allowed to open a pack of a medicinal product in order to supply part of that pack to the public, it is necessary to verify those drugs in question, too (A Royal Pharmaceutical Society Publication, 2017; European Comission, 2016). We plan that our development with on-product marking would help to verify each pill even in the absence of original packaging.

The ideal mark for medical applications is indelible, easy to read, difficult to copy or alter, contains unique serialization information, and does not change product functionality in any way (Heller, 2015).

Film coating is used in the pharmaceutical industry for solid dosage form because of visual attractiveness, trade marking issues, identifying, taste masking, improved product stability, shelf life increase or controlled release of the active pharmaceutical ingredient (API) (Koller et al., 2011; Korasa et al., 2016; Markl et al., 2014). Besides the above, colored coatings can also help to prevent counterfeiting. Since most of the tablets are round and white and, consequently, easier to fake, a unique and distinctive shape and color can improve identification and make counterfeiting more difficult (Pérez-Ibarbia et al., 2016).

Coloring and special shape are not enough to distinguish each tablet from one another. Further marking is necessary, especially for unique identification.

From among many different options, printing is one of the most attractive methods for marking as the capital equipment cost is relatively low. However, the printing process necessitates contact between the substrate and some form of ink carrier, toner reservoir, or stamp, so it could be a source of contamination. High printing speed is required for some of the fastest production lines and that can result in a loss of image quality and the risk of unreadable codes (Davison, 2011). Furthermore, the ink formulation has to be designed with respect to its viscosity and surface tension to guarantee continuous printing and high reproducibility of the forming droplets (Genina et al., 2012). In addition, chemical markers or colorants that are used on the surface of the dosage form must be materials that are tested and accepted as safe by the pharmaceutical authorities (Davison, 2011).

One of the other ways of marking could be done with infrared (IR) laser. It produces a surface mark through intense localized heating and it could cause damage in heat-sensitive materials (Gaebler, 2017).

Ultraviolet (UV) lasers overcome the drawbacks of the above-mentioned ink printing and IR laser printing technologies. UV laser marking is a non-contact method that avoids the problems of contamination and eliminates the cost of consumables. It undergoes a cold photochemical, rather than photothermal interaction. Since this is a cold process, there is essentially no Heat Affected Zone (HAZ) or changes to the surrounding material. Finally, since UV light can be more tightly focused than IR, UV lasers support complex, high-resolution marks such as 2D barcodes.

In the past UV lasers were rarely utilized because of their cost. However, over the past decade, companies reduced UV laser price by a factor of nearly five over this period (Heller, 2015).

The final aim of the present work is to develop a technology to mark an individual traceability code directly on the tablet. The plan is to make 2 layers of coatings on the surface. The first one is the functional one, and the other on the top of it would be applied because of the marking. The colors of the 2 coatings should contrast each other. By ablating the upper coating, we should be able to read the 2D data matrix code that will be formed of those two layers. The basic experiment for this article started with only one layer. We examined how the coated film behaves when it is treated with 3 different types of laser to be able to select the right instrument for further research. With excimer UV laser we made a square shape ablation for a start, which we plan to replace in the future with 2D code forming mask. With semiconductor laser we were able to mark a 2D barcode on the surface of the tablet. Unfortunately, the pulsed Nd:YAG laser damaged the coating film. By analytical quality tests, we were planning to select the right instrument for unique drug marking.

This investigation suggests the use of excimer UV laser for marking the tablet surface because this treatment minimizes the chemical degradation of the coating film during the process.

2. Materials and methods

2.1. Materials

2.1.1. Tablet core and coating materials

Tablet samples for laser marking preformulation were original tablets from the legal supply chain: Sinecod (GSK), Telfast (Sanofi), Klacid (Abbott), furthermore Eudraguard® control and HPMC coated placebo tablets.

In the further research round placebo tablets were used, with no break line (diameter: 7 mm, crown height: 4 mm). Aqueous-based enteric coating solution was prepared. It consisted of 52% w/w dry substance of a neutral copolymer based on ethyl acrylate and methyl methacrylate with a ratio of 2:1 (Eudraguard® control dispersion 30% w/w (Evonik Nutrition & Care GmbH)), 16% w/w talc, 28% w/w alginic acid sodium salt, 4% w/w glycerol, and distilled water. Coatings were colored with 1% w/w patent blau 85 (blue), 3% w/w Gelborange (orange), 1.5% w/w Azorubin (cherry) or 1.5% w/w Iron Oxide Red (red).

Table 1
Coating parameters of placebo tablets.

Step	Inlet-air temperature (°C)	Exhaust-air temperature (°C)	Tablet bed temperature (°C)	Drum speed (rpm)	Air flow rate (m^3/min)
Warm up	50		Until 30	5	0.50
Coating	49 ± 2	32	30 ± 2	18	0.50
Drying & cooling	40	27	25	5	0.50

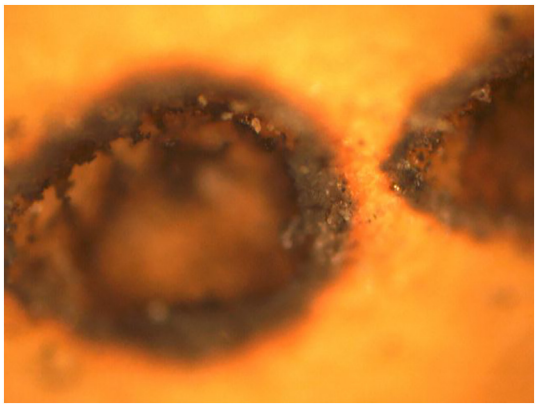

Fig. 1. Coated tablet treated by Nd:YAG laser.

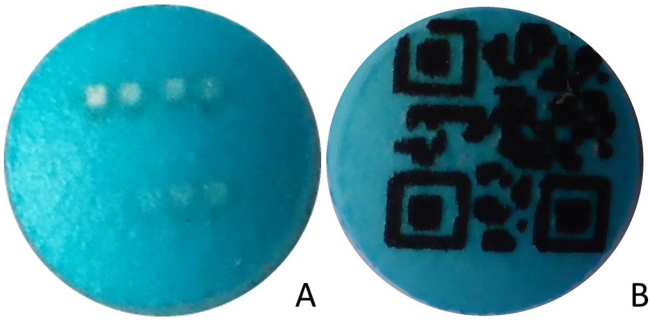

Fig. 2. Coated tablet treated with excimer laser: from bottom line left: 10, 20, 30, 40, upper line from right: 50, 60, 70, 80 impulses (A) and coated tablet treated with semiconductor laser (B).

2.2. Methods

2.2.1. Tablet coating procedure

The spray coating process was performed using a 4M8 Pancoat (Pro-C-epT, Zelzate, Belgium) perforated coating pan on a batch of 500 g tablet. The process was divided into three stages. The coating parameters are shown in Table 1. For the application of the atomized spray coating solution, 0.8 mm spray nozzle was used for 140 min, with an atomizing air pressure of 1.5 bars and an air flow rate of 0.50 m^3/min. The drying and cooling processes together lasted for 30 min.

The final coating thickness was determined by Zeiss Stereomicroscope. Measurements were performed at a magnification of 500. After calibration, we examined 4–4 half-cut tablets (differently colored), each at 10 places. Coating thickness averages measured on different tablets are: yellow: 60.79 ± 9.11 µm, blue: 59.31 ± 11.82 µm, cherry: 49.19 ± 10.18 µm and red: 88.02 ± 18.98 µm.

2.2.2. Irradiation of tablets using 3 types of laser

The coated tablets were irradiated with a pulsed Lambda Physik EMG 201 type ArF excimer laser (wavelength: 193 nm, energy: 3 ± 0.2 mJ, fluence: 444 mJ/cm^2, FWHM: 20 ns, spot size: 375 µm), CW (continuous wave) semiconductor laser (wavelength: 405 nm, spot size: 73 µm, power: 1000 mW, irradiation time: 15–20 ms) and pulsed Nd:YAG laser (wavelength: 1064, power: 1–2.6 W, frequency: 1 kHz).

2.2.3. Surface profilometer

Profilometry measurements were performed on a Veeco, Dektak 8 Advanced Development Profiler®. The tips employed had a radius of curvature ~2.5 µm, and the force applied to the surface during scanning was ~30 µN. The horizontal resolution was 0.1–0.13 µm. The vertical resolution was 40 Å.

Data has been evaluated by Dektak software (Microsoft® Windows XP®: interactive data acquisition) and Vision® 32 software (data processing, 2-D and 3-D image analysis) (Veeco Instruments Inc., New York, USA).

2.2.4. Scanning electron microscope (SEM)

The morphology of the ablated film was observed by using a scanning electron microscope (SEM, Hitachi Tokyo, Japan S4700). The tablets were stuck to a double-sided carbon adhesive tape and a conductive golden layer was deployed with the use a sputter apparatus (Polaron Ltd., UK). The measurements were performed at a magnification of 100–2000, applying 10.0 kV of electron energy and 1.3–13 MPa of air pressure.

2.2.5. Raman spectra

In our method, the effect of laser light was analyzed by Raman surface mapping. To investigate the components, Raman spectra were

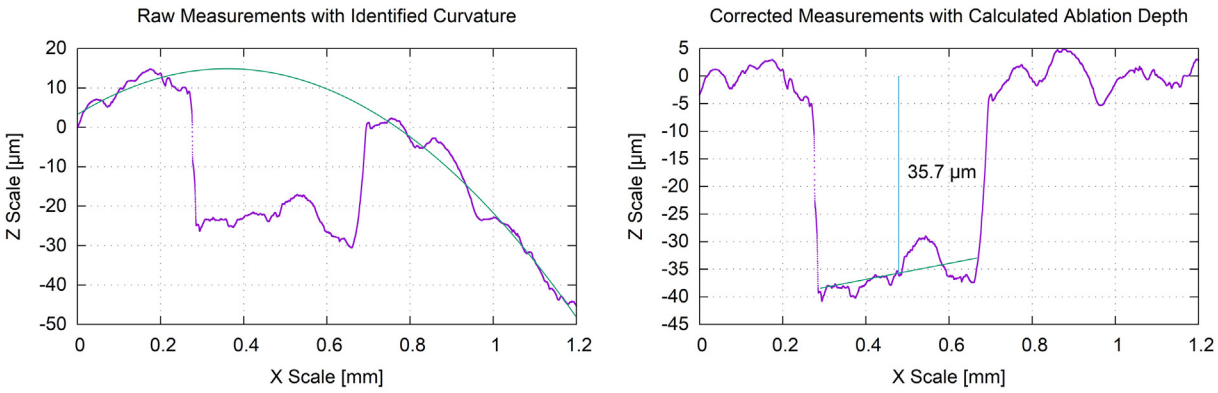

Fig. 3. The ablation depth calculation process.

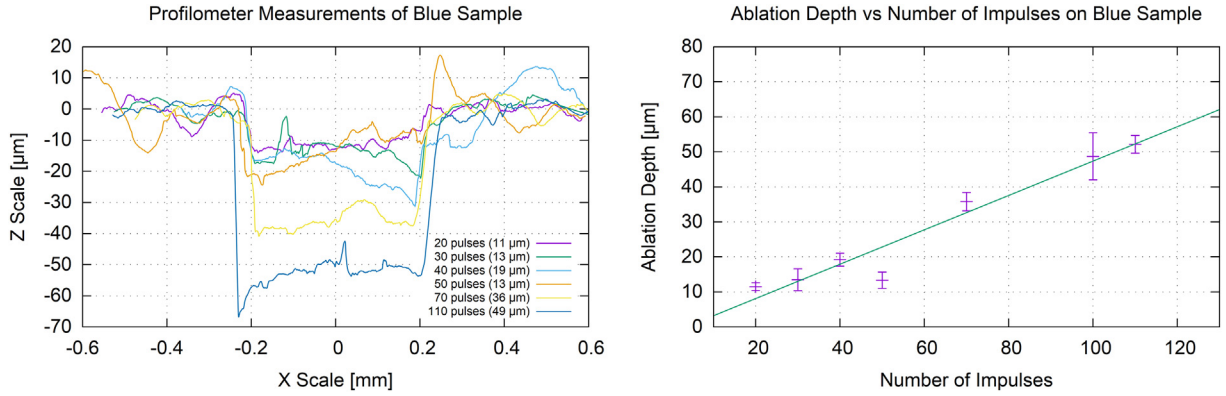

Fig. 4. The profilometer analysis of the ablated holes. (For interpretation of the references to color in this figure, the reader is referred to the web version of this article.)

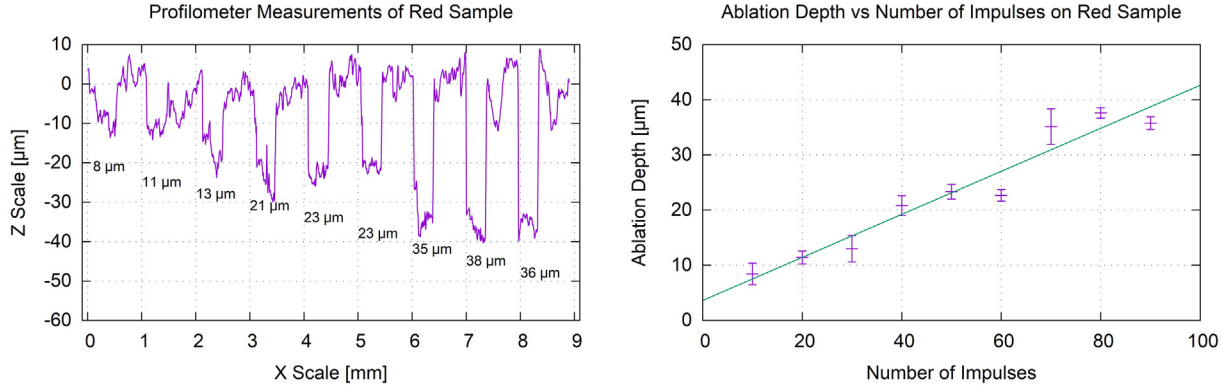

Fig. 5. The profilometer analysis of the red tablet surface.

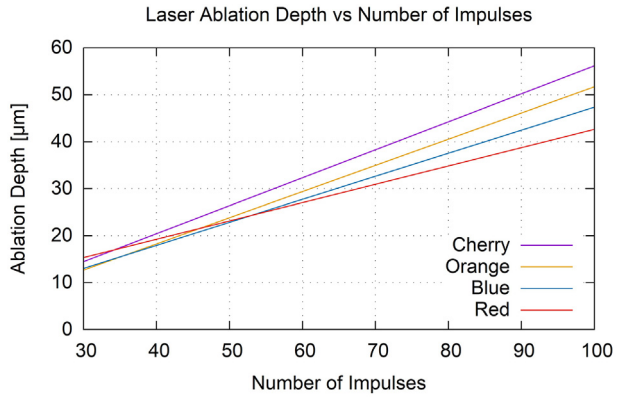

Fig. 6. Comparison of the measurements of the ablated hole depth of tablets with different colors. (For interpretation of the references to color in this figure legend, the reader is referred to the web version of this article.)

acquired with a Thermo Fisher DXR Dispersive Raman (Thermo Fisher Sco. Inc., Waltham, MA, USA) equipped with a CCD camera and a diode laser operating at a wavelength of 780 nm. Raman measurements were carried out with a laser power of 6 and 24 mW at 25 µm slit aperture size on a 2 µm spot size. The spectra of the individual substances were collected using an exposure time of 6 s, a total of 48 scans in the spectral range of 1700–200 cm^{-1} with cosmic ray and fluorescence corrections.

2.2.6. Thermal gravimetric analysis (TGA)

The thermal gravimetric analysis of the samples was carried out with a Mettler-Toledo TGA/DSC1 instrument (Mettler-Toledo GmbH, Switzerland). The start temperature was 25 °C, the end temperature was 500 °C, the applied heating rate was 10 °C/minute. Nitrogen atmosphere was used (Cell gas: 50 ml/min, method gas: 70 ml/min). 5 ± 1 mg samples were measured into aluminum pans (40 µl). The TG curves were evaluated with Mettler-Toledo STAR^e Software.

2.2.7. Mass spectrometry (MS)

The gas analysis of the tablet coating material was carried out with the Thermo Star (Pfeiffer Vacuum, model ThermostarTM GSD 320, Germany) quadruple mass spectrometer (maximum 300 amu) for gas analysis that was coupled to the TG instrument. The measurements were carried out in a flow of nitrogen atmosphere. The connection between the TG and the mass spectrometer was made by means of a silica capillary, which was maintained at 120 °C. Ions with various mass numbers were determined with the SEM MID measurement module of the Quadera software. Continuous recordings of sample temperature and sample mass were performed. The obtained results were exported and then plotted in one coordinate system with the TG curves using the Mettler-Toledo STAR^e software.

3. Results and discussion

Coated tablets were marked with 3 different types of lasers. After marking polymer films, we made an analytical quality control of them to check if there occurred any change during the laser intervention.

Since the Nd:YAG laser treatment burned the tablet's coating during the preformulation study, that tool was not a part of our further research. The treatment result is presented in Fig. 1.

3.1. Examination of tablet surface

Firstly, film coted tablets were treated by excimer laser with 10, 20, 30, 40, 50, 60, 70 and 80 pulses, which is seen in Fig. 2, Part A. The

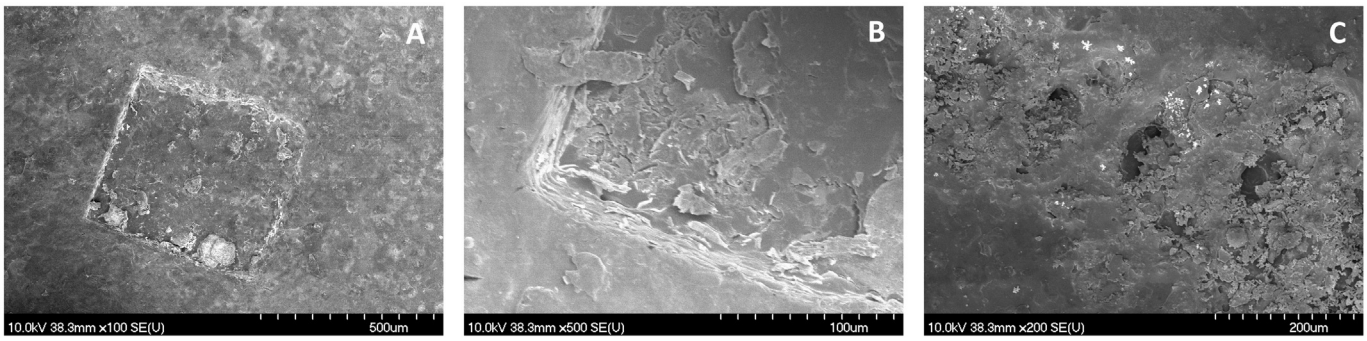

Fig. 7. The SEM micrograph of excimer laser treated film (magnification of 100×: A, magnification of 500×: B) and semiconductor laser treated film (magnification of 200×: C).

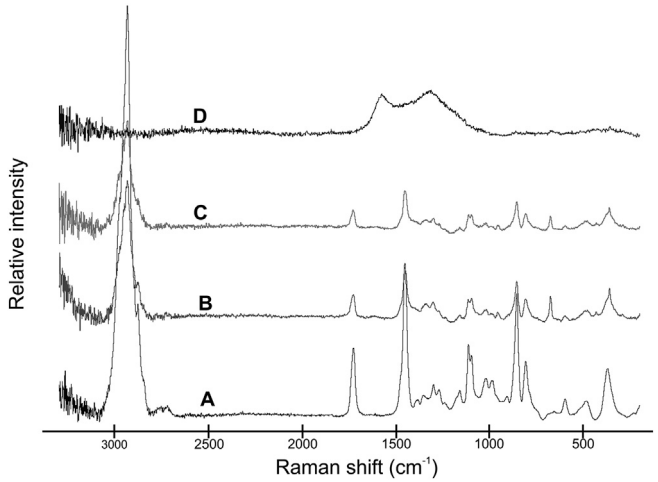

Fig. 8. Raman spectra of film coatings (A: Eudraguard® control dispersion, B: prepared free film of Eudraguard® control, C: prepared free film of Eudraguard® control treated by excimer laser, D: prepared free film of Eudraguard® control treated by excimer semiconductor laser).

holes have a shape of a regular square, sharply separated from the environment, returning the shape of the mask used. Secondly, coated tablets were treated by semiconductor laser. With this instrument we were able to mark a two-dimensional QR code on tablets. The photograph of it can be seen in Fig. 2, Part B. It shows that the laser beam blackened the coating. Factors changing the color of the coating by the semiconductor laser irradiation were not cleared.

The ablated holes of the excimer laser were examined by a surface profilometer and their extent was measured. Also, the influence of the differently colored coatings on the ablative depth was examined.

The results of profilometer were evaluated as follows: the raw data were detrended by fitting the second order polynomial to the region not affected by laser treatment (Fig. 3). This correction was applied to the data in order to eliminate the tablet curvature effect. The obtained data was used to calculate the ablation depth by fitting a line to the points in the ablation hole. The distance of the line segment's center point from zero level was assumed as the average ablation depth (Fig. 3).

The results of the ablations on the blue colored tablet are shown in Fig. 4. The curves in the left figure show the deepness of the holes made by different numbers of laser pulses. The measurements and the fitted line in the right figure show near lineal relation between the applied number of impulses and ablation depth up to 100 impulses.

The series of the ablated holes were examined with a full profilometer scan on the red tablet surface (Fig. 5). The tablet coating was treated by excimer laser using 10, 20, 30, 40, 50, 60, 70, 80, 90 impulses. The ablation depths were also calculated by extracting the affected regions from the dataset. The aggregated data show a similar linear relation between the applied number of impulses and ablation depth as was determined in the case of other colors.

We found some influence of the different colors on the ablation depth (Fig. 6). The quantitative analysis of this effect needs more profilometer and optical property measurements. The weighted average of the ablation performance is 0.411 ± 0.025 μm/impulse using 2.8–3.2 mJ impulses in Eudraguard® control film.

3.2. Scanning electron microscope

The pre- and post-laser structure was examined by SEM as well. In Fig. 7, Parts A, B the micrographs of the film treated with excimer laser can be seen. They show the same ablation square at different magnifications. It is seen that the ablated surface of the sample exhibits no large destructions, the structure of the film is relatively intact. The

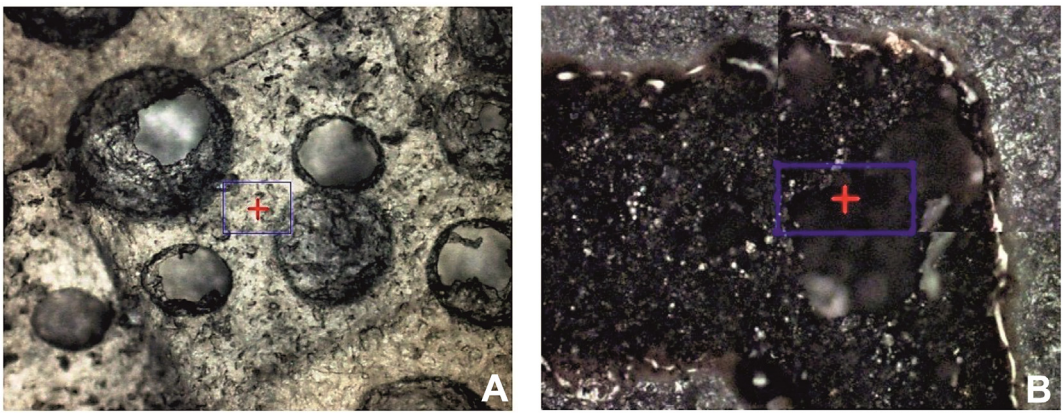

Fig. 9. Microscopic picture of films treated by excimer laser (A) and treated by semiconductor laser (B).

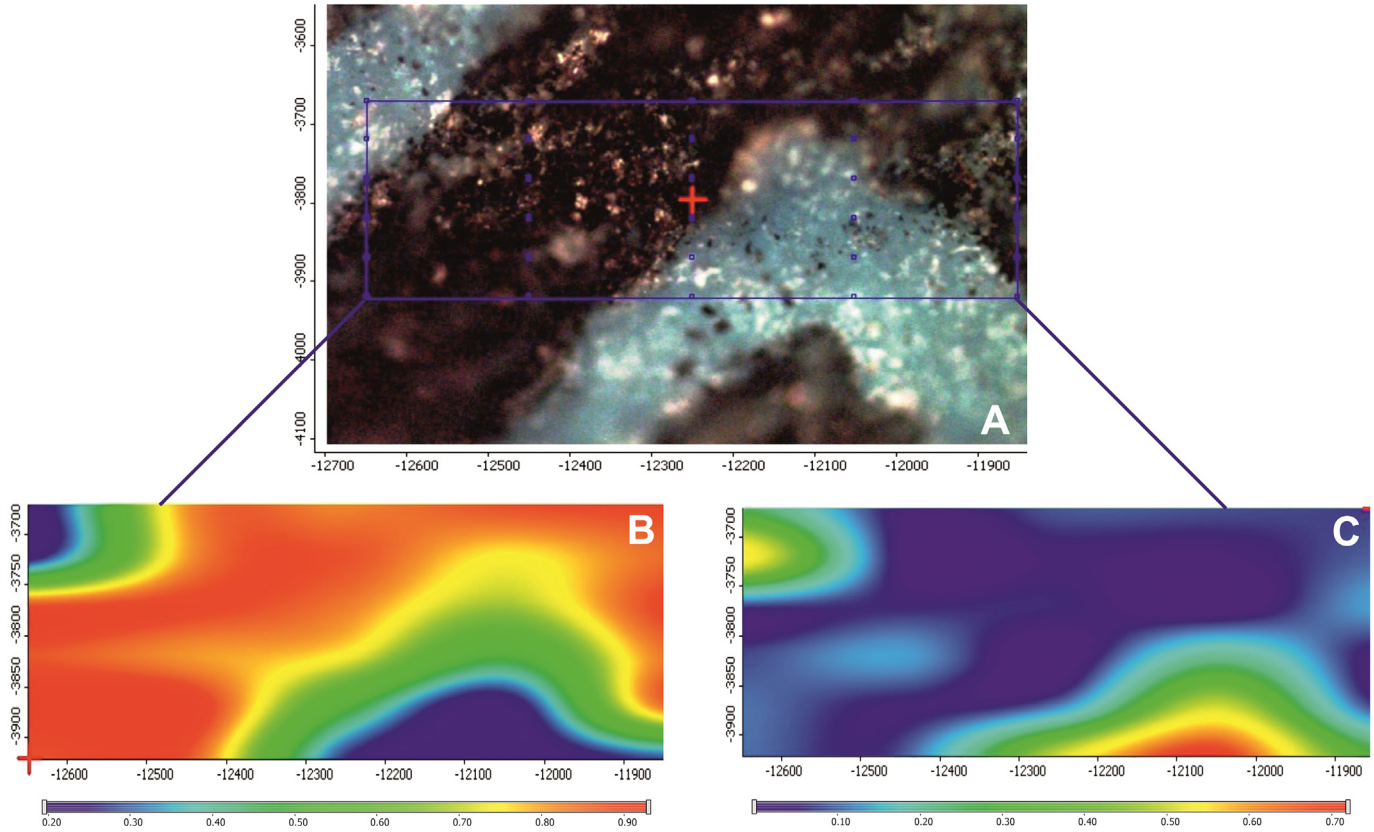

Fig. 10. Microscopic picture of film treated by semiconductor laser (A), chemical maps profiled to special changed area of spectra which was treated by semiconductor laser (B), chemical maps profiled to untreated Raman spectra of film coating (C). (For interpretation of the references to color in this figure legend, the reader is referred to the web version of this article.)

Table 2
Decomposition behavior of the raw polymer film and the film treated by laser.

TG-DTG data	Eudraguard® control film	Eudraguard® control film treated with excimer laser	Eudraguard® control film treated with semiconductor laser
First step			
Thermal range (°C)	30–120	30–120	30–120
Mass loss (%)	4.31	3.90	4.12
Normalized integral (s/°C)	−0.11	−90.41e-03	−0.13
Peak (°C)	72.83	57.03	64.65
Second step			
Thermal range (°C)	120–290	120–290	120–290
Mass loss (%)	15.03	14.28	18.75
Normalized integral (s/°C)	−0.57	−0.59	−0.60
Peak (°C)	232.99	233.74	230.66
Third step			
Thermal range (°C)	290–500	290–500	290–500
Mass loss (%)	50.59	51.88	69.96
Normalized integral (s/°C)	−2.12	−2.12	−2.79
Peak (°C)	362.78	360.07	358.40

shape of the hole is a well distinguished regular square, returning the shape of the mask used. It is clearly visible at the edge of the ablative pit that the film has a layered texture due to the drying of droplets during the coating procedure. It looks as if these layers came off one after another in accordance with the number of laser impulses used. Despite the lack of bigger destructions, there are some cracks in the affected area, which may be the result of loss of water caused by the local temperature elevation or by a photocatalytic reaction.

Part C of Fig. 7 shows that, in contrast with the excimer laser, the semiconductor laser induced considerable damage in the coating structure during the treatment. Holes are seen in every 200 µm on the film, surrounded by a wide range of burn traces. There are blistering, snow-flake like crystals around the holes, melting, and recrystallization. It is unclear whether these are the results of a consequential loss of water or the melting of the coating material.

The changes described above were observed macroscopically. In the following, the chemical structure degradation was analyzed by Raman and TG-MS analytical tests.

3.3. Raman investigations

Raman spectroscopy is a promising analytical method to monitor the preparation process and to implement the PAT requirements. In this article, a Dispersive Raman spectrometer was used to detect the effect

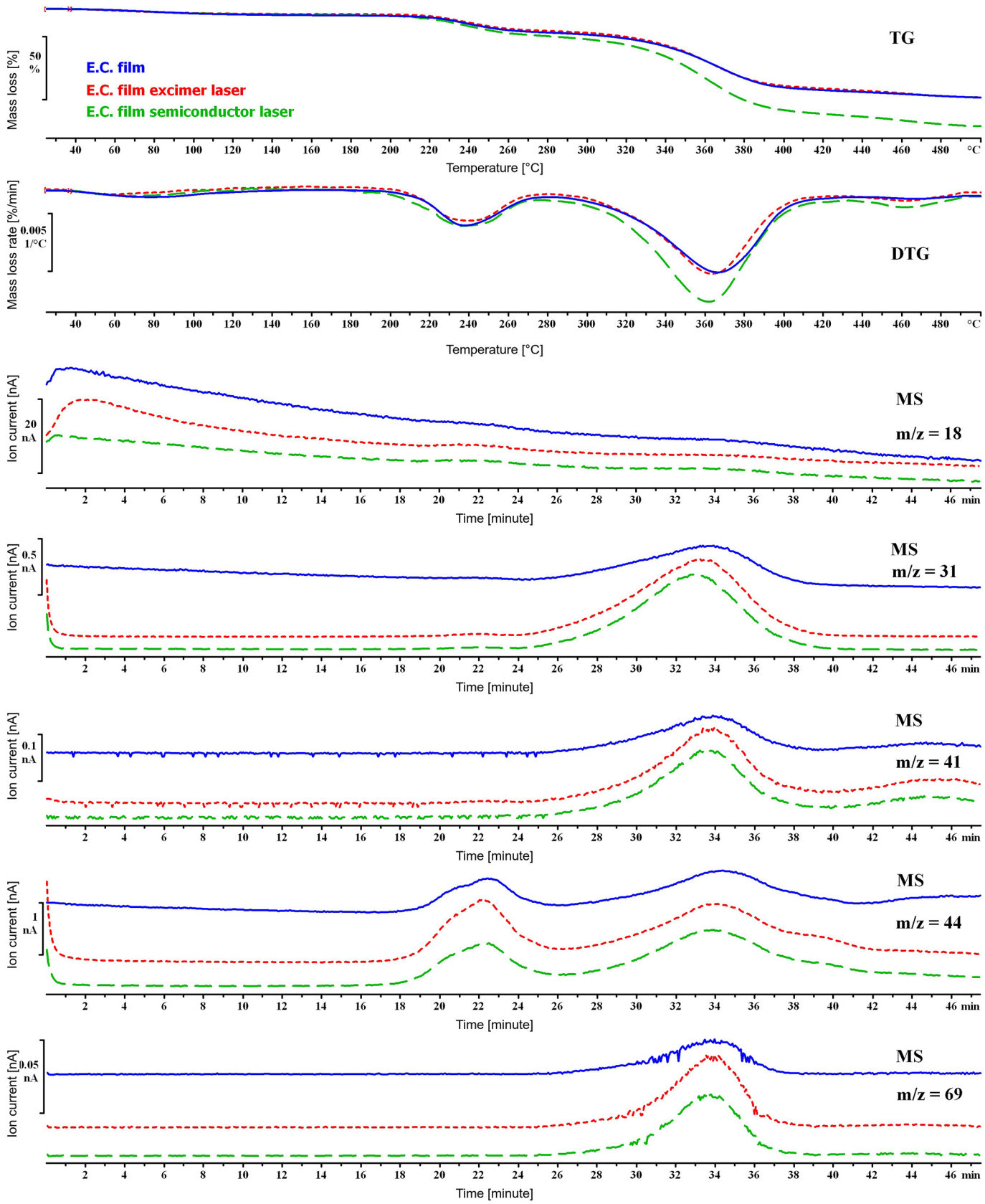

Fig. 11. TG, DTG and MS curves of Eudraguard® control film (E.C. film), Eudraguard® control film treated with excimer laser (E.C. film excimer laser), Eudraguard® control film treated with semiconductor laser (E.C. film semiconductor laser).

of different laser sources on the surface of coated tablets. Raman spectroscopy is used for the non-invasive and fast, qualitative investigation of pharmaceutical dosage forms.

To investigate the effect of different laser sources on film coating, we used Raman spectroscopy. The finger print region of Eudraguard® control is 1800 cm^{-1}–500 cm^{-1}. In Fig. 8 we summarized the spectra of raw film dispersion, raw free film and films treated by different laser sources. The spectra of the film treated by semiconductor laser changed completely, the fingerprint region of Eudraguard® control smoothed. The result of this laser treatment, black burst signal, is seen in the microscopic picture (Fig. 9, Part B). The square shaped 'print' on the surface of the film returned the shape of the mask used after the excimer laser ablation (Fig. 9, Part A).

To confirm the chemical degradation of the film polymer, Raman chemical mapping was chosen. We selected an area treated by semiconductor laser which contained burst and intact film, too. The microscopic mosaic photo is presented in Part A of Fig. 10. The area framed with blue lines is the chemically mapped part. The spectra were determined in the blue points. Then this chemical map was profiled to the special changed area of the spectra which was treated by semiconductor laser (1800 cm^{-1}–500 cm^{-1}). The warm colors show the area which contains these spectra (Part B of Fig. 10). Then the chemical map was profiled to the untreated Raman spectra of the film coating (Part C of Fig. 10). In this picture the warm colors show the original (raw) intact film. This picture is the inverse of Part B of Fig. 10. So, we have concluded that chemical changes were caused by the semiconductor laser source.

3.4. Thermal gravimetric analysis (TGA)

TGA is a method of thermal analysis which provides curves corresponding to mass loss characteristics. As the measured substance degrades, basic information is given about their behavior during temperature rise. Data from mass reduction through this system alone does not allow classification of the molecules.

The burning characteristics of samples obtained from thermogravimetric analysis may be used to effectively compare the decomposition characteristics of the raw polymer film and films treated by different laser beams.

Table 2 shows TG temperature ranges, mass loss, DTG normalized integral of examined materials and peak temperatures. The main characteristics of the samples derived from TG curves as corresponding mass loss values were used to define the thermal behavior and combustion characteristics of films.

It is seen that mass loss in coating films comes in three stages. The first mass loss occurred between 30 and 120 °C, the second stage between 120 and 290 °C, and the third between 290 and 500 °C. Thermogravimetry showed that the decomposition of the material occurred sooner in films marked by semiconductor laser, in higher temperature ranges, which is probably due to the decomposition process that had already started during the laser marking process. We did not experience anything like this in the case of using excimer laser.

3.5. Evolved gas analysis with mass spectrometry

To clarify the decomposition mechanism of the films, the mass loss should be characterized during each decomposition process by the identified evolution of gas components. The mass spectra were interpreted on the basis of degassing profiles of the molecule ions and ion fragments of various gases.

The evolution of released gas species was followed in situ by the coupled system of TG-MS instruments. The evolution curves are shown as current ion versus time curves. The characterization of water release by means of MS is possible with the molecule H_2O, $m/z = 18$, (peak at 50 °C). It can be safely concluded from Fig. 11 that water is given out at about 50 °C from the samples, which is consistent with the mass loss observed from the TG curves. The dehydration of the film takes place at around this temperature.

An important increase in the concentration of methyl methacrylate is recorded for $m/z = 41$ and for $m/z = 69$ due to the decomposition of the polymer at temperatures at around 360 °C. The abundance of the $m/z = 41$ and $m/z = 69$ signals vs. temperature can be seen in Fig. 11. The $m/z = 69$ signal corresponds to the monomer after the loss of $-OCH_3$ from the side chain, and the $m/z = 41$ signal corresponds to the monomer after the loss of the entire side chain ($-COOCH_3$).

The evolution of gas of CO_2, $m/z = 44$ signal was detected in two steps at slightly higher temperatures around 240 °C and 365–370 °C, as it is seen on the MS curves in Fig. 11.

The release of ethanol, $m/z = 31$ by means of MS curves seen in Fig. 11, happens at a temperature around 355 °C.

The results of mass spectroscopy are consistent with the mass loss observed from the TG curves, as the decomposition of the material occurred slightly sooner in the film treated with semiconductor laser in the case of $m/z = 44$ and $m/z = 69$, where the decomposition started sooner as the deacylation had taken place earlier during the laser treatment.

Also, there were other gases evolved from the treated material, which are under examination for the interpretation of further mass loss difference seen in the TG curves of the original film compared to the films treated by lasers.

4. Conclusions

Anti-counterfeiting unique laser marking of the tablet surface operation was investigated in this article.

It was found that from among the three types of coding instruments examined, excimer laser ablation did not cause a qualitative change in the material during laser marking.

In this study we examined how the depth of ablation can be controlled by changing only the number of impulses delivered by excimer laser. We found that the correlation is completely linear. We were able to ablate even 100 μm deep in the coating, so it is possible to trim the outer layer even if it is that thick.

Raman spectroscopy is becoming one of the most widely used and applicative approaches for analyzing pharmaceutical materials. It was shown that Raman was capable of distinguishing films treated by different laser sources. We have concluded that chemical changes were caused by semiconductor laser source compared to the original film, and the film treated by excimer laser.

The main finding of the TG measurement showed that the decomposition of the material occurred sooner in films marked by semiconductor laser, in higher temperature ranges, which is probably due to the decomposition process that had already started during the laser marking intervention. We did not experience anything like this in the case of using excimer laser.

Based on our measurement results, it can be stated that the excimer UV laser is clearly the most suitable marking instrument for anti-counterfeiting coding on solid coated tablet form.

Acknowledgements

I would like to thank Evonik Industries AG for providing the polymers.

This research did not receive any specific grant from funding agencies in the public, commercial, or not-for-profit sectors.

References

A Royal Pharmaceutical Society Publication, 2014. Pharmaceutical industry fights back against counterfeit medicines. Pharm. J. 292, 392. https://doi.org/10.1211/PJ.2014.11136787.

A Royal Pharmaceutical Society Publication, 2017. Falsified medicines directive:

opportunity or obstacle? Pharm. J. 298, 1–10. https://doi.org/10.1211/PJ.2017.20202646.
Attaran, A., Barry, D., Basheer, S., Bate, R., Benton, D., Chauvin, J., Garrett, L., Kickbusch, I., Kohler, J.C., Midha, K., Newton, P.N., Nishtar, S., Orhii, P., McKee, M., 2012. How to achieve international action on falsified and substandard medicines. BMJ 345, 1–6. https://doi.org/10.1136/bmj.e7381.
CSIP, 2016. The internet pharmacy market in 2016 trends, challenges, and opportunities. [WWW Document]. URL. http://safemedsonline.org/wp-content/uploads/2016/01/The-Internet-Pharmacy-Market-in-2016.pdf, Accessed date: 28 February 2018.
Davison, M., 2011. Pharmaceutical Anti-counterfeiting Combating the Real Danger From Fake Drugs. John Wiley & Sons, Inc., Publication, pp. 103–140.
European Comission, 2016. REGULATIONS COMMISSION DELEGATED REGULATION (EU) 2016/161 of 2 October 2015 supplementing Directive 2001/83/EC of the European Parliament and of the Council by laying down detailed rules for the safety features appearing on the packaging medicinal product. Off. J. Eur. Union L 32/1-L32/27.
European Commission Staff Working Document, 2015. COMMISSION DELEGATED REGULATION (EU) No …/… Supplementing Directive 2001/83/EC of the European Parliament and of the Council by Laying Down Detailed Rules for the Safety Features Appearing on the Packaging of Medicinal Product for Human Use. European Commision.
European Medicines Agency, 2014. European Medicines Agency alerts EU healthcare professionals after vials of falsified Herceptin identified. [WWW Document]. EMA - Press release. URL. http://www.ema.europa.eu/ema/index.jsp?curl=pages/news_and_events/news/2014/04/news_detail_002076.jsp&mid=WC0b01ac058004d5c1, Accessed date: 5 March 2018.
European Medicines Agency, 2018. Falsified medicines. [WWW Document]. URL. http://www.ema.europa.eu/ema/index.jsp?curl=pages/regulation/general/general_content_000334.jsp&mid=WC0b01ac05800ba1d9, Accessed date: 28 February 2018.
Gaebler, F., 2017. Make your mark: using UV light for medical device marking. [WWW Document]. URL. https://edge.coherent.com/assets/pdf/Medical_Plastics_News_2017-06.pdf, Accessed date: 28 February 2018.
Genina, N., Fors, D., Vakili, H., Ihalainen, P., Pohjala, L., Ehlers, H., Kassamakov, I., Haeggström, E., Vuorela, P., Peltonen, J., Sandler, N., 2012. Tailoring controlled-release oral dosage forms by combining inkjet and flexographic printing techniques. Eur. J. Pharm. Sci. 47, 615–623. https://doi.org/10.1016/j.ejps.2012.07.020.
Heller, J., 2015. Precision Laser Marking for Medical Applications [WWW Document]. Ind. Laser Solut. Manuf., URL. https://www.industrial-lasers.com/articles/print/volume-30/issue-6/features/precision-laser-marking-for-medical-applications.html, Accessed date: 28 February 2018.
Interpol, 2013. Pharmaceutical crime: operations. [WWW Document]. URL. http://www.interpol.int/Crime-areas/Pharmaceutical-crime/Operations/Operation-Pangea, Accessed date: 28 February 2018.
IRACM, 2013. Organized crime in the network of drug falsification. [WWW Document]. URL. http://www.iracm.com/en/thematic-observatory/organized-crime, Accessed date: 28 February 2018.
Koller, D.M., Hannesschläger, G., Leitner, M., Khinast, J.G., 2011. Non-destructive analysis of tablet coatings with optical coherence tomography. Eur. J. Pharm. Sci. 44, 142–148. https://doi.org/10.1016/j.ejps.2011.06.017.
Korasa, K., Hudovornik, G., Vrečer, F., 2016. Applicability of near-infrared spectroscopy in the monitoring of film coating and curing process of the prolonged release coated pellets. Eur. J. Pharm. Sci. 93, 484–492. https://doi.org/10.1016/j.ejps.2016.08.038.
Markl, D., Hannesschläger, G., Sacher, S., Leitner, M., Khinast, J.G., 2014. Optical coherence tomography as a novel tool for in-line monitoring of a pharmaceutical film-coating process. Eur. J. Pharm. Sci. 55, 58–67. https://doi.org/10.1016/j.ejps.2014.01.011.
Pérez-Ibarbia, L., Majdanski, T., Schubert, S., Windhab, N., Schubert, U.S., 2016. Safety and regulatory review of dyes commonly used as excipients in pharmaceutical and nutraceutical applications. Eur. J. Pharm. Sci. 93, 264–273. https://doi.org/10.1016/j.ejps.2016.08.026.
Przyswa, E., 2013. Counterfeit Medicines and Criminal Organisations. pp. 1–129. https://doi.org/10.2139/ssrn.1725072.
Sukkar, E., 2014. Taking stock of counterfeit medicines. Pharm. J. 292, 570–572. https://doi.org/10.1211/PJ.2014.11138907.
The European Parliament and the Council of the European Union, 2011. Directive 2011/62/EU Of The European Parliament and of the Council of 8 June 2011. Off. J. Eur. Union L 174/74, 74–87.
UNICRI, 2012. Counterfeit Medicine and organised crime. [WWW Document]. URL. http://www.unicri.it/topics/counterfeiting/medicines/report/Ctf_medicines_and_oc_advance_unedited2013.pdf, Accessed date: 28 February 2018.
Wajsman, N., Arias Burgos, C., Davies, C., 2016. The Economic Cost of IPR Infringement in the Pharmaceutical Industry.
WHO, 2018. Media centre substandard and falsified medical products. [WWW Document]. URL. http://www.who.int/mediacentre/factsheets/fs275/en/, Accessed date: 28 February 2018.
WHO IMPACT, 2006. Counterfeit Medicines: An Update on Estimates 15 November 2006.

International Journal of Pharmaceutics 570 (2019) 118665

Contents lists available at ScienceDirect

International Journal of Pharmaceutics

journal homepage: www.elsevier.com/locate/ijpharm

Comparison of conventionally and naturally coloured coatings marked by laser technology for unique 2D coding of pharmaceuticals

Krisztina Ludasi[a], Orsolya Jójárt-Laczkovich[a], Tamás Sovány[a], Béla Hopp[c], Tomi Smausz[b,c], Géza Regdon jr[a,*]

[a] Institute of Pharmaceutical Technology and Regulatory Affairs, University of Szeged, Eötvös utca 6, 6720 Szeged, Hungary
[b] MTA-SZTE Research Group on Photoacoustic Spectroscopy, University of Szeged, Dóm tér 9, 6720 Szeged, Hungary
[c] Department of Optics and Quantum Electronics, University of Szeged, Dóm tér 9, 6720 Szeged, Hungary

ARTICLE INFO

Keywords:
Personalised medicines
Falsified medicines
Identification
Anti-counterfeiting
Laser marking
Unique laser coding
Naturally coloured coating

ABSTRACT

Substandard and/or falsified medicines are a growing global threat for health and they cause serious social and economic damage. In low- and middle-income countries the failure rate of these medical products is approximately 10.5%. 50% of medicines purchased over the Internet may be fake.

According to Directive 2011/62/EU as regards the prevention of falsified medicines from entering into the legal supply chain, a unique identification should be put on each box of drugs in the EU from 9th February 2019.

The current project is focusing on the development of a laser technology to mark an individual traceable code on the surface of the tablet. Usually, coatings contain titanium dioxide for sufficient coverage, which makes precision laser coding more difficult. New naturally coloured films do not include those excipients. In this research, we would like to compare the physical-chemical properties of conventionally and naturally coloured coatings after the laser marking procedure by using two types of lasers.

This unique identification technology can be used for marking personalized medicine with the doses tailored for each patient, too.

To sum up, the present findings may contribute to efficient and reliable laser marking solutions in the unique identification procedure. Based on our measurement results, it can be stated that excimer UV lasers are promising candidates as marking instruments for the polymer film in both conventionally and naturally coloured coatings.

1. Introduction

Substandard and falsified (SF) medicinal products are a growing problem, as they damage patients' health, the society and the economy. The World Health Organization, (WHO) adopted the name SF for the medical products that fail to meet either national or international quality standards or specifications at its 70th World Health Assembly in 2017 (WHO, 2017a; World Health Assembly, 2017).

According to the reports from WHO (2017), in low- and middle-income countries the failure rate of SF medical products is approximately 10.5% (WHO, 2017b, 2017c), which means that due to SF medicines each year 72,000 to 169,000 children may die of pneumonia, or 64,000–158,000 additional deaths of malaria could be caused according to the estimations of the University of Edinburgh and London School of Hygiene and Tropical Medicine, respectively (WHO, 2017d). In 2013 an estimated 122,350 (IQR: 91,577–154,736) under-five deaths were associated with the consumption of poor-quality antimalarials only in 39 sub-Saharan African countries, which suggests that these poor-quality medicines are important contributors to child mortality (Renschler et al., 2015) and may help the spread of growing resistance geographically. The number of drugs is also growing in the global marketplace, especially sales on the Internet (Nayyar et al., 2019), which has become an accepted, and more and more popular way to purchase medications in high-income countries since the establishment of the first Internet pharmacies (Gallagher and Colaizzi, 2000; Ghinea et al., 2006). Unfortunately, by now about 50% of medicines purchased over the Internet are falsified because of the increase of illegal activities (UNICRI, 2012; WHO IMPACT, 2006; Wilczyński, 2015), as they can easily circumvent regulatory oversight (Siva, 2010), and globalization makes it harder to regulate the medical products that are sold in this way (Bichell, 2017).

Most of the counterfeiters produce and print packaging in different

* Corresponding author at: University of Szeged, Institute of Pharmaceutical Technology and Regulatory Affairs, H-6720 Szeged, Eötvös u. 6, Hungary.
E-mail address: geza.regdon@pharm.u-szeged.hu (G. Regdon).

https://doi.org/10.1016/j.ijpharm.2019.118665
Received 31 May 2019; Received in revised form 30 August 2019; Accepted 4 September 2019
Available online 06 September 2019
0378-5173/

countries, shipping components to the final destination, where they are assembled and distributed (WHO, 2017d). Parallel imports also pose a significant risk to the safety of patients, especially when the product has to be repackaged, which is generally not allowed, but sometimes it is objectively necessary, e.g., to suit the target country's national language (European Commission, 2003; Said et al., 2011). Nevertheless, the removal of blister packs from their original external packaging and their insertion with one or more original packages into new external packaging, or their insertion into another original package, the insertion of new user instructions in national languages, or the fixing of self-stick labels on original external packaging or blister packs is considered as an activity which shall not affect the condition of the medicinal product inside the packaging. The necessity of repackaging must be justified by the parallel distributor in the course of a notification procedure (European Medicines Agency, 2019).

Managing illicit drug trafficking and limiting access to potentially counterfeit medicines should be a priority for governments and drug delivery systems (Vida et al., 2017). Recently, global pharmaceutical supply chains have been developing stricter regulatory requirements. In the USA, the FDA's Drug Supply Chain Security Act sets out the necessary steps to implement an electronic, interoperable system to identify and trace prescription drugs distributed in the US (FDA, 2014).

To prevent falsified medicines from entering the legal supply chain, the European Union adopted Directive 2011/62/EU (European Commission Staff Working Document, 2015; The European Parlament and the Council of the European Union, 2011). The EU Commission gave additional technical details for the further design of security features with the Delegated Regulation (EU) 2016/161. From 9th February 2019 serialization, traceability and verification for prescription-only medicines are obligatory requirements in the EU. This requires a new safety feature, a unique 2D data matrix barcode, which should be put on each box of drugs (European Comission, 2016).

To protect medical products, a large number of security technologies can be used for authentication. The choice of technology depends on the available financial resources, security level, feasibility, etc. It is recommended to use more than one technology at the same time to provide an effective protection against counterfeiting. The technologies that can be used include, but are not limited to the following: Printing technologies (offset lithography, flexography, gravure, screen printing, laser printing, pad printing, embossing and debossing, laser engraving, inkjet printing), security labels (adhesive, frangible, security cuts and perforation, void labels, holograms) and/or tracking technologies (serial numbers, linear bar codes, matrix codes, radio frequency identification (RFID)) may be used on the packaging of the medicines(Davison, 2011). Furthermore, various methods such as unique coating colours, shapes, tooling, texture, sizes, physical feature, unique tablet designs, logos, texts, pearlescent film, printing etc. may be used for on-dose visual identification, while physical-chemical identifiers (PCIDs) include inks, pigments, flavours, and molecular taggants. For example, TruTag's on-dose authentication (TruTag Technologies, 2019), Microtag (Nogaja, 2013), may be incorporated into solid oral dosage forms as in-dose features. Some PCIDs could require the use of instrumental detection.

The final aim of the present project is to extend the regulation provided by the Directive and to develop a technology for marking individual traceable 2D codes directly on the surface of the tablet. With this process, it would be easier to provide tablet authentication and to avoid illegal repackaging. As most existing anti-counterfeit technologies are on the drug packaging, it is easy for unscrupulous traders to exchange quality drugs (You et al., 2016). The QR code on the surface of the tablet is an excellent opportunity because of its high-capacity and error-correctability, its comprehensive reading ability, and its rapid and easy generation (Fei and Liu, 2016).

Besides anti-falsification, this unique identification technology is also suitable to label personalized medicines with codes tailored for each patient on each tablet. This information is increasingly needed for older persons following a prolonged complex drug regimen as they make mistakes when taking their medication (Mira et al., 2015), or when dose flexibility is needed for specific patient groups depending on age, gender, weight and genetic background (Edinger et al., 2018; Vakili et al., 2015). Coding could have benefits in terms of remote monitoring like tracking of medicine, or medicine reminder and monitoring system (Zanjal and Talmale, 2016). Furthermore, in hospitals, it is important to have a method to keep track of individual medicines dispensed to patients to avoid severe health risks. When the medicine leaves its packaging, it becomes impossible to identify the drug unless the leaflet remains accessible. The problem is the lack of information on the medicine itself (Kato et al., 2010).

Other research groups are also investigating alternative techniques for the direct marking of dosage forms. You et al., applied a fluorescent 3D QR code consisting of three different colour layers directly printed on the surface of the drug capsules. By using the multilayer printing and splitting technology, where each layer encodes information of different aspects of the drug and may be decoded by a specific smartphone application, the information storage capacity per unit area increases (You et al., 2016). Another study reports the interface between 3D printing and 2D inkjet printing technologies in order to fabricate a drug-loaded 3D printed tablet with a unique track-and-trace measure in a single step process. 2D codes were printed onto the surface of polymeric based printlets for scanning using a smartphone device and were designed to encode tailored information pertaining to the drug product, patient and prescriber. Plus, a novel anti-counterfeit strategy was designed, which involved the deposition of a unique combination of material inks for detection using Raman spectroscopy (Trenfield et al., 2019). In a third case, CO2 laser engraving was used to achieve roughness over different surfaces causing a difference in the grey levels on tranFslucent materials. This effect and the micro mold process was used to achieve micro pattern of the QR code and to obtain drug-laden biodegradable label (Fei and Liu, 2016).

In the present study laser ablation has been chosen for marking because it overcomes the drawbacks of the most popular printing methods (like offset-, ink-jet-, and pad printing), where the clear printing pattern may easily be affected by the environmental conditions of the process room, uniformity, temperature, and drying of the ink (Hosokawa and Kato, 2011). Printability is also affected by ink viscosity and surface tension, the size of the nozzle (Daehwan et al., 2009), the surface roughness of tablets, which may cause problems such as mottled appearance, blur, or dirt of the inks (Kato et al., 2010). Most of the ink printing requires contact between the substrate and some form of ink carrier, toner reservoir, or stamp so that could be a source of contamination (Davison, 2011). In addition, organic solvents which are harmful to the employees' health and the environment are often used for the inks (Kato et al., 2010). In contrast, laser ablation is a non-contact method that avoids the problems of the above-mentioned ink printing technologies and eliminates the cost of consumables using ink.

The final plan is to put two coatings on the tablet surface in different colours, a functional one and a second one for marking. After the laser ablation of the upper film layer, the differently coloured code could be read even by the patient using a mobile phone with the appropriate application. In the literature, there are several studies on mobile phones as a device capturing image and processing data for the authentication of fake drugs (Edinger et al., 2018; Fei and Liu, 2016; Karen Langhauser, 2013; Mackey and Nayyar, 2017; Ur Rehman et al., 2011). This coding process could have benefits for tracking drugs across the distribution chain and for adding information for personalised medicines. However, the 2D code on the surface of the medicine could have an impact on the visual appearance and affect the acceptance of medication by patients (Trenfield et al., 2019).

Preliminary studies (Ludasi et al., 2018) have shown that the use of conventional coatings, containing titanium dioxide and talc to achieve better surface coverage, could make precision laser coding more difficult. Therefore, as a response to the growing demand for natural

materials, and since new naturally coloured film formulations do not include the excipients mentioned above, the current research is focusing on the comparison of the physical-chemical properties of conventionally and naturally coloured coatings after the laser marking procedure by two different types of lasers.

The selection criteria for lasers were the comparison of completely different types of instruments to provide a broader overview of the effects of different lasers. The pulsed mode excimer laser works with photochemical ablation, which seems to have a more gentle effect on the structure of the coating. However, it uses gas mixtures, usually noble gas and halides, and the running costs are high due to the maintenance and equipment costs (E. Kannatey-Asibu Jr., 2009; Steen and Mazumder, 2010). In contrast, the continuous mode semiconductor (diode) laser ablates by the photothermal effect and has the advantages of being compact, efficient, with a quick modulation response and reliability. It is relatively small in size and easy to fabricate by mass production, thereby it has a low cost. In addition, they operate at different wavelengths.

2. Materials

2.1. Coating materials

HPMC based ready-to-use coating formulas: Sepifilm PW Red, PW Green, PW White and naturally coloured Sepifilm NAT Pink and NAT Green (Seppic S.A., Paris La Defense, France) were used dispersed in distilled water.

3. Methods

3.1. The plastic ball coating procedure

In this study, experiments were done on coating films, sprayed on the surface of polyethylene balls (Primary Balls Kft., Budaörs, Hungary) with an outer diameter of 2.5 cm under the same conditions as previously used on tablets. Thereafter the film was removed from the ball, marked by laser and examined.

The aqueous HPMC coating solutions consisting of 15% w/w dry substance in the case of SEPIFILM™ NATurally COLoured coatings agents, and 20% w/w dry substance in the case of Sepifilm™ PW coating systems, according to the supplier's recommendation, were prepared by dispersing them in distilled water. The total mixing time lasted for 45 min, followed by passing the dispersion through a 0.5 mm sieve.

4 M8 Pancoat (ProCepT, Zelzate, Belgium) perforated coating pan was used for spray coating. 35 pieces of balls were coated at the same time in four stages. The coating parameters are shown in Table 1. A 0.8 mm spray nozzle was used for the application of the atomised spray coating solution for 55 min, with an atomising air pressure of 2.0 bars and an air flow rate of 0.70 m^3/min. The drying and cooling process lasted for 15 min each.

3.2. Irradiation of coating films with 2 types of laser

In the first step the coating films were irradiated with a LLG TWINAMP type ArF excimer laser (wavelength: 193 nm, energy: 3 ± 0.2 mJ, fluence: 444 mJ/cm2, FWHM: 20 ns, spot size: 375 μm), using a simple square-shaped mask, which has resulted in a 1 mm^2 square-shaped ablation hole, to study the effect of the laser on the coating film. The extension of the ablation procedure to achive the planned 2D imaging requires the combination of the laser with a precise CNC stage.

Table 1
The coating parameters of balls.

Step	Inlet air temperature (°C)	Exhaust air temperature (°C)	Ball temperature (°C)	Drum speed (rpm)
Warm-up	60	N/A	Until 50	3
Coating	50–55	40–42	45	9
Drying	40	30	27	3
Cooling	25	25	25	3

The effect of a CW semiconductor laser (wavelength: 405 nm, spot size: 73 μm, power: 1000 mW, irradiation time: 15–20 ms) on the quality of the coating films was also tested. In this case a full QR code was generated using online ZXing ("Zebra Crossing") code generator software, an open-source, multi-format 1D/2D barcode image processing and code generator library implemented in Java. The standard QR code was generated (ISO/IEC 18004:2015) with 8 numerical characters using 300 dpi resolution and lowest error correction (Level L). For reading the QR code, the same software application was used by a mobile phone. The 3D geometric correction has not yet been applied to the 2D images, since it was projected to the coating film, which has a negligible curvature compared to the real tablet surface.

3.3. Digital microscope

The surface morphology of the ablated film was observed by using a Digital Microscope (KEYENCE, VHX-6000). This instrument is equipped with a newly developed REMAX VI High-Performance Graphics Engine and D.F.D. 2.0 image processing engine. This enables the creation of a precise 3D image by analysing small changes in texture after capturing numerous images at different heights and different angle positions, HDR and image-stitching. Through line roughness and surface roughness measurements, reliable evaluation of surfaces can be performed and converted to a figure.

Data was evaluated by HDR playback / measurement / stitched image playback software developed by KEYENCE.

3.4. Surface profilometer

Profilometry measurements were performed on a Veeco, Dektak 8 Advanced Development Profiler®. The tips employed had a radius of curvature ~2.5 μm, and the force applied to the surface during scanning was ~30 μN. The horizontal resolution was 0.1–0.13 μm. The vertical resolution was 40 Å. Data was evaluated by Dektak software (Microsoft ® Windows XP ®: interactive data acquisition) and Vision ® 32 software (data processing, 2-D and 3-D image analysis) (Veeco Instruments Inc., New York, USA)

3.5. Raman spectra

Films treated by a laser were investigated by Raman spectroscopy. Spectra were acquired with a Thermo Fisher DXR Dispersive Raman (Thermo Fisher Scientific Inc., Waltham, MA, USA) equipped with a CCD camera and a diode laser operating at a wavelength of 780 nm. Raman measurements were carried out with a laser power of 12 and 24 mW at 25 μm slit aperture size. Spectra of the individual films and films treated by two different lasers were collected using an exposure time of 6 sec. The data were collected in the spectral range of 3407–24 cm^{-1} using automated fluorescence corrections. OMNIC 8 software was used for data collection, averaging the total of 20 scans and making the spectral corrections. For the removal of cosmic rays, a convolution filter was applied to the original spectrum using Gaussian kernel.

3.6. Thermal gravimetric analysis (TGA)

The thermal gravimetric analysis of the samples was carried out with a Mettler-Toledo TGA/DSC1 instrument (Mettler-Toledo GmbH, Switzerland). The start temperature was 25 °C, the end temperature was 500 °C, the applied heating rate was 10 °C/min. Nitrogen atmosphere was used (cell gas: 50 ml/min, method gas: 70 ml/min). 5 ± 1 mg of

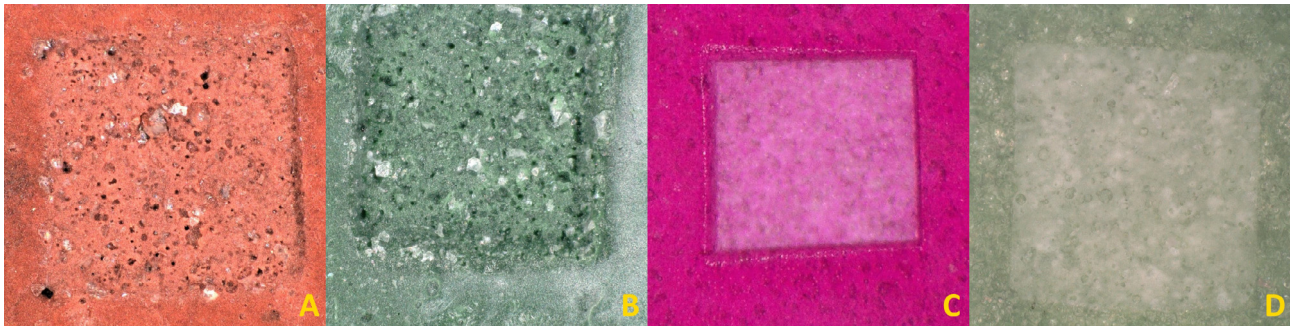

Fig. 1. Coating films treated by excimer laser: Sepifilm PW Red (A), PW Green (B), Sepifilm Naturally Coloured Pink (C) and Green (D).

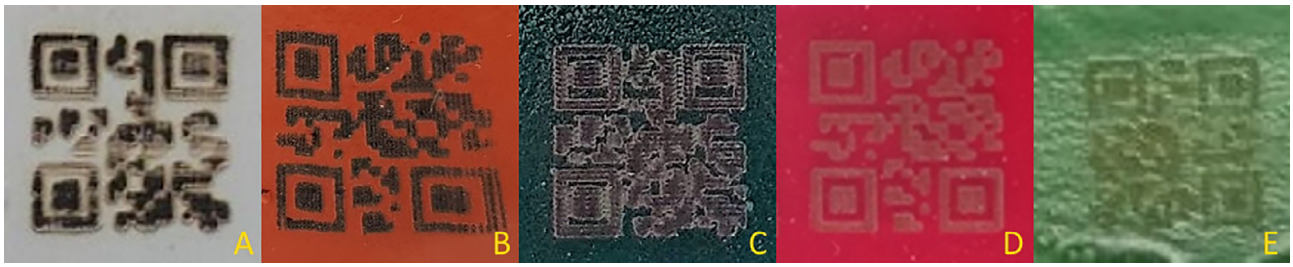

Fig. 2. The coating films treated by semiconductor laser: Sepifilm PW White (A), PW Red (B), PW Green (C) and Sepifilm Naturally Coloured Pink (D) and Green (E).

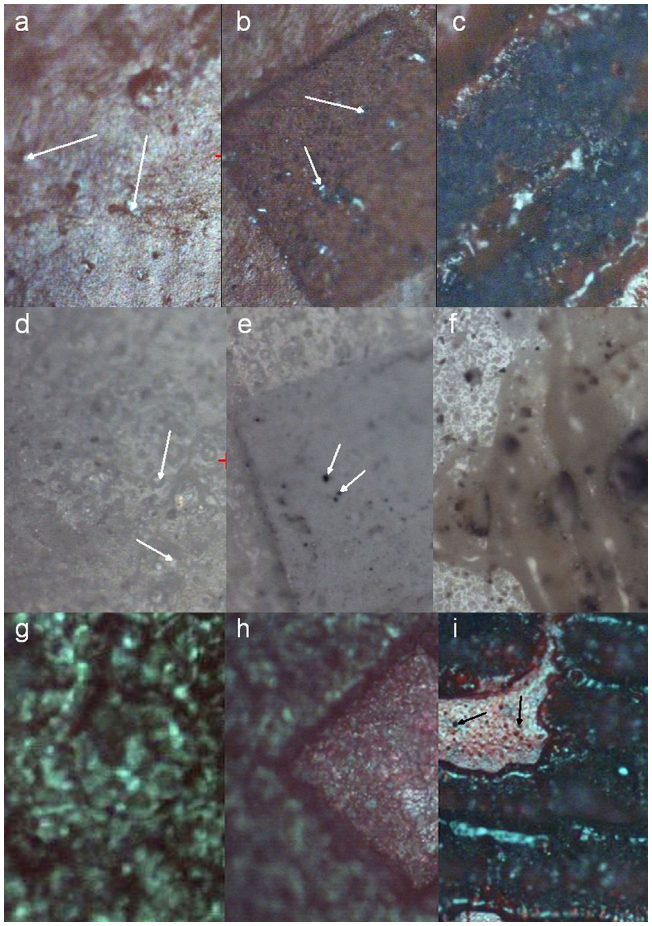

Fig. 3. Microscopic picture of untreated films (first column: a, d, g), films treated by excimer laser (second column: b, e, h) and films treated by semiconductor laser (third column: c, f, i). Sepifilm PW Red (a, b, c), PW White (d, e, f), and Sepifilm Naturally Coloured Pink (g, h, i).

samples were measured into aluminium pans (40 µl). The peak areas were evaluated with Mettler-Toledo STARe Software.

4. Results and discussion

The present study is focusing on the comparison of conventionally coloured and naturally coloured coatings that are talc- and titanium dioxide-free, to clarify how the titanium dioxide particles interfere with laser ablation. Films were sprayed on the surface of polyethylene balls, removed and marked with 2 different types of lasers. After marking the polymer films, a detailed quality analysis was made to check if there occurred any change during the laser intervention in different films.

4.1. Surface

Laser marked films were examined first by a 3D digital microscope. The investigated lasers had different effects on the films. The excimer laser's material removal mechanism is photochemical ablation. The energy of the ultraviolet photon is between 3.5 and 6.5 eV, which is similar to the molecular bonding energy for many organic materials (the energy associated with the C—C bond is roughly 4.6 eV, while that of the C—H bond is about 4.2 eV and 6.42 eV in our case). When an organic material is irradiated with an ultraviolet beam, the compounds efficiently absorb the beam's energy in a very thin layer of the order of submicron, near the surface. This breaks molecular bonds, causing ablative decomposition of the irradiated area. The process occurs almost instantaneously, there is no time for any heat transfer. The resulting edges are well defined, with minimal thermal damage to the surrounding area, which is why the process is also called cold ablation.

In contrast, semiconductor lasers ablate material by a photothermal effect. Heat flows by thermal conduction and material evaporates by boiling after prior melting or burning. However, this thermal heating may cause material removal by routes other than straight boiling. By the sufficient heating of the material, the vibrations can break the weaker bonds, and the boiling point of the broken structure may be lower than that of the original structure and evaporation occurs without the reaching of the melting point, which is of particular relevance to polymers (Kannatey-Asibu Jr., 2009; Steen and Mazumder, 2010).

The effects of the different lasers on the ablated polymer films are

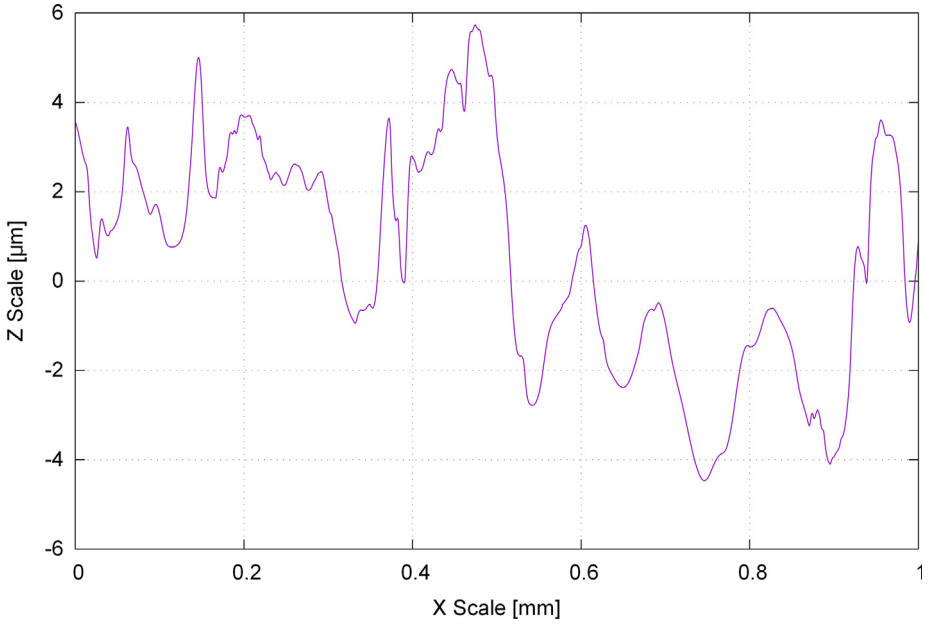

Fig. 4. Typical untreated tablet surface roughness measured with profilometer.

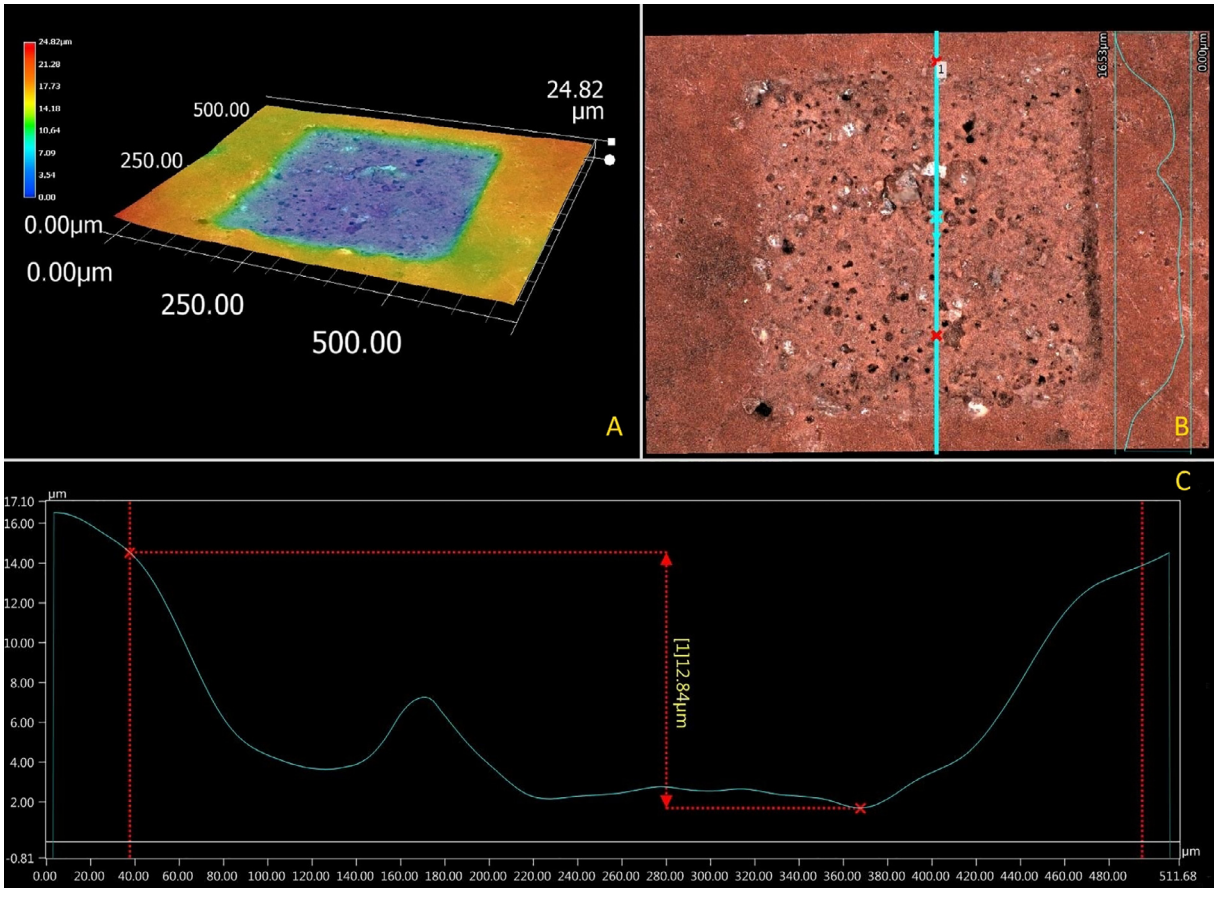

Fig. 5. Surface analysis by KEYENCE 3D microscope of the excimer laser treated region of Sepifilm PW Red coating. A – 3D surface graph, B – top view with original colours of the ablation hole, C – profile analysis. The white titanium dioxide particle is marked with a yellow circle.

seen in Figs. 1 and 2, showing the holes ablated by the excimer laser, and the markings achieved by the semiconductor laser, repectively. During the excimer laser ablation, the square-shaped holes on the film returned the shape of the mask used. The ablations of the differently coloured coatings were considerably different: coatings PW Red and PW Green, containing titanium dioxide and talc, are seen in Fig. 1 A and B, where white and black particles are visible. The is no similar phenomenon on the laser treated surface of the naturally coloured NAT Pink and NAT Green coatings (Fig. 1C and D). The resulted shape is much sharper, and the surface is much smoother in this type of coating

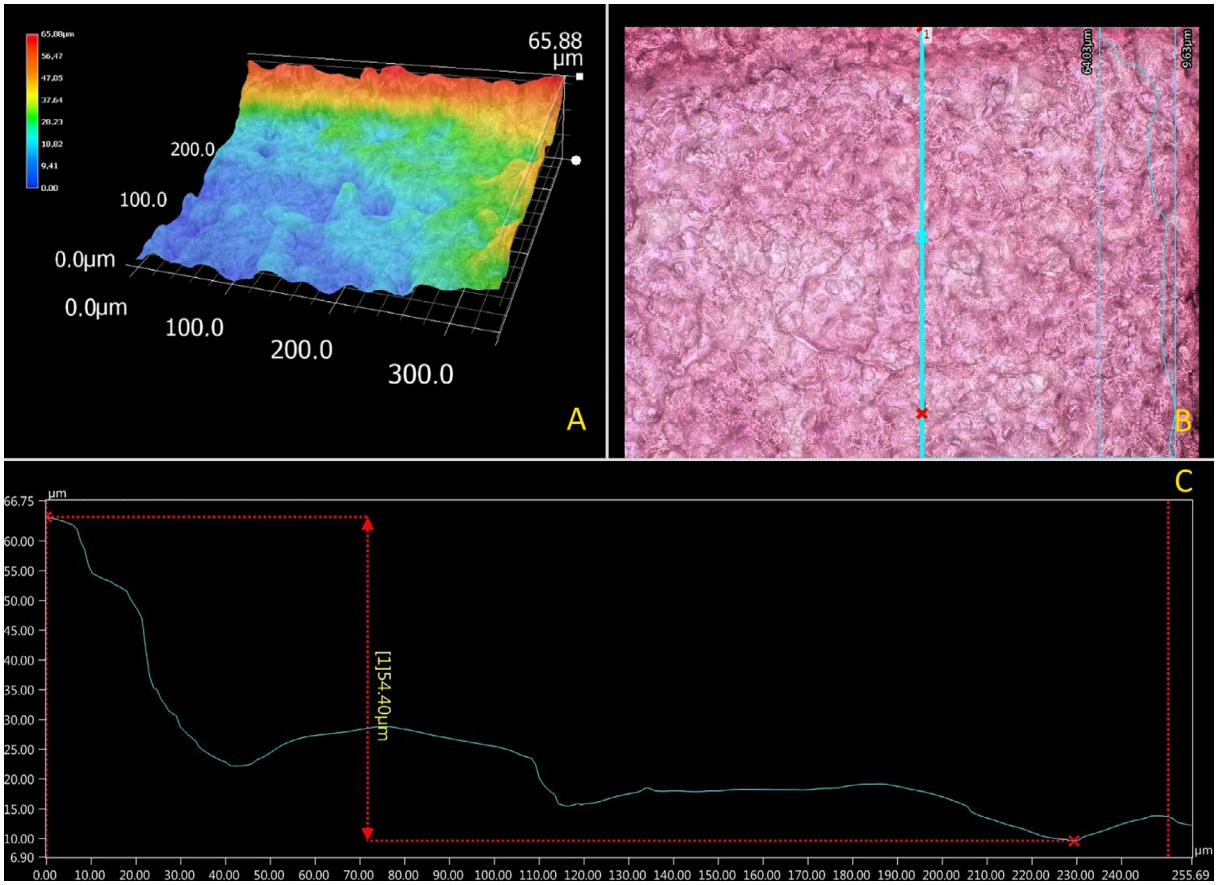

Fig. 6. Surface analysis by 3D microscope of the excimer laser treated region of the Sepifilm NAT Pink coating. A – 3D surface graph, B – top view with original colours of the ablation hole, C – profile analysis.

Table 2
The compositions and Raman spectroscopic references of conventionally (PW) and naturally (NAT) coloured coatings.

PW coloured films		Literature background Raman activity of components	NAT coloured films		Literature background Raman activity of components
HPMC		(Romann et al., 2010)	HPMC		(Romann et al., 2010)
PEG		(Romann et al., 2010)	glycerine		(Romann et al., 2010)
Talc		(Szostak and Mazurek, 2002)	MCC		(Fechner et al., 2003)
Titanium dioxide		(Kato et al., 2010)			
Pigments	white: -		Colouring food agents		
	red: iron oxide	(Li et al., 2012)		pink: beetroot extract	(de Oliveira et al., 2010)
	green: chlorophyll	(Koyama et al., 1986)		green: algae extract	(Weiss et al., 2010)

films due to the lack of the disturbing particles.

The result of the treatment by semiconductor laser is black burst signals or the fading of the colour of coatings, which may be seen in Fig. 2A–C or D and E, repectively. To clarify the nature of changes on the treated surface, further investigations were made.

The microscopic pictures of the untreated, excimer laser treated and semiconductor laser treated films may be seen in the first (Fig. 3a, d, g.), second (Fig. 3b, e, h) and third (Fig. 3c, f, i) columns of Fig. 3 respectively. Arrows are pointing at the little white titanium dioxide particles. However, in the square shaped 'print' both black and white particles are seen in Fig. 3b, e.

This phenomenon may be connected to the three existing crystal structures of titanium dioxide, rutile, anatase, and brookite (Hosokawa and Kato, 2011). By the laser treatment of titanium dioxide, apart from ablation, three main events are expected to occur: reduction, phase transition and melting. These can be qualitatively graded according to the respective characteristic temperatures of 500 °C, 750 °C, and 1870 °C. It was reported by Robert et al. that the irradiation of titanium dioxide by KrF excimer UV pulsed laser at wavelength 248 nm induced a colour change from white to dark blue, which was the phase transition of anatase to rutile indicating surface reduction (Robert et al., 2003). Furthermore, Kato et al. were studying the mechanism of printing film-coated tablets containing titanium dioxide by using a tripled Nd: YVO4 UV laser printing machine (wavelength of 355 nm). They marked clear numbers and letters on the surface of the tablet by turning the colour of the film from white to grey, as a result of the appearance of many black particles in the coloured part of the film. The black particles are formed by the agglomeration of the greyed oxygen-defected titanium dioxide by the UV laser irradiation (Kato et al., 2010). It was assumed that in the present case the white and black points in Fig. 3b and e are also associated with the laser irradiated titanium dioxide, since the reactions of titanium dioxide to laser ablation differ significantly from other ingredients of the coating material. Each material has its characteristic ablation threshold. This value is specific

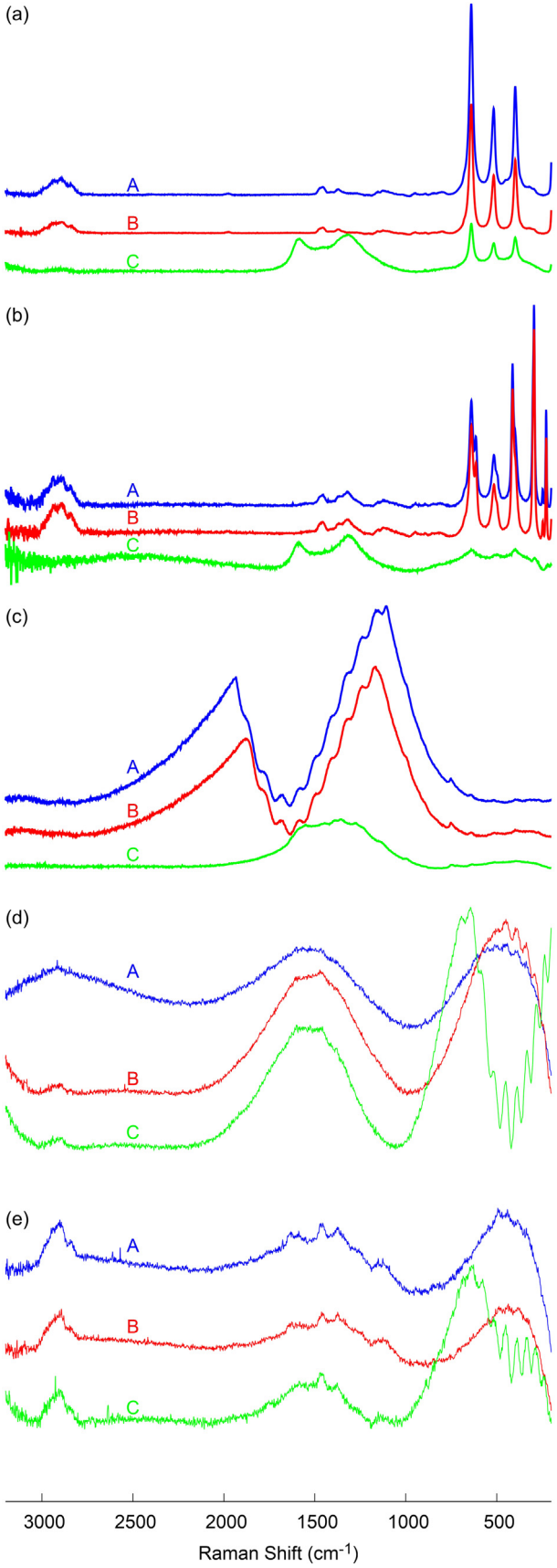

Fig. 7. Raman spectra of film coatings treated with different lasers (a) Sepifilm PW White, (b) Sepifilm PW Red, (c) Sepifilm PW Green, (d) Sepifilm NAT Pink, (e) Sepifilm NAT Green (A – original, B – excimer laser, C – semiconductor laser). Raman measurements were carried out with a laser power of 12 mW and in the case of Sepifilm NAT Green 24 mW.

to the material, to the type of laser, to the ablation method and to the wavelength and the fluence (Kannatey-Asibu Jr., 2009; Steen and Mazumder, 2010). In the studies of Laude et al., the ablation of talc started at 250 mJ/cm^2 fluence at 248 nm wavelength, so it is likely that talc has been ablated during the laser treatment (Laude et al., 1997). The ablation of titanium dioxide requires higher fluence than other ingredients of the coating material, and it is likely to require higher fluence than our laser can provide. In the present case the excimer laser was used at 193 nm wavelength and 444 mJ/cm^2 fluence, whereas literature data about the ablation threshold of titanium dioxide is available only at 248 nm wavelength and 1.44 J/cm^2 (Van Overschelde et al., 2006) or 910 mJ/cm^2 fluence (Robert et al., 2003). The threshold value in this study was still below the ablation threshold of titanium dioxide and was not enough for its removal, but it was enough for the removal of the rest of the coating. Therefore the presence of these excipients makes precision laser coding by the excimer laser more difficult as particles remain, increasing overall surface roughness and degrading the uniform colour distribution. In the case of the titanium dioxide-free naturally coloured coatings (Fig. 3g and h), those black and white particles are not visible.

The QR code requires a certain spatial resolution when encoding the desired amount of data. The required (RMS-Root mean squared) surface roughness of the treated region should be less than 10 µm. In most cases, the untreated tablet surface fulfils that criterion, see Fig. 4.

The previously discussed titanium dioxide enrichment can disturb the 2D code recognition by increasing surface roughness. The remaining particle size can be about half of the ablation depth, as shown by the results of the excimer laser treated PW Red film as an example (Fig. 5). The designated line where the measurement was taken is passing through the ablation hole (Fig. 5A and B) and the corresponding profile of the ablation hole is shown in Fig. 5C.

The metal oxide and pigment ratio also changed during the ablation procedure. This effect modifies the treated coating colour and, as a result, degrades the 2D code contrast. In contrast, no disturbing white particles are seen in the case of NAT Pink coating (Fig. 6), and the lasered surface is found to be smoother.

According to the literature, it was supposed that the thermal effect of pulsed UV radiation of 193 nm is negligible, only rapid photochemical reactions take place in the irradiated volume “exploding” the molecules from the surface (photoablation), and there is no time for any heat transfer. This hypothesis was supported by the microscopic pictures where no sign of thermal degradation or modification of the film structure were visible. In contrast, the 404 nm wavelength diode (semiconductor) laser has a higher wavelength, greater heat effect, and operates with continuous irradiation, where there is enough time for heat transfer, heat propagation and heat accumulation, which can lead to thermal degradation. The signs of melting and burning, causing structural changes and modified porosity of the films are well visible in Figs. 2 and 3c, f, i.

4.2. Raman investigations

As it was discussed above, the 2 types of lasers have a completely different effect on the coatings, which was displayed in the microscopic pictures (Fig. 3). The semiconductor laser seemingly burned or faded out the films. To find out what kind of chemical changes happened, Raman investigations were carried out. Nevertheless, the complex composition of the coatings, - especially the ones that contain natural colourings (e.g., extracts of fruits, vegetables, plants or algae) -, where the exact composition is not known, makes analysis difficult.

The components and the related relevant literature for Raman spectroscopic examinations are listed in Table 2.

The fingerprint region of Sepifilm is 1800 cm^{-1}–500 cm^{-1}. The spectra of raw free films and films treated by different lasers are summarized in Fig. 7. In all cases, the spectra of the films treated by the semiconductor laser changed the fingerprint region of Sepifilm, while

Table 3
Decomposition behavior of the raw polymer film and the film treated by laser.

TG data	Sepifilm® NAT. P. film	Sepifilm® NAT. P. film treated with excimer laser	Sepifilm® NAT. P. film treated with semiconductor laser
First step			
Thermal range (°C)	25–120	25–120	25–120
Mass loss (%)	2.85	4.05	4.91
Second step			
Thermal range (°C)	290–430	290–430	290–430
Mass loss (%)	58.26	59.98	68.94
TG data	Sepifilm® PW R film	Sepifilm® PW R film treated with excimer laser	Sepifilm® PW R film treated with semiconductor laser
First step			
Thermal range (°C)	25–120	25–120	25–120
Mass loss (%)	1.07	1.15	1.80
Second step			
Thermal range (°C)	290–440	290–440	290–440
Mass loss (%)	51.88	52.11	55.12
TG data	Sepifilm® PW W film	Sepifil® PW W film treated with excimer laser	Sepifilm® PW W film treated with semiconductor laser
Thermal range (°C)	25–500	25–500	25–500
Mass loss (%)	56.06	54.80	65.63

the excimer laser did not cause considerable alteration in the coatings.

Firstly, it should be emphasized that the polymer films containing the extract of colouring foodstuffs, Sepifilm PW Green, NAT Pink and NAT Green (Table 2) exhibited severe fluorescence during the measurement (Fig. 7c–e). This effect could not be corrected by photobleaching, and it has made the analysis difficult or impossible. In the case of PW Green, fluorescence disappeared after marking it by the semiconductor laser, presumably because of a change in the structure of chlorophyll, which resulted in the change of the colour of the coating (Fig. 2).

Among the listed components, titanium dioxide is one of the most important that had an effect on the lasering results, which has already been discussed above. In the corresponding articles, the peaks of the Raman spectra of titanium dioxide may be found at 396, 516 and 638 cm^{-1}, which characteristic peaks were found in the Raman spectra of Seppic PW films (Fig. 7a–c). These peaks exhibited a minor decrease in films treated by the excimer laser, and a more considerable decrease in intensity when they were lasered by the semiconductor laser, in the same way as Kato et al. have reported (Kato et al., 2010). In the same spectra, considerable fluorescence was detectable in the region of 1700 cm^{-1} to 1200 cm^{-1} in the case of the semiconductor laser treated films, which is likely due to the product degradation that had occurred during the laser treatment.

4.3. Thermal gravimetric analysis (TGA)

To reveal the effect of the assumed chemical changes on the structure of the films, TGA measurements were performed. The main characteristics of the samples derived from TG curves as corresponding mass loss values (Table 3) were used to define the thermal behaviour and combustion characteristics of films. It is seen that mass loss in Sepifilm NAT Pink and Sepifilm PW Red coating comes in two stages. The first mass loss occurred between 25 and 120 °C with both coatings, the second stage between 290 and 430 °C in the case of NAT Pink film, and between 290 and 440 °C in the case of PW Red. The mass loss of Sepifilm PW White film was observed between 25 and 500 °C.

The TG curves revealed that the decomposition occurred sooner in Sepifilm NAT Pink, PW White, and PW Red coatings if they were marked by a semiconductor laser, as it may be seen in Fig. 8. These results correlate with the results of our previous research (Ludasi et al., 2018). It may be seen from the microscopic mosaic picture of the pre- and post-lasered films that in contrast with the untreated intact films (Fig. 3a, d, g), the semiconductor laser treated films (Fig. 3c, f, i) exhibit damaged structures. Holes may be seen, especially on the Sepifilm PW White film (Fig. 3f) surrounded by a wide range of melted area. A damaged structure and larger pores appeared, suggesting that water can escape more easily from the internal parts of the material as a result of the heat effect. Therefore, it can be concluded that the weight loss seen in the first step of the TG curve may show the water loss of the films (Fig. 8a and c). The visual signals of the damage (Fig. 3c, f, i) and the corresponding TG curves of semiconductor laser treated films, - where all of these curves reveal that decomposition occurred sooner -, all indicate that the decomposition process had already started during the laser marking process. In contrast, in the micrographs of the excimer laser treated films (Fig. 3b, e, h) it is seen that the ablated surface of the sample exhibits no considerable destruction, the structure of the film is relatively intact. The TG curves of the excimer laser marked films run together with the curves of the original, untreated film. Overall, the earlier the mass loss of TG curves began, the more damaged the surface of semiconductor laser-coded coatings was, and the lack of these signs on the excimer laser treated ones indicates well the different effects of different lasers on the films.

5. Conclusion

In this study, the behaviour of conventional coating compared to ones containing natural colourings was examined during marking with different lasers. The results demonstrated that the excimer laser could be the right instrument for marking functional coatings, since it caused no structural damage in the treated films. However, the laser treatment of the naturally coloured material can be performed more accurately, with greater precision due to the lack of remaining particles disturbing the reading of the ablated codes. It can also be concluded that laser ablation differentiates the ingredients of the conventional coating as the white titanium dioxide particles stay in place and they change the overall surface colour, which can affect drug identification. Marking pills by excimer laser could be a promising solution for pharmaceutical companies that would like to have additional protection against drug counterfeiters or to mark personalized medicines. It is also an important conclusion that, despite the resulting chemical modifications, semiconductor lasers may be useful and cheaper alternative for tablet coding if marking is performed on non-functional coating which is thick enough to avoid heat transfer into the tablet core, and if no harmful by-product is formed as a result of the heat. These technologies would not be mandatory, but the option is there to use them as they could have several useful features, too.

Declaration of Competing Interest

The authors declare that they have no known competing financial interests or personal relationships that could have appeared to influence the work reported in this paper.

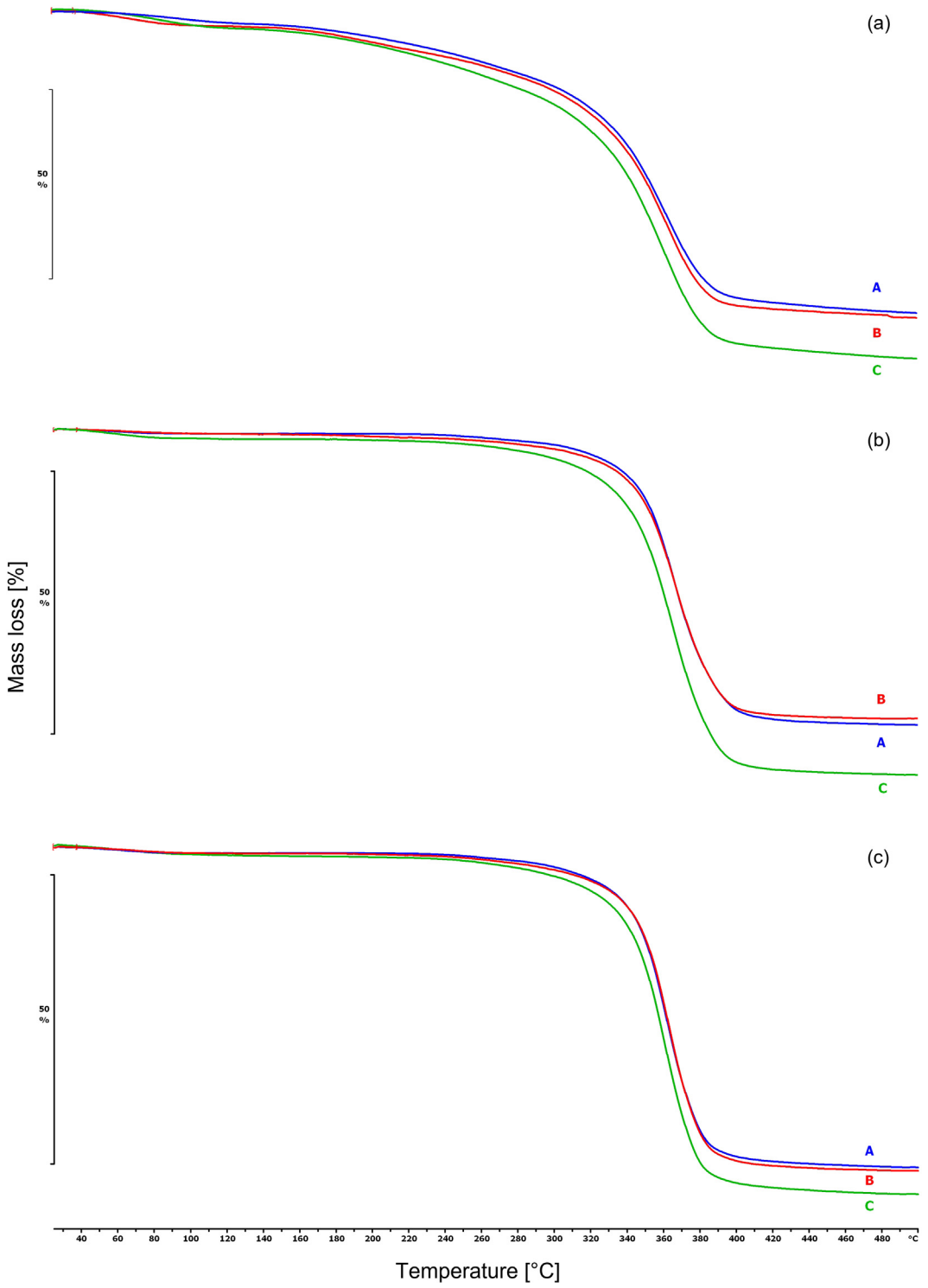

Fig. 8. TG curves of Sepifilm (a) NAT Pink, (b) PW White, (c) PW Red film treated with different lasers (A – original, B – excimer laser, C – semiconductor laser).

Acknowledgement

I would like to thank Seppic S.A. for supplying the polymers, KEYENCE Corporation for providing the digital microscope with knowledgeable technical assistance, and Imre Gódány, who helped with the measurements.

This research was supported by the EU-funded Hungarian grant EFOP-3.6.1-16-2016-00008

References

Bichell, R.E., 2017. Fake drugs are a major global. Problem, WHO Reports.
Daehwan, J., Dongjo, K., Jooho, M., 2009. Influence of fluid physical properties on ink-jet printability. Langmuir 25, 2629–2635.
Davison, M., 2011. Pharmaceutical Anti-Counterfeiting Combating the Real Danger from Fake Drugs. John Wiley & Sons Inc., Publication, pp. 103–140.
de Oliveira, V.E., Castro, H.V., Edwards, H.G.M., de Oliveiraa, L.F.C., 2010. Carotenes and carotenoids in natural biological samples: A Raman spectroscopic analysis. J. Raman Spectrosc. 41, 642–650. https://doi.org/10.1002/jrs.2493.
Kannatey-Asibu Jr., E., 2009. Principles of Laser Materials Processing. John Wiley&Sons.
Edinger, M., Bar-Shalom, D., Sandler, N., Rantanen, J., Genina, N., 2018. QR encoded

smart oral dosage forms by inkjet printing. Int. J. Pharm. 536, 138–145. https://doi.org/10.1016/j.ijpharm.2017.11.052.
European Comission, 2016. REGULATIONS COMMISSION DELEGATED REGULATION (EU) 2016/161 of 2 October 2015 supplementing Directive 2001/83/EC of the European Parliament and of the Council by laying down detailed rules for the safety features appearing on the packaging medicinal product. Off. J. Eur. Union L 32/1-L32/27.
European Commission. 2003. Commission Communication on parallel imports of proprietary medicinal products for which marketing authorisations have already been granted EN.
European Commission Staff Working Document, 2015. COMMISSION DELEGATED REGULATION (EU) No/ supplementing Directive 2001/83/EC of the European Parliament and of the Council by Laying Down Detailed Rules for the Safety Features Appearing on the Packaging of Medicinal Product for Human Use. European Commision.
European Medicines Agency. 2019. Human Regulatory, Frequently asked questions about parallel distribution. < https://www.ema.europa.eu/en/human-regulatory/post-authorisation/parallel-distribution/frequently-asked-questions-about-parallel-distribution > (accessed 3.29.19).
FDA. 2014. Drug Supply Chain Security. < http://www.fda.gov/Drugs/DrugSafety/DrugIntegrityandSupplyChainSecurity/DrugSupplyChainSecurityAct/ > (accessed 3.4.19).
Fechner, P.M., Wartewig, S., Füting, M., Heilmann, A., Neubert, R.H.H., Kleinebudde, P., 2003. Properties of microcrystalline cellulose and powder cellulose after extrusion/spheronization as studied by fourier transform raman spectroscopy and environmental scanning electron microscopy. AAPS J. 5, 1–13.
Fei, J., Liu, R., 2016. Drug-laden 3D biodegradable label using QR code for anti-counterfeiting of drugs. Mater. Sci. Eng. C 63, 657–662. https://doi.org/10.1016/j.msec.2016.03.004.
Gallagher, J.C., Colaizzi, J.L., 2000. Issues in internet pharmacy practice. Ann. Pharmacother. 34, 1483–1485. https://doi.org/10.1345/aph.10130.
Ghinea, G., Asgari, S., Moradi, A., Serif, T., 2006. A Jini-based solution for electronic prescriptions. IEEE Trans. Inf. Technol. Biomed. 10, 794–802. https://doi.org/10.1109/TITB.2006.879586.
Hosokawa, A., Kato, Y., 2011. Factors affecting color strength of printing on film-coated tablets by UV laser irradiation: TiO_2 particle size, crystal structure, or concentration in the film, and the irradiated UV laser power. Drug Dev. Ind. Pharm. 37, 901–906. https://doi.org/10.3109/03639045.2010.548816.
Langhauser, Karen, 2013. If You Drop QR Codes, Do They Bounce Back ? Phamaceutical Manuf.
Kato, Y., Nakashima, Y., Shino, N., Sasaki, K., Hosokawa, A., Ishihara, H., 2010. Studies on the mechanism of printing film-coated tablets containing titanium dioxide in the film by using UV laser irradiation. Drug Dev. Ind. Pharm. 36, 405–412. https://doi.org/10.3109/03639040903213725.
Koyama, Y., Umemoto, Y., Akamatsu, A., Uehara, K., Tanaka, M., 1986. Raman spectra of chlorophyll forms. J. Mol. Struct. 146, 273–287. https://doi.org/10.1016/0022-2860(86)80299-X.
Laude, L.D., Soudant, S., Beauvois, S., Renaut, D., Jadin, A., 1997. Laser ablation of charged polymers. Nucl. Instrum. Methods Phys. Res. Sect. B Beam Interact. Mater. Atoms 131, 211–218. https://doi.org/10.1016/S0168-583X(97)00137-7.
Li, Y.S., Church, J.S., Woodhead, A.L., 2012. Infrared and Raman spectroscopic studies on iron oxide magnetic nano-particles and their surface modifications. J. Magn. Magn. Mater. 324, 1543–1550. https://doi.org/10.1016/j.jmmm.2011.11.065.
Ludasi, K., Sovány, T., Laczkovich, O., Hopp, B., Smausz, T., Regdon, G., 2018. Unique laser coding technology to fight falsified medicines. Eur. J. Pharm. Sci. 123, 1–9. https://doi.org/10.1016/j.ejps.2018.07.023.
Mackey, T.K., Nayyar, G., 2017. A review of existing and emerging digital technologies to combat the global trade in fake medicines. Expert Opin. Drug Saf. 16, 587–602. https://doi.org/10.1080/14740338.2017.1313227.
Mira, J.J., Guilabert, M., Carrillo, I., Fernández, C., Vicente, M.A., Orozco-Beltrán, D., Gil-Guillen, V.F., 2015. Use of QR and EAN-13 codes by older patients taking multiple medications for a safer use of medication. Int. J. Med. Inform. 84, 406–412. https://doi.org/10.1016/j.ijmedinf.2015.02.001.
Nayyar, G.M.L., Breman, J.G., Mackey, T.K., Clark, J.P., Hajjou, M., Littrell, M., Herrington, J.E., 2019. Falsified and substandard drugs: stopping the pandemic. Am. J. Trop. Med. Hyg. 00, 1–8. https://doi.org/10.4269/ajtmh.18-0981.
Nogaja, J.S., 2013. Micro-tag: a novel technique of security in pharmaceuticals. Int. J. Pharm. Sci. Res. 4, 29–33.
Renschler, J.P., Walters, K.M., Newton, P.N., Laxminarayan, R., 2015. Estimated under-five deaths associated with poor-quality antimalarials in sub-saharan Africa. Am. J. Trop. Med. Hyg. 92, 119–126. https://doi.org/10.4269/ajtmh.14-0725.
Robert, T.D., Laude, L.D., Geskin, V.M., Lazzaroni, R., Gouttebaron, R., 2003. Micro-Raman spectroscopy study of surface transformations induced by excimer laser irradiation of TiO_2. Thin Solid Films 440, 268–277. https://doi.org/10.1016/S0040-6090(03)00819-8.
Romann, J., Valmalette, J.C., Chevallier, V., Merlen, A., 2010. Surface interactions between molecules and nanocrystals in copper oxalate nanostructures. J. Phys. Chem. C 114, 10677–10682. https://doi.org/10.1021/jp9082344.
Said, M.M., Gibbons, S., Moffat, A.C., Zloh, M., 2011. Near-infrared spectroscopy (NIRS) and chemometric analysis of Malaysian and UK paracetamol tablets: A spectral database study. Int. J. Pharm. 415, 102–109. https://doi.org/10.1016/j.ijpharm.2011.05.057.
Siva, N., 2010. Tackling the booming trade in counterfeit drugs. Lancet 376, 1725–1726. https://doi.org/10.1016/S0140-6736(10)62118-6.
Szostak, R., Mazurek, S., 2002. Quantitative determination of acetylsalicylic acid and acetaminophen in tablets by FT-Raman spectroscopy. Analyst 127, 144–148. https://doi.org/10.1039/b108240j.
The European Parlament and the Council of the European Union, 2011. Directive 2011/62/EU of the European parliament and of the council of 8 June 2011. Off. J. Eur. Union L 174 (74), 74–87.
Trenfield, S.J., Xian Tan, H., Awad, A., Buanz, A., Gaisford, S., Basit, A.W., Goyanes, A., 2019. Track-and-trace: Novel anti-counterfeit measures for 3D printed personalized drug products using smart material inks. Int. J. Pharm. 567. https://doi.org/10.1016/j.ijpharm.2019.06.034.
TruTag Technologies. 2019. Brand Protection for Pharmaceutical + Nutraceutical. < https://trutags.com/pharmaceutical-nutraceutical/ > .
UNICRI. 2012. Counterfeit Medicine and organised crime. < http://www.unicri.it/topics/counterfeiting/medicines/report/Ctf_medicines_and_oc_advance_unedited2013.pdf > (accessed 5.8.19).
Ur Rehman, S., Ur Rasool, R., Ayub, M.S., Ullah, S., Kamal, A., Rajpoot, Q.M., Anwar, Z., 2011. Reliable identification of counterfeit medicine using camera equipped mobile phones. 8th Int. Conf High-Capacity Opt. Networks Emerg. Technol. HONET 2011, 273–279. https://doi.org/10.1002/pi.4602.
Vakili, H., Kolakovic, R., Genina, N., Marmion, M., Salo, H., Ihalainen, P., Peltonen, J., Sandler, N., 2015. Hyperspectral imaging in quality control of inkjet printed personalised dosage forms. Int. J. Pharm. 483, 244–249. https://doi.org/10.1016/j.ijpharm.2014.12.034.
Van Overschelde, O., Dinu, S., Guisbiers, G., Monteverde, F., Nouvellon, C., Wautelet, M., 2006. Excimer laser ablation of thin titanium oxide films on glass. Appl. Surf. Sci. 252, 4722–4727. https://doi.org/10.1016/j.apsusc.2005.07.147.
Vida, R.G., Fittler, A., Mikulka, I., Ábrahám, E., Sándor, V., Kilár, F., Botz, L., 2017. Availability and quality of illegitimate somatropin products obtained from the Internet. Int. J. Clin. Pharm. 39, 78–87. https://doi.org/10.1007/s11096-016-0398-y.
Weiss, T.L., Chun, H.J., Okada, S., Vitha, S., Holzenburg, A., Laane, J., Devarenne, T.P., 2010. Raman spectroscopy analysis of botryococcene hydrocarbons from the green microalga botryococcus braunii. J. Biol. Chem. 285, 32458–32466. https://doi.org/10.1074/jbc.M110.157230.
WHO, 2017a. Seventieth World Health Assembly Update, 29 May 2017, Who.
WHO, 2017b. WHO Global Surveillance and. Monitoring System.
WHO, 2017c. A study on the public health and socioeconomic impact of substandard and falsified medical products.
WHO. 2017d. 1 in 10 Medical Products in Developing Countries Is Substandard or Falsified. Who. < http://www.who.int/mediacentre/news/releases/2017/substandard-falsified-products/en/ > (accessed 11.7.18).
WHO IMPACT. 2006. Counterfeit Medicines: an update on estimates 15 November 2006.
Wilczyński, S., 2015. The use of dynamic thermal analysis to distinguish between genuine and counterfeit drugs. Int. J. Pharm. 490, 16–21. https://doi.org/10.1016/j.ijpharm.2015.04.077.
Steen, W.M. and Mazumder, J. 2010. Laser Material Processing, 4th ed. Springer.
World Health Assembly, 2017. WHO Member State Mechanism on Substandard/Spurious/Falsely-Labelled/Falsified/Counterfeit (SSFFC) Medical Products. Seventieth World Heal. Assem. A70 (23), 33–36.
You, M., Lin, M., Wang, S., Wang, X., Zhang, G., Hong, Y., Dong, Y., Jin, G., Xu, F., 2016. Three-dimensional quick response code based on inkjet printing of upconversion fluorescent nanoparticles for drug anti-counterfeiting. Nanoscale 8, 10096–10104. https://doi.org/10.1039/c6nr01353h.
Zanjal, S.V., Talmale, G.R., 2016. Medicine Reminder and Monitoring System for Secure Health Using IOT. Phys. Procedia. https://doi.org/10.1016/j.procs.2016.02.090.

International Journal of Pharmaceutics 605 (2021) 120793

Contents lists available at ScienceDirect

International Journal of Pharmaceutics

journal homepage: www.elsevier.com/locate/ijpharm

Anti-counterfeiting protection, personalized medicines – Development of 2D identification methods using laser technology

Krisztina Ludasi [a], Orsolya Jójárt-Laczkovich [a], Tamás Sovány [a], Béla Hopp [b], Tamás Smausz [b], Attila Andrásik [b], Tamás Gera [b], Zsolt Kovács [c,d], Géza Regdon jr [a,*]

[a] Institute of Pharmaceutical Technology and Regulatory Affairs, University of Szeged, Eötvös utca 6., 6720 Szeged, Hungary
[b] Department of Optics and Quantum Electronics, University of Szeged, Dóm tér 9., 6720 Szeged, Hungary
[c] Department of Experimental Physics, University of Szeged, Dóm tér 9., 6720 Szeged, Hungary
[d] Department of High Energy Experimental Particle and Heavy Ion Physics, Wigner Research Centre for Physics, Konkoly-Thege Miklós út 29-33., 1121 Budapest, Hungary

ARTICLE INFO

Keywords:
Falsified medicines
Identification
Anti-counterfeiting medicines
Personalized medicines
Laser marking
Unique laser coding

ABSTRACT

Counterfeiting of the products for healing is as old as trading, and it is difficult to quantify the magnitude of the problem. It is known that substandard and/or falsified (SF) medicines are a growing global threat to health, and they cause serious social and economic damage. The EU has a strong legal framework for medicines, it is mandatory to meet the requirements of Directive 2011/62/EU. Serialisation prevents SF medicinal products from entering the legal distribution chain. The present study is an extension of the original idea and aims to develop a laser technology-based method to mark an individual traceable code on the surface of the tablet, which technology can also be used for marking personalized medicines. The method is based on the ablation of the upper layer of a double-layer, differently coloured coating. The 2D code should be formed without harming the functional layer, and anyone with a smartphone integrated with a camera should be able to authenticate these drugs with a suitable application. The present findings confirmed that KrF excimer laser and Ti:sapphire femtosecond laser are efficient and reliable for marking. These should be promising candidates for pharmaceutical companies that would like to have additional protection against drug counterfeiters.

1. Introduction

Counterfeiting of the products for healing is as old as trading, dating back to 1495 BCE, when there was a hunt for genuine medicinal plants at the request of Queen Hatshepsut of Egypt because the market was full of worthless fakes (Brickell, 2001). In the 18th century, when malaria was still endemic in Europe, the continent was flooded with false cinchona bark used to treat fevers (WHO, 2017a).

Substandard and falsified (SF) medicinal products pose a growing threat to public health as they can deliver hazardous treatment or even cause death (Han et al., 2012a). Moreover, in health institutions physicians and pharmacists may not even be aware of patients buying medicines from uncertain or illegal sources, but these products are likely to influence the success of therapies (Fittler et al., 2018b). Bringing these drugs under control is a considerable challenge globally (Han et al., 2012a).

Substandard medicines are authorized medical products that fail to meet either their quality standards or specifications, or both, while falsified medical products are those that deliberately misrepresent their identity, composition or source (WHO, 2017b).

Some falsified medical products are almost visually identical to the genuine product and very difficult to detect. However, many can be identified (WHO, 2018). Possible techniques for detection: **visual analysis** (inspection of packaging condition, labelling, spelling mistakes, dosage units, expiry dates, or various product security features like watermarks, holograms or microprinting, etc.), **physical analysis** (observation of discolourations, surface investigations by microscopy, furthermore, evaluation of disintegration or dissolution measurements, etc.), and **chemical analysis** (classical chemistry or instrumental analysis such as spectroscopy, spectrometry, chromatography, etc.) (Davison, 2011; Roth et al., 2019).

The EU has a strong legal framework for medicines. At the end of the distribution chain, only licensed pharmacies and approved retailers are allowed to sell medicines, including legitimate sale via the Internet

* Corresponding author.
E-mail address: geza.regdon@pharm.u-szeged.hu (G. Regdon jr).

https://doi.org/10.1016/j.ijpharm.2021.120793
Received 10 March 2021; Received in revised form 4 June 2021; Accepted 7 June 2021
Available online 10 June 2021

(European Medicines Agency, 2018a). For EU Member States, since February 2019, it has been mandatory to satisfy the requirements of Commission Delegated Regulation (EU) 2016/161(European Commission, 2015) and Directive 2011/62/EU (The European Parlament and the Council of the European Union, 2011) of June 2011. Serialisation prevents SF medicinal products from entering the legal distribution chain. It involves tracing an individual product from the manufacturer through the wholesaler to the patient, by a unique 2D identification that is put on each box of prescription drugs. The 2D code should include the product code, the batch number, the serial number, the expiry date, and the national identification number if required by the Member State where the product is placed on the market (European Commission, 2015). In order to combat drug counterfeiting, pharmaceutical manufacturers and suppliers are working on adopting a worldwide standardized identification system (Trenfield et al., 2019).

The aim of this research is to support the regulation and to develop a technology for marking an individual traceable code directly on the surface of the medicine. Oral drug delivery is the most preferred and convenient route of drug administration (Viswanathan et al., 2017), and from among these, tablets are the most chosen pharmaceutical drug delivery systems. They are physically and chemically stable during storage, simple-to-use, have sustainable production and generally excellent content uniformity (Haaser et al., 2013). Therefore, tablets were chosen for marking in this study. The laser coding technology allows the authentication of tablets and avoids illegal repackaging.

For encoding, the Quick Response (QR) Code was chosen, which contains information in vertical and horizontal directions. It offers high-capacity encoding so it can hold a great volume of information. QR codes have different features and data capacities. Some have a maximum storing capacity of approximately 7000 figures (Denso Wave, 1994). They have an error correction capability that can restore data from a partially damaged code, and they offer omnidirectional reading. Because of these features, the QR code is suitable for encoding a high-level authentication capability (Han et al., 2012b). In the case of tablets, it is possible to encode in the QR code the name of the drug or information relevant to the patient, the usage, the dose, the ID of the producer and the batch number or the expiration date, etc. (Edinger et al., 2018). Further research is needed to determine the maximum information density of QR codes produced by the laser ablation technique on curved drug surfaces. In 2018, the European Medicines Agency (EMA) published a guideline on the use of mobile scanning and other technologies, such as QR coding in labelling and packaging of medicines (European Medicines Agency, 2018b).

If marking of individual tablets is aimed at or necessary, the following cases should be considered when laser coding is applied: if the tablets to be marked do not have a coating, at least one coloured layer should be applied to the drug so that the laser coding process can be performed on the surface. In cases when tablets have a coloured coating (for example, for improved swallowability or identification purposes), that layer could be marked. When a functional coating is needed because of the therapy, an extra coating is required on top of it to enable marking without the loss of coating functionality.

In our previous study, the results demonstrated that marking functional coatings by ArF 193 nm excimer laser caused no structural damage in the treated films (Ludasi et al., 2018), although titanium dioxide particles remained in the film during ablation. Those white particles made the accurate reading of the QR codes difficult due to the reduced contrast. To eliminate the problem, naturally coloured coatings were used (Ludasi et al., 2019). That solution seemed to work, but since most coatings contain titanium dioxide for better coverage and/or improved photostability, it would greatly restrict the use of this method. So, another solution had to be found. Each material has an ablation threshold, and for successful marking, the threshold value of the material has to be exceeded (Kannatey-Asibu, 2009). The ablation threshold of a substance is determined by several parameters, which are mostly related to the laser beam. These include the repetition rate of the laser (Hz), wavelength, pulse energy and duration, energy density and the absorption properties of the substrate. By selecting the proper laser parameters, the desired ablation depth can be achieved (Elliott, 1995). To solve the difficulty with titanium dioxide, other types of lasers were tested in this study. In the first case, a KrF excimer laser with a higher wavelength (248 nm) (hereinafter: UV248) was chosen, as it was known from previous experience that the excimer laser was safe. Also, the laser exceeded the ablation threshold of titanium dioxide at the wavelength of 248 nm known from the literature (Van Overschelde et al., 2006). In the second case, a near-infrared (800 nm), short pulse femtosecond laser was used. The assumption was if the pulse is ultrashort, the heat effect is negligible, and no or just little chemical or thermal damage occurs during the removal of the material. In addition, it can create very fine structures, it is more accurately adjustable, faster and also cleaner (Steen and Mazumder, 2010).

In the present experiment, tablets (white) were coated with 2 layers of differently coloured coatings. The transparent bottom layer was the functional one, while the red-coloured top layer was applied to enable marking. The 2D codes were drawn by ablating specific parts of the upper coating layer. Anyone with a camera-enabled phone and a suitable application should be able to authenticate these drugs. In addition, as for healthcare it is increasingly important that each patient receive personalized drug therapy instead of a ‘one-size-fits-all’ treatment (Ayyoubi et al., 2021), these codes could be used as a label in personalized medicine.

We would like to emphasize that, in addition to all kinds of protection and coding, the most important strategy that can be adopted for the patients’ safety is to organize communication and education campaigns to inform them and to educate the public on the safe use of Internet pharmacies. People must be taught to be able to differentiate between legal and illegal medication suppliers (Fittler et al., 2018a). Mobile phone applications that recognize information encoded on tablets can dramatically reduce the time for education, especially for the upcoming generation.

2. Materials

2.1. Tablet core and coating materials

The active ingredient of the model tablet was Ibuprofen DC 85 (Ibu, BASF, Germany) 16.66% (w/w), and excipients: microcrystalline cellulose (Vivapur 102, JRS Pharma, Germany) 74.33% (w/w), crospovidone (Kollidon CL-M, BASF, Germany) 5% (w/w), talc (Molar Chemicals, Hungary) 3% (w/w) and magnesium-stearate (Molar Chemicals, Hungary) 1% (w/w) were used as received.

The shape of the tablets was as follows: Nr1 type: round with flat surface and no break line on it (diameter: 12 mm, crown height: 4.1 mm, average weight: 600 mg). Nr 2 type: round with flat surface and no break line on it (diameter: 10 mm, crown height: 3.1 mm, average weight: 300 mg). Nr 3 type: round with flat surface and no break line on it (diameter: 10 mm, crown height: 4.8 mm, average weight: 500 mg).

Placebo tablets were also used as coating aid for reasons of saving time and material. The placebo tablets were round with biconvex surface and had no break line on them (diameter: 10 mm, crown height: 4.2 mm, average weight: 350 mg).

The first (functional) film-forming agent was an aqueous-based enteric coating dispersion: Eudragit L30 D55® (Evonik Nutrition & Care, Germany). The second film-forming substance was a hydroxypropyl–methylcellulose (HPMC)-based coating formula, Sepifilm PW Red (Seppic S.A., France).

3. Methods

The ingredients of the tablet were homogenized with a Turbula mixer (Willy A. Bachofen Maschienenfabrik, Switzerland) for 8 min, and 2 min after the addition of the lubricant. The homogenous powder

mixture was compressed with a Korsch EK0 (E. Korsch Maschienenfabrik, Germany) single punch eccentric tablet press.

3.1. Coating procedure

330 g of placebo tablets and 70 g of API (Active Pharmaceutical Ingredient) containing tablets were coated together at the same time in order to save material and time.

Eudragit® L30-D55 aqueous polymer dispersion was prepared. It consisted of 16.76% w/w dry substance of a methacrylic acid - ethyl acrylate copolymer with a ratio of 1:1 (dispersion 30% w/w) (Evonik Nutrition & Care GmbH), PlasAcryl® HTP 20 (Evonik Nutrition & Care GmbH) 2.9% w/w dry substance was added to the dispersion as plasticizer/anti-tacking agent and distilled water 1 h before coating.

The aqueous HPMC coating solutions consisted of 20% w/w dry substance in the case of Sepifilm™ PW Red coating system. According to the supplier's recommendation, they were dispersed in purified water. The total mixing time took 45 min, followed by sieving the dispersion through a 0.5 mm sieve.

Spray coating was performed in a 4 M8 Pancoat (ProCepT, Belgium) perforated coating pan. 2 layers of coatings were put on the tablets. The first layer was Eudragit L30 D55. A 0.8 mm spray nozzle was used for the application of the atomised spray coating solution for 75 min, with an atomising air pressure of 1.0 bar, a spray rate of 3 g/min and an air flow rate of 0.70 m^3/min. The drying and cooling process lasted for 15 min. Other coating parameters are shown in Table 1.

The second layer was the HPMC-based ready-to-use coating formula. A 0.8 mm spray nozzle was used for the application of the atomised spray coating solution for 45 min in the case of Sepifilm PW coating, with an atomising air pressure of 2.0 bars, a spray rate of 2 g/min and an air flow rate of 0.70 m^3/min. The drying and cooling process lasted for 15 min. Other coating parameters for the second layer are shown in Table 2.

The final coating thickness was measured with a stereomicroscope (Zeiss, Germany). Measurements were performed at a magnification of 500. After calibration, 4–4 tablets were examined, which were cut in half along the middle of the tablet band, and each was measured at 10 places and averaged.

3.2. Irradiation of coated tablets

2 different types of lasers were used for the irradiation of the tablets. The experimental setup for the laser processing is outlined in Fig. 1.

KrF excimer laser (UV248) was used for the UV-regime ablation, a twin-tube hybrid dye-excimer laser-system (Szatmári, 1994, Szatmári and Schäfer, 1988). The current laser setup produced 60 mJ laser pulses with a pulse length of 700 fs. The central part of unfocused 4 cm × 4 cm pulses was cut out by an aperture 2 cm in diameter and the remaining pulses were attenuated with dielectric coated plates to about 1–2 mJ in order to avoid plasma formation in the air. The parameters of irradiation using excimer laser were the following: wavelength: 248 nm, energy: 0.5 mJ, number of impulses: 10, spot size: 100 μm, FWHM: 700 fs, fluence: 6.37 J/cm^2.

Ti:sapphire Femtosecond laser (Femto), operating in the TeWaTi laser lab at the University of Szeged (TeWaTi, 2019) provided amplified pulses with a repetition rate of 200 Hz and maximum pulse energy of 1 mJ. An achromatic lens with a focal length of 150 mm focused the beam onto the target placed into the focal plane, allowing beam imaging of f/19 (F-number) and processing of the target surface with 135 fs pulses. Irradiation of tablets using Femto laser: wavelength: 800 nm, energy: 0.62 mJ, number of impulses: 20, spot size: 110 μm, FWHM: 135 fs, repetition rate: 200 Hz, fluence: 6.52 J/cm^2.

A computer-controlled, movable desktop, a motorized translator was created to be able to change the position of the tablet during lasering (Fig. 1). The QR code was ablated hole by hole. During UV248 laser ablation, the oval-shaped holes in the film followed the shape of the beam. It took 1.5–2 h to create such a code with the UV248 laser and 10 mins with the Femto laser.

Table 1
Coating parameters of Eudragit L30 D55.

Step	Inlet air temperature (°C)	Exhaust air Temperature (°C)	Tablet temperature (°C)	Drum speed (rpm)
Warm-up	60		Until 50	3
Coating	45–55	40–45	30–35	15
Drying	50	38–40	35–37	3
Cooling	25	25	25	3

Table 2
Coating parameters of Sepifilm films.

Step	Inlet air temperature (°C)	Exhaust air Temperature (°C)	Tablet temperature (°C)	Drum speed (rpm)
Warm-up	60		Until 50	3
Coating	55	40–42	35	9
Drying	40	30	27	3
Cooling	25	25	25	3

3.3. Surface profilometer

Veeco, Dektak 8 Advanced Development Profiler® was used for profilometry measurements. The tips employed had a radius of curvature ~2.5 μm, and the force applied to the surface during scanning was ~30 μN. The horizontal resolution was 0.1–0.13 μm, and the vertical resolution was 40 Å. Dektak software (Microsoft® Windows XP®: interactive data acquisition) and Vision® 32 software (data processing, 2D and 3D image analysis) were used for data evaluation (Veeco Instruments Inc., New York, USA).

3.4. Determination of the ablation threshold

The characteristics of the ablation holes were examined with a surface profilometer. The laser parameters required for ablation were determined from the data obtained using a profilometer according to the method described below.

The ablation threshold indicates the minimal laser energy required to remove the material from the substrate (i.e., tablet surface). The threshold value is a fundamental parameter for laser fine-tuning. In most of the cases, the laser operates close to the threshold but with slightly higher energy to avoid unwanted side effects, such as the thermal distortion of the material. The final etching depth is controlled by the number of laser impulses and not by fluence (Lawrence, 2010).

As the spatial distribution of fluence was different for the two laser types (homogeneous flat top and Gaussian), two different methods were applied to determine the corresponding ablation threshold.

The first method is based on the measured ablation rate (ablation depth per number of laser impulses). The ablation rate shows a logarithmic correlation with the applied fluence (impulse total energy per unit surface area) close to the threshold. The $l = (1/\alpha)\ \ln(F/F_{th})$ logarithmic function was fitted to the measurements by using nonlinear least-squares (NLLS) Marquardt-Levenberg algorithm in this case.

The second method is based on the measured ablation diameter. The linearized model log(energy) versus estimated impact surface was used in this case to calculate the zero crossing by fitting the linear trend to the measurements.

Fig. 2 summarizes the threshold calculation results for the UV248 laser. Only the first method was used for threshold estimation in this case. Fig. 3 shows the results for the Femto laser, where the second method was used for threshold estimation in two measurement sessions.

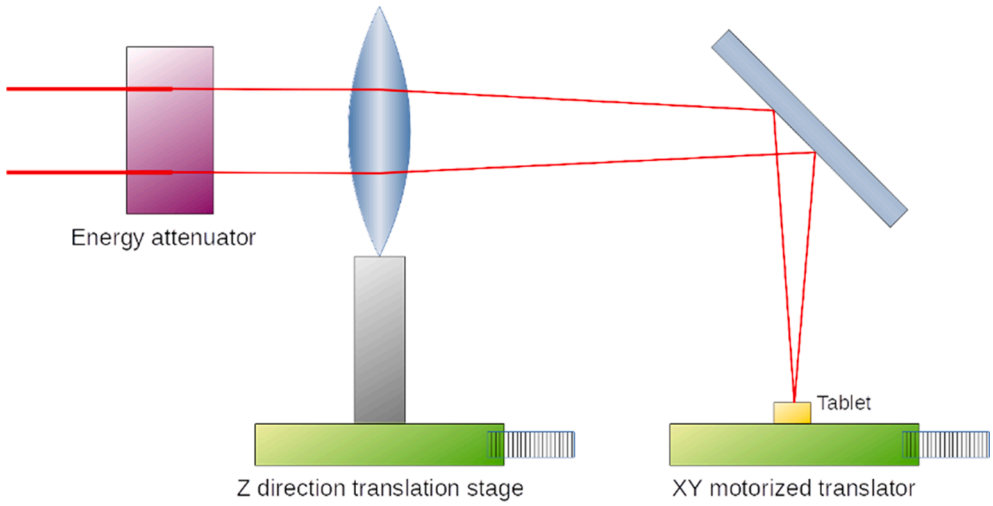

Fig. 1. Experimental setup for laser processing. The tablet position was adjusted with a motorized XY translator during the QR code engraving. The Z direction translator stage was used to set the focus plane precisely on the surface of the tablet.

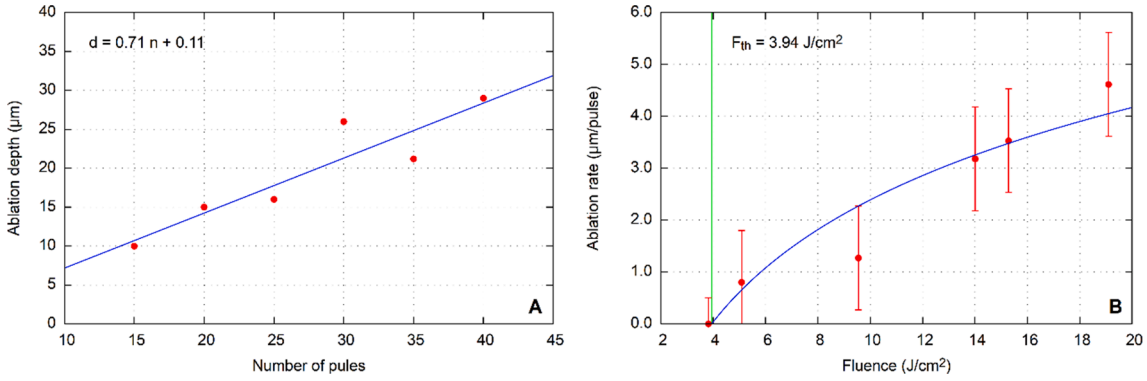

Fig. 2. UV248 laser ablation threshold determination. A: Ablation depth estimation based on the number of the applied laser pulses. B: Threshold calculation result based on ablation depth by using logarithmic model fit.

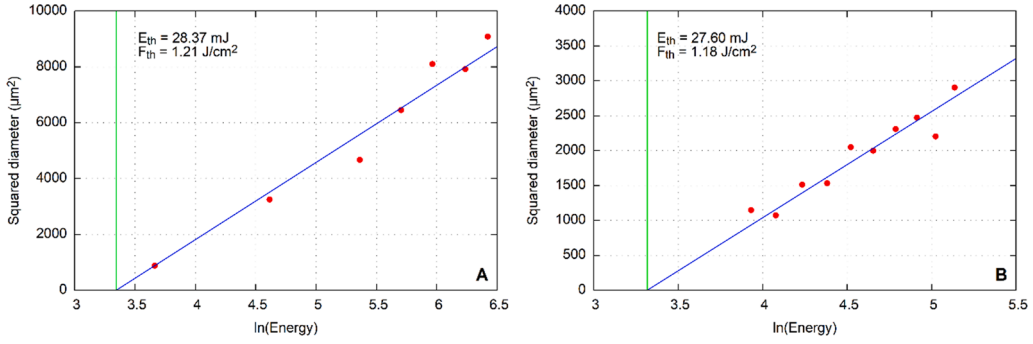

Fig. 3. Femto laser ablation threshold determination. A, B: Threshold calculation result based on ablation diameter using a linearized model. Diagrams A and B represent two measurement sets with different pulse energy ranges.

3.5. Scanning electron microscope (SEM)

The ablated tablet was observed by using a scanning electron microscope (SEM, Hitachi, Japan S4700). The tablets were mounted rigidly on a specimen holder with a double-sided carbon adhesive tape and a conductive ultrathin golden layer was deployed on them with a sputter device (Polaron, UK). The measurements were performed at a magnification of 30–5000, applying 10.0 kV electron energy and 1.3–13 MPa air pressure.

3.6. Raman spectra

Raman spectroscopy was used for the examination of the tablets treated by lasers. Spectra were acquired with a Thermo Fisher DXR Dispersive Raman spectrometer (Thermo Fisher Scientific Inc., MA, USA), a diode laser operating at a wavelength of 780 nm and equipped with a CCD camera. Raman measurements were carried out with a laser power of 4 mW (Ibu) and 12 mW (Eudragit L30 D55, Sepifilm PW Red) at a slit aperture size of 25 µm. The spectra of the tablets treated by lasers were collected by using an exposure time of 6 sec, and 10 spectra were

averaged in the spectral range of 3200–200 cm^{-1} with cosmic ray and fluorescence corrections.

Raman chemical mapping was also performed with the same equipment. Spectral data were collected on the surface of the lasered tablet, and on the fracture surface of the halved tablet, including the treated and the intact region, too. The spectra were determined at certain points in a defined area, while the sample had a translational motion between each discrete measurement. The point scan system measures each spectrum individually at a series of predefined points. The chemical map was profiled to the spectra of Eudragit L30 D55 and to the spectra of Sepifilm PW Red. In the case of Ibu, profiling was made to the peak at 1604 cm^{-1} because it was found to be the most typical for the API, and it was the most separated from the spectra of the other investigated components.

Furthermore, sample analyses were performed on the cross-section surface of both types of laser-treated tablets (10 points directly below the lasered coated surface and 10 points in the core of the lasered tablets). The mean of these 10 spectra was compared with the mean of the 10 spectra taken from the core of the untreated tablet and the spectrum of Ibu. These averaged spectra were normalized to peak 1604 cm^{-1} of the Ibu spectrum.

Data was evaluated with Spectragryph - optical spectroscopy software (F. Menges, 2020).

3.7. In vitro drug disintegration

In the disintegration studies, the tablets were tested according to the standard method of the European Pharmacopoeia with an Erweka model ZT71 apparatus (Erweka, Germany). First, 900 ml of artificial enzyme-free gastric juice (pH = 1.22) was preheated and maintained at a temperature of 37 ± 0.5 °C. According to the guideline, enteric coating should be intact for 2 h in acidic media. After 2 h, the medium was changed to a phosphate buffered saline solution (pH = 6.82). The time necessary for each tablet to disintegrate in acidic and intestinal solution was recorded automatically by the apparatus.

3.8. In vitro drug dissolution

In the present study, the investigation of drug release kinetics from marked tablets was carried out with an Erweka DT 700 (Erweka GmbH, Germany) dissolution tester according to the standards of the European Pharmacopoeia. A rotating basket method was used for the dissolution tests, where the rotation speed was 100 rpm, the dissolution medium was 900 ml of artificial enzyme-free gastric juice (pH = 1.22) for 2 h, and then it was replaced with 900 ml of phosphate buffered saline solution (pH = 6.82) for 1 h. The pH value was checked with a pH meter. The temperature was maintained at 37 ± 0.5 °C. As a sample, 5 ml of the dissolution medium was taken manually at predetermined intervals without being replaced. Medium loss was not taken into account during the calculations. Samples were filtered through a 10 μm Poroplast filter (Erweka, Germany). The absorbance of ibuprofen DC85 was analyzed at 222 nm, using a spectrophotometer (Genesys 10S UV–VIS, Thermo Fisher Scientific Inc., MA, USA). Four tablets were tested, and samples were taken at the following time intervals: at 120 min in the case of gastric juice, and after changing to intestinal fluid at 5, 10, 15, 30, 45 and 60 min.

4. Results and discussion

The present study focuses on demonstrating the effectiveness of a QR code-based authentication process of film-coated tablets, from the formulation of the QR-coded tablets by laser ablation to the decoding step using a QR code reader application on a smartphone.

The primary focus was on removing the titanium dioxide particles that remained in the film during previous ablation studies (Ludasi et al….) by comparing the effectiveness of two different types of lasers in marking. The 2D codes were formed by removing particular parts of the upper coloured coating. After marking, a detailed quality analysis was made to check if any change occurred in the quality of films or in the API during the laser intervention. Also, the disintegration and dissolution of the lasered products were investigated to confirm that it was possible to mark the tablets with functional coating without damaging them during the procedure.

4.1. Microscopic analysis of the coated surface

The QR code (Fig. 4A) that was lasered on the tablets was generated by the QR code generator library libqrencode. (Fukuchi, 2020). A simple code (with content: 12345678) was made as the secondary aim was to find out if it was possible to ablate a decodable QR code on the surface of the tablet by these lasers. Further research is being done on how much information can be encoded in a QR code of a given size to keep the decoding accuracy.

The present study confirmed that titanium dioxide particles did not interfere with decoding when coding had been done by UV248 or Femto lasers. The QR codes applied on the tablets are readable by a smartphone with QR code scanner applications downloaded from the Internet, for example, with QRbot (https://qrbot.net/) or with the photo mode of the mobile phone. The only requirement is that the application must be able to read the “inverse” QR code (Fig. 4B), as in this case the tablet is coloured and the ablated part is white, just the opposite of the usual QR codes.

The results of the UV248 laser treatment are seen in Fig. 5. It can be observed through visual inspection that the 5 × 5 mm QR code is made up of dots.

It is known that a usable QR code can also be created by not overlapping parts, such as dots. The UV248 laser-ablated oval-shaped holes in the film were in accordance with the shape of the beam. It was possible to make a readable code from oval-shaped holes, too, even in cases where laser irradiation was not perfect, as the code has error correction capability that can restore the missing data, as seen on the ablated QR code that is made up of individual points (Fig. 5B,D). Better coverage can be obtained by overlapping the holes, which results in a more readable code. Nevertheless, care must be taken not to punch through the Eudragit layer. The depth of ablation can be controlled by changing the number of pulses on the sample place or the fluence, which allows the accurate setting of the penetration depth to the coating layer. It took 1.5 and 2 h to create such a code by the UV 248 laser depending on whether there was an overlap between the holes or not. Fewer shots mean faster but still effective marking.

The same computer-controlled movable desktop was coupled with the Femto laser to mark the tablet, as in the previous case. At this time, the shape of the beam was round, thus the ablated holes were too, and they overlapped, as shown in Fig. 6. The ablation of the QR code took about 10 min, as the most important limiting factor of overall ablation is the repetition rate of the laser. Therefore, the higher frequency (200 Hz) of the Femto laser dramatically shortens the marking procedure.

Fig. 7A–C displays the scanning electron micrographs of the 4 × 4 mm QR code on the tablet treated by the UV248 laser.

Fig. 7A shows a part of the QR code on the tablet surface, and it is

Fig. 4. Sample QR code ablated on the tablet. A: The common form of the QR code. B: The inverse of the QR code ablated onto the coloured tablet. C: The same QR code but made of dots, prepared for laser and desktop control.

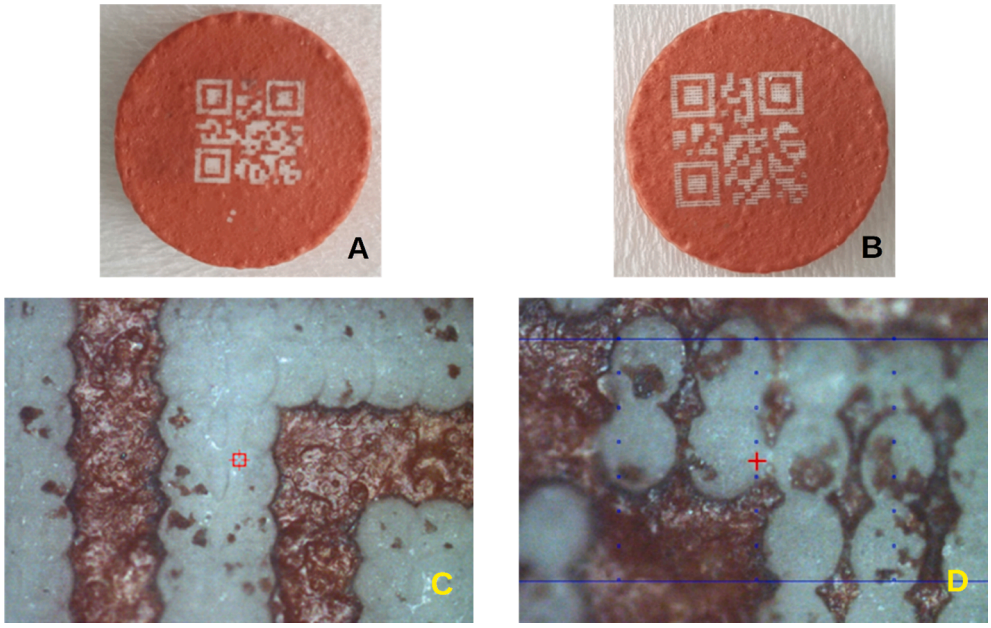

Fig. 5. Tablet encoded by UV248 laser. A: The size of the QR code is 4 × 4 mm. B: The size of the QR code is 5 × 5 mm. C: Microscopic picture of the 4 × 4 mm QR code. D: Microscopic picture of the 5 × 5 mm QR code.

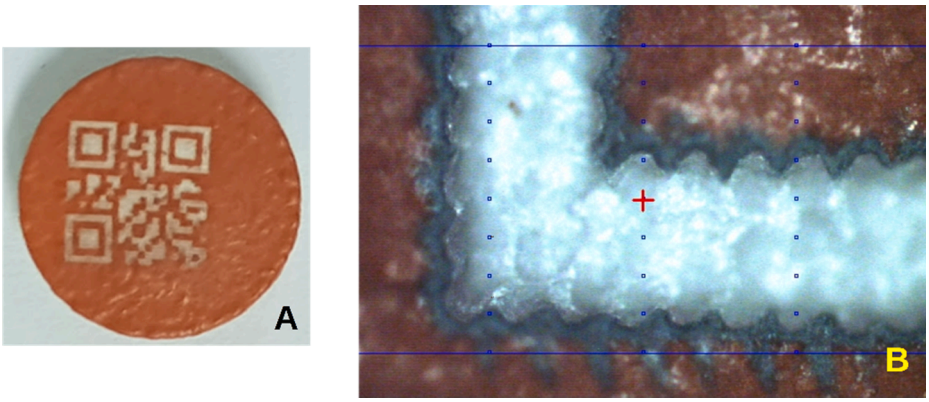

Fig. 6. Tablet encoded by Femto laser. A: Visible to the naked eye. B: Microscopic picture.

clearly visible that it is made of overlapping dots, as described above. The holes are deeper at the overlapping parts. It can also be seen that the surface of the untreated coating is uneven, and the holes visible on the untreated surface may have remained from the bubbles formed during the coating process due to too quick drying since the air did not have time to diffuse out. Fig. 7B displays the lasered tablet surface at greater magnification. The holes in the ablated surfaces could also have resulted from bubble formation. Fig. 7C shows the cross-section surface of the tablet, where the place of lasering is seen in the framed part. The glossy part on the top of the tablet is the PW red coating, which is about 5–10 μm thick. The bottom coating, which is 60–70 μm thick, seems to be intact. The ablated surface of the sample has no large damage. Only a physical change is observed in the structure as a result of the removal of the coating by the UV248 laser, and no obvious sign of chemical change is detected.

Fig. 7D-G displays the micrographs of the Femto lasered tablet. In Fig. 7D, a part of a QR code is seen on a halved tablet. The dots which compose the QR code are clearly visible. The penetration depth seems to be greater with the Femto laser than with the UV248. In Fig. 7E the lasered surface is visible at higher magnification, where intact regions may be identified between the holes. Fig. 7F shows one hole at higher magnification. At the bottom of the ablation cavity a different material is detected, which is thought to be the functional coating because of its different, more porous structure. The laser penetration here seems to have taken place right up to the bottom of the coating. In Fig. 7G, the cross-section surface of the halved tablet is seen. The tablet was fixed to the holder upside down. The ablation area is visible in the framed part. The Femto laser removed the upper coating, which is about 50 μm thick, and in some places, the laser also penetrated into the functional Eudragit coating. Nevertheless, because its thickness is about 150 μm, functionality may still be intact despite its partial absence.

Similarly to the UV248 laser, it may be seen that the Femto laser did not cause considerable damage in the coating structure during the treatment, either. Only a physical change may be detected in the ablated area, fragments of the coating film are visible where the coating was removed. No visible sign of chemical changes was detected in the upper or in the bottom layer. Overall, it can be stated that no visible chemical change occurred on the treated surface when using either of the two lasers.

4.2. Disintegration test

In the disintegration studies, six pieces of coated and ablated tablets were tested from tablet type Nr 3. The tablets remained intact during the

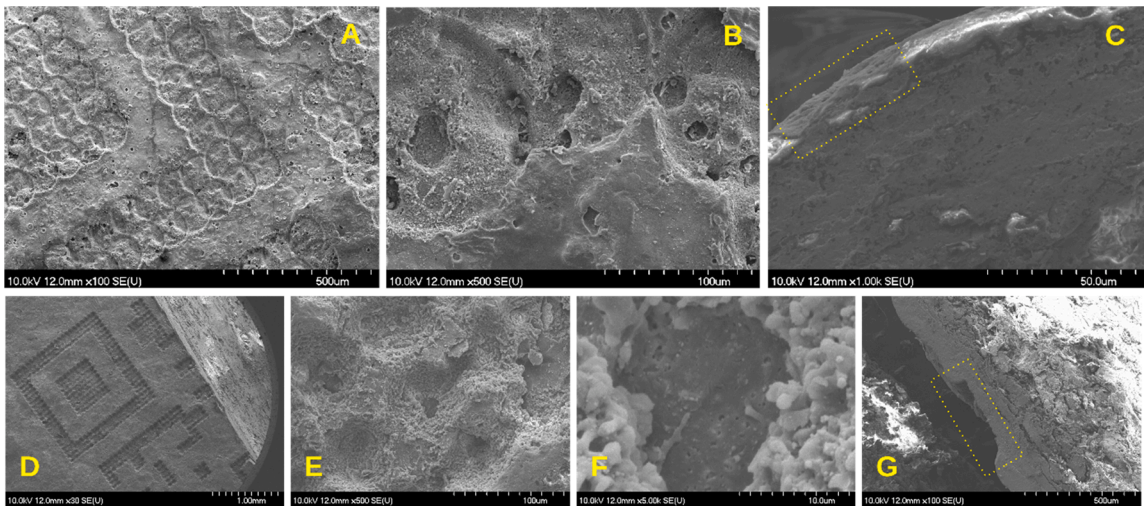

Fig. 7. SEM micrographs of laser-treated tablets. First row: Films A, B, C treated by UV248 laser. A: Tablet surface at a magnification of 100×. B: Tablet surface at a magnification of 500×. C: The tablet's cross-section surface at a magnification of 1000×. Second row: Tablets D, E, F, G treated by Femto laser. D: Tablet surface at a magnification of 30×. E: Tablet surface at a magnification of 500×. F: Ablation hole at a magnification of 5000×. G: The tablet's cross-section surface at a magnification of 100×. C,G: The place of lasering is shown in the framed section.

2-hour disintegration process in the artificial enzyme-free gastric juice, which corresponds to the result expected according to the European Pharmacopoeia, as they had a gastro-resistant coating. After changing to the intestinal fluid, the disintegration test was complete in 30 min for all tablets. This result confirmed our preliminary conclusion based on SEM analysis, according to which the lasering of the upper coating left the functional coating in the bottom intact, and it is possible to mark functionally coated tablets.

4.3. *In vitro drug dissolution test*

For in vitro drug dissolution tests, tablets of different shapes were used: A: Type Nr1, B: Type Nr2, C and D: Type Nr3. Three of the investigated tablets remained intact after 120 min in the gastric medium. The amount of the dissolved API was 0.15%, 2.12%, and 0.92%, for A, C and D, respectively, while the dissolved API was 35.2% for Tablet B, which partially disintegrated during this period.

In order to save time and material, the differently shaped API containing tablets were coated together with placebo tablets. Presumably, due to their different geometry, they were mixed inappropriately during coating, therefore they might have different coating thicknesses. Tablet coating thickness may also vary in the case of identical tablets, as observed by M. Wolfgang et al., where it varied between 56.3 μm and 86.9 μm (Wolfgang et al., 2019). The literature also confirms that the shape of the tablet directly influences intra-tablet coating uniformity. The most likely reason for intra-tablet coating variability is the preferred orientation of tablets when passing through the spray zone of the coater (Wilson and Crossman, 1997). There was another investigation of inter-tablet coating layer thickness, where a comparison of both sides of the tablet surface was made. It shows that the thickness of the coating layer of some tablets on one side of the tablet is up to 10 μm thicker than on the other one (Ho et al., 2007). Achieving a high level of intra-tablet uniformity is especially important for functional film coatings (Dong et al., 2017), where uniform thickness is required to guarantee the desired drug release rate to the patient (Sacher et al., 2019). In the present study, it can be assumed that in the case of tablet B, the coating was thinner and had been damaged during the marking. It is likely that if only tablets of the same shape are coated at a time, the layer thickness will be more uniform and the inner, functional layer can be protected from damage.

The dissolution profile of the tablets in phosphate buffered saline solution is shown in Fig. 8. It can be concluded that during the one-hour

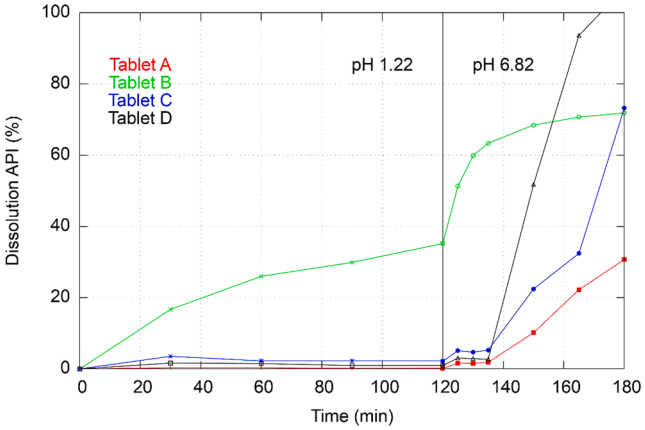

Fig. 8. Drug dissolution curves of the 4 coated and lasered tablets.

in vitro studies, the tablets acted in accordance with pharmacopoeial standards and the disintegration and dissolution process started. It is seen that the dissolution of tablet B started earlier than that of the others, and the final concentration was lower. The explanation for this phenomenon is that the dissolution of tablet B had already started in the gastric medium.

4.4. *Coating film thickness*

To confirm the assumption that not only the inter-tablet but also the intra-tablet variability of final coating thickness is spread over a wide range, microscopic film thickness measurement was applied. Fig. 9 shows the difference in the thickness of the coating on the top and on the side of the tablet. Coating thickness averages measured on different tablets, determined on the basis of measurements at 10 places of 4–4 half tablets, are presented in Table 3.

4.5. *Raman*

Finally, to confirm that the ablation process causes no chemical change, a dispersive Raman spectrometer was used to detect possible changes in the coated tablets. Chemical mapping was chosen to determine if there was a laser-induced change in the coating layers or in the

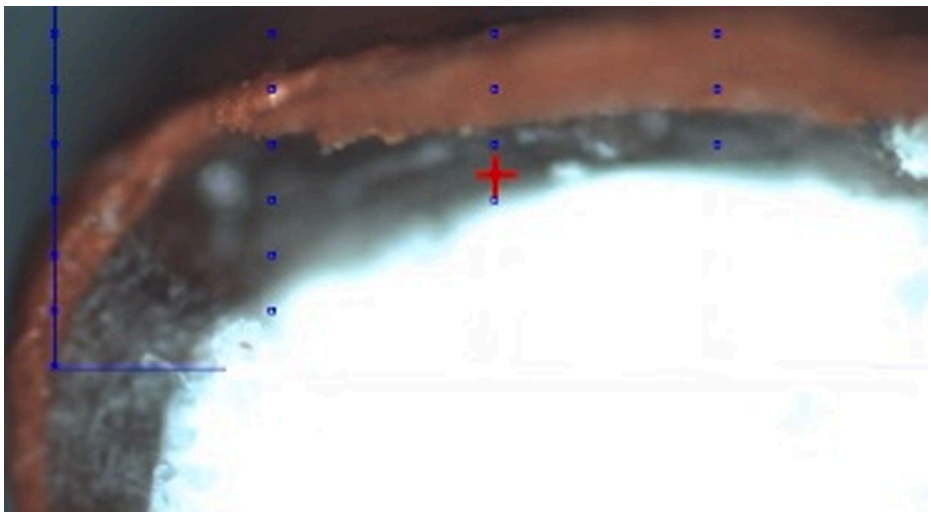

Fig. 9. Uneven thickness of tablet coatings.

Table 3
Thickness of the different coatings.

	12 mm diameter round flat tablet (600 mg)	10 mm diameter round flat tablet (300 mg)	10 mm diameter round flat tablet (500 mg)
PW red coating thickness (μm)	49.43 ± 9.23	16.19 ± 9.19	88.02 ± 18.98
	63.12 ± 14.72	61.78 ± 14.67	95.42 ± 13.45
	59.31 ± 11.82	34.81 ± 11.76	73.26 ± 22.65
	76.75 ± 13.98	45.78 ± 14.56	69.76 ± 16.54
	182.34 ± 22.44	79.62 ± 17.79	155.45 ± 19.57
Eudragit coating thickness (μm)	145.93 ± 29.54	123.65 ± 29.67	98.02 ± 23.77
	204.54 ± 17.57	97.43 ± 23.65	136.23 ± 29.76
	163.78 ± 32.23	134.75 ± 36.76	102.43 ± 13.65

API in the core during marking. The examination was done on the surface of the lasered tablet and on the fracture surface of the halved tablet. The chemical map was profiled based on the spectra that are summarized in Fig. 10. The full spectrum was applied for raw free films (Eudragit L30-D55, Sepifilm PW Red) and a single peak (1604 cm^{-1}) for the API Ibuprofen DC85.

Figs. 11–14 present the data of the obtained chemical maps. Part "A" of the figures shows the microscopic mosaic photo of the laser-treated region, the chemically mapped area is framed with a blue or a red line. The spectra were collected from places marked by blue or red points. The other parts of the Figures show chemical maps, where "B", "C" and "D" show the profiling result of the Eudragit, Ibu and PW red film, respectively. In these maps, warm colours show a higher concentration of the profiled materials. Profiling of the PW red spectrum was performed only for tablet cross-sections.

The UV 248 nm laser-treated tablet surface is presented in Fig. 11 and Fig. 12. The results confirm that the PW red upper layer (Fig. 12D) was completely ablated in the places that were lasered. Based on Fig. 11C, it can be assumed that the laser had reached the API because

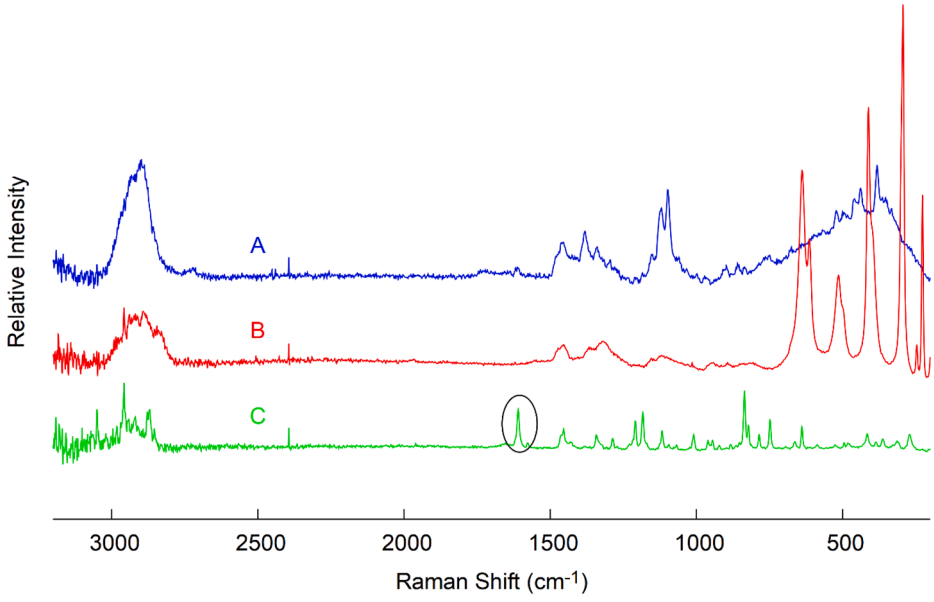

Fig. 10. Raman spectra of film coatings and the API. A: Eudragit L30-D55, B:Sepifilm PW Red, C: API Ibuprofen DC85. Chemical map profiling was performed on spectra A, B and a single peak, which is circled on the spectrum C (1604 cm^{-1}). (For interpretation of the references to colour in this figure legend, the reader is referred to the web version of this article.)

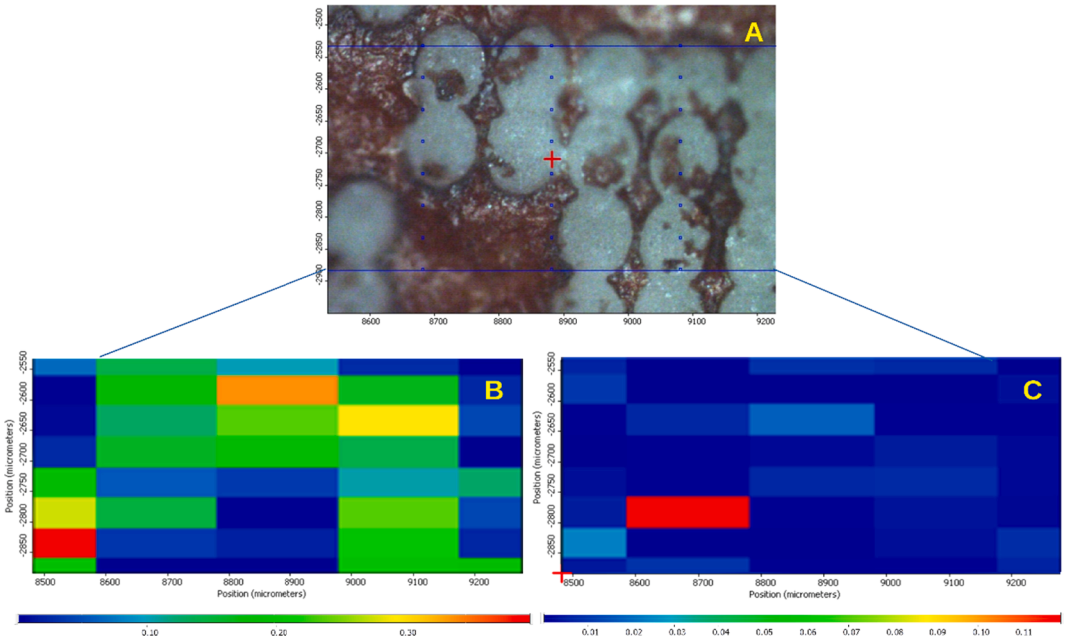

Fig. 11. Surface of the tablet treated by UV248 laser. A: Microscopic picture of the surface of the lasered tablet. B: Chemical map profiled to Eudragit L30-D55. C: Chemical map profiled to Ibu.

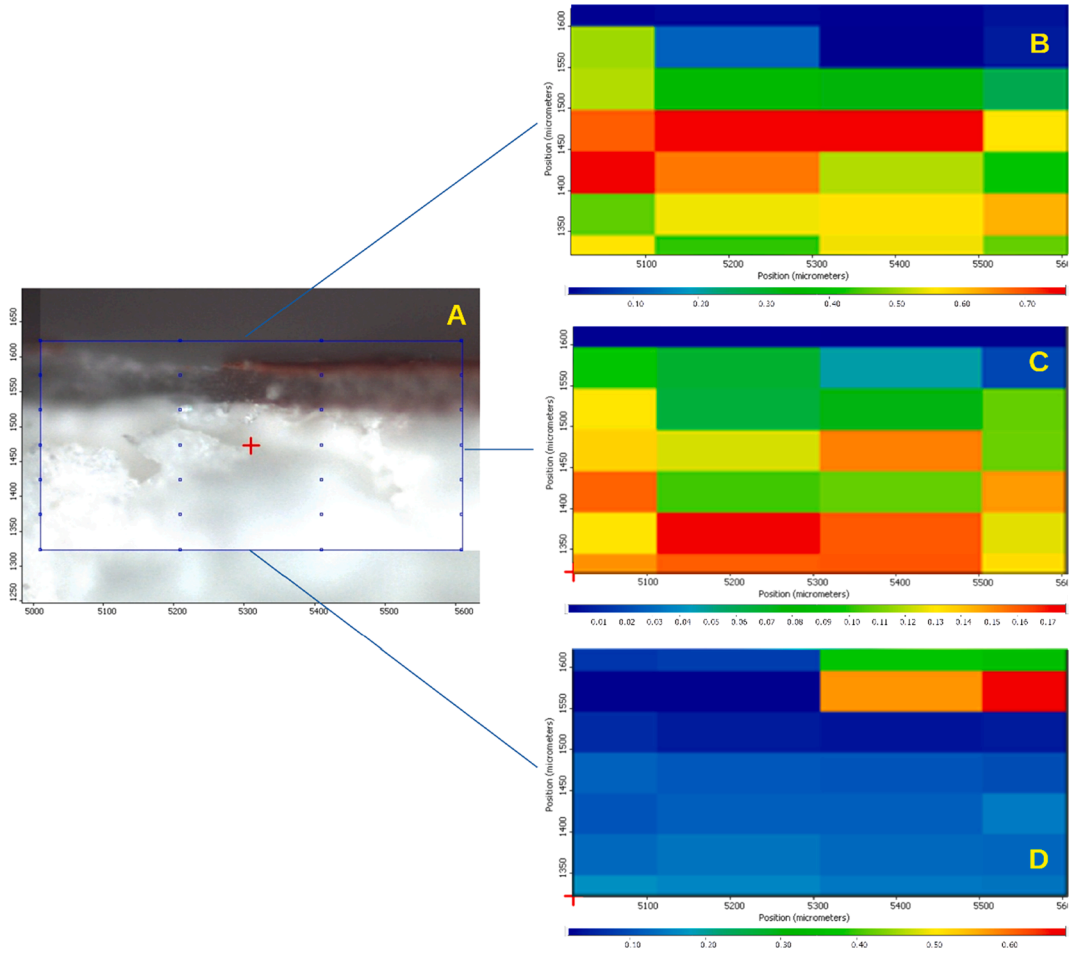

Fig. 12. Fracture surface of a tablet treated by UV248 laser after halving. A: Microscopic picture of the fracture surface of the lasered tablet. B: Chemical map profiled to Eudragit L30-D55. C: Chemical map profiled to Ibu peak. D: Chemical map profiled to Sepifilm PW red. (For interpretation of the references to colour in this figure legend, the reader is referred to the web version of this article.)

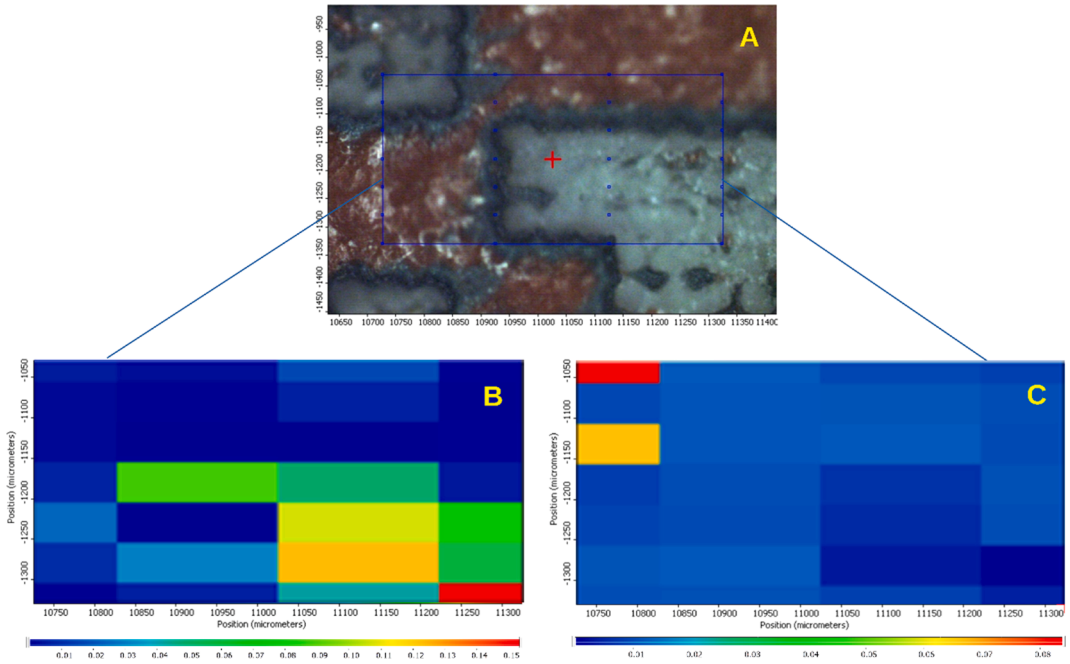

Fig. 13. Surface of the tablet treated by Femto laser. A: Microscopic picture of lasered tablet. B: Chemical map profiled to Eudragit L30-D55. C: Chemical map profiled to Ibuprofen.

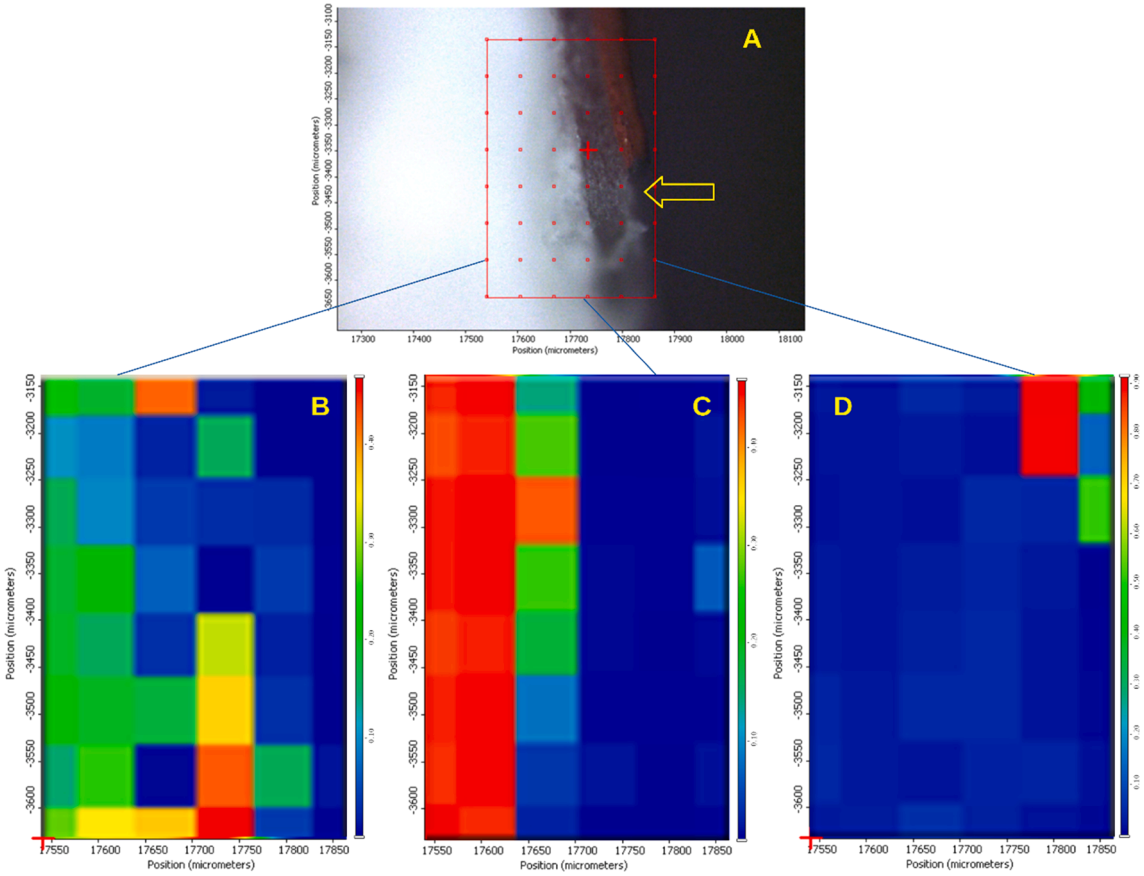

Fig. 14. Cross-section surface of the Femto laser treated tablet. A: Microscopic picture of the halved tablet, arrow pointing at the missing PW red coating. B: Chemical map of the tablet surface profiled to Eudragit L30-D5. C: Chemical map of the tablet surface profiled to Ibuprofen. D: Chemical map of the tablet surface profiled to Sepifilm PW red. (For interpretation of the references to colour in this figure legend, the reader is referred to the web version of this article.)

the thickness of the coating was not consistently even, and furthermore because the API might have penetrated into the Eudragit coating (Fig. 12C).

Fig. 13 and Fig. 14 display the tablet surface and the cross-section of Femto laser-treated tablets, respectively. In Fig. 13B Eudragit is seen in the laser-treated areas, while in Fig. 13C the warm colours show the API Ibu, which suggests that the coating thickness was not consistently even, and the laser might have reached the API or penetrated into the coating in this case as well.

In Fig. 14A the arrow points to the missing PW red coating, and the mapping (Fig. 14D) confirms that it was ablated by the laser. The profiling shows that the API is mostly in the tablet core (Fig. 14C), but in the same picture, the area of the inner coating is green, which means that the API partly migrated from the tablet core to the Eudragit film. According to the literature, such migration during the coating process can happen if the coating is aqueous-based. Migration is enhanced if a component is soluble in the coating solution, and it also depends on the spray conditions used during the coating operation (Dansereau et al., 1993; Guo et al., 2002). Ibu is a Biopharmaceutics Classification System (BCS) class II drug with low solubility at pH = 1.2 and pH = 4.5 but high solubility at pH = 6.8 (Álvarez et al., 2011).

To determine if there was a laser-induced change in the API, Raman measurements were performed on the fracture surface of the tablets treated by the two lasers. Sample analyses were made at 10 points directly below the lasered coating surface and at 10 points in the core of the lasered tablets. As described in the "Methods" section, 10 spectra were averaged at each point. The mean of these spectra was compared with the average of 10 spectra taken from the core of an untreated tablet and with the spectrum of Ibu. These spectra were normalized to peak 1604 cm^{-1} of the Ibu spectrum and are shownin Fig. 15.

There was no significant difference between the spectra taken from the lasered area compared with the spectra taken from the non-lasered area. The most characteristic peaks of Ibu are present in all the spectra, with no slip visible. The observed peak intensities can be attributed to the relative inhomogeneity of the materials in the tablet, depending on how rich or poor Ibu was in the studied region. Sampling with a small laser spot may also result in different intensities due to the inhomogeneous composition of the tablet. It can be stated that no chemical structural change was observed after the labelling. Overall, despite the fact that, mainly due to the uneven thickness of the coating, the laser might occasionally reach the functional coating besides the removal of the PW red layer and also that Ibu may penetrate from the core of the tablet into the functional coating, no chemical structural change was observed in the coatings during labeling.

5. Conclusions

During laser ablation, it is important not to cause any change in the medicine. Commonly, it is the thermal effect which can cause problems in the material's quality. At the same time, the coating has to be removed at specific points. This can be achieved by choosing the right laser and setting the optimal parameters.

It can be concluded that in the experiment, the threshold exceeded the ablation threshold of titanium dioxide during lasering, and it was sufficient in its removal. Titanium dioxide did not interfere with QR code recognition, which was performed with a mobile phone.

It was found that ablation with UV248 laser and Femto laser did not cause a qualitative change in the material during laser marking. The UV248 laser is a laser for laboratory use, while Femto lasers are commonly used in the industry. However, the higher repetition rate of the Femto laser allows faster and more efficient coding, which has key importance in the production. Furthermore, the results show that due to the high performance in the fs pulse length, the wavelength is no longer a critical parameter as it is for ns or longer pulses. The thermal effects are negligibly low in the fs region even at high peak powers. The thermal effects of laser ablation can be avoided by reducing the wavelength or the impulse length based on the current study.

It is known that the efficient use of this technology requires further development in speed. Other high energy near-infrared pulse lasers that operate at multi-kHz versions (with a repetition frequency of multi ten-kHz and also MHz), could potentially further shorten the ablation time. Those devices could even be used for line speed marking in pharmaceutical companies. Also, these devices are scalable in energy and they are capable of implementing the one-shot technique. Further research is needed in this direction by testing new lasers and new techniques.

In conclusion, we propose a functionally advanced marking by the lasers mentioned in this article, highlighting the Femto laser as a solution for pharmaceutical companies that would like to have additional protection against drug counterfeiters or to label personalized medicines, knowing that the technique needs further improvement.

CRediT authorship contribution statement

Krisztina Ludasi: Conceptualization, Data curation, Writing - original draft, Investigation. **Orsolya Jójárt-Laczkovich:** Data curation, Investigation. **Tamás Sovány:** Formal analysis. **Béla Hopp:** Methodology, Supervision. **Tamás Smausz:** Methodology, Investigation. **Attila Andrásik:** Investigation, Visualization. **Tamás Gera:** Investigation, Visualization. **Zsolt Kovács:** Investigation. **Géza Regdon jr:** Writing -

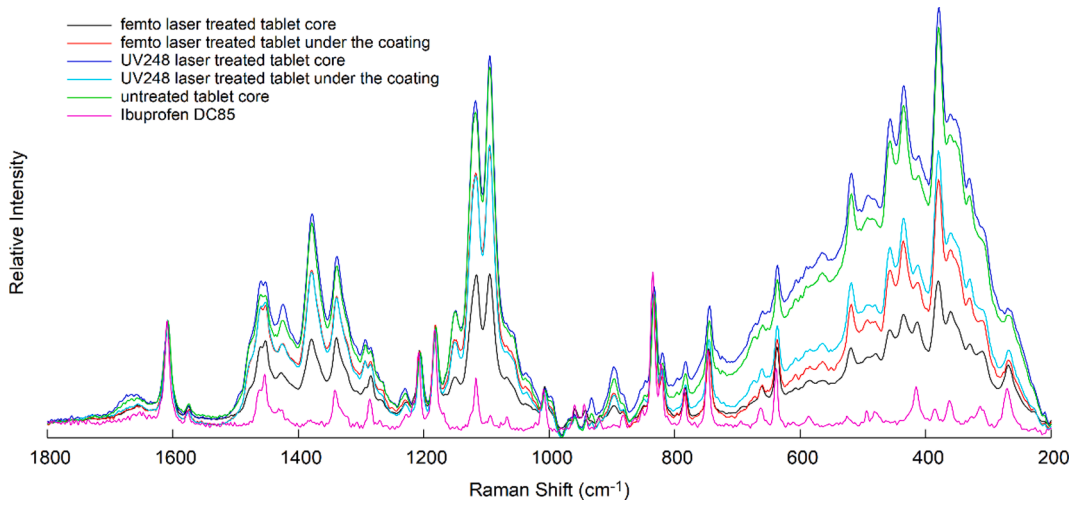

Fig. 15. Averaged and normalised (to Ibu peak 1604 cm^{-1}) spectra taken from the lasered and non-lasered places (both Femto and UV248 laser-treated tablets), spectra of untreated tablet core and Ibuprofen DC85 spectrum.

review & editing, Supervision.

Declaration of Competing Interest

The authors declare that they have no known competing financial interests or personal relationships that could have appeared to influence the work reported in this paper.

Acknowledgement

I would like to thank Seppic S.A. for supplying the polymers.

This work was supported by the EU-funded Hungarian grant EFOP-3.6.1-16-2016-00008.

References

Álvarez, C., Núñez, I., Torrado, J.J., Gordon, J., Potthast, H., García-Arieta, A., 2011. Investigation on the possibility of biowaivers for ibuprofen. J. Pharm. Sci. 100, 2343–2349. https://doi.org/10.1002/jps.22472.

Ayyoubi, S., Cerda, J.R., Fernández-garcía, R., Knief, P., Lalatsa, A., Healy, A.M., Serrano, D.R., 2021. 3D printed spherical mini-tablets: Geometry versus composition effects in controlling dissolution from personalised solid dosage forms. Int. J. Pharm. 120336 https://doi.org/10.1016/j.ijpharm.2021.120336.

Brickell, C.D., 2001. New introductions and the use of genetic resources. Acta Hortic. 552, 159–163. https://doi.org/10.17660/actahortic.2001.552.17.

Dansereau, R., Brock, M., Redman-Furey, N., 1993. The Solubilization of Drug and Excipient Into a Hydroxypropyl Methylcellulose (Hpmc)-Based Film Coating As a Function for the Coating Parameters in a 24“ Accela-Cotab. Drug Dev. Ind. Pharm. 19, 793–808.

Davison, M., 2011. Pharmaceutical Anti-Counterfeiting Combating the Real Danger from Fake Drugs. John Wiley & Sons Inc, Publication, pp. 103–140.

Denso Wave, 1994. QR code development story [WWW Document]. Denso Wave Technol. URL https://www.denso-wave.com/en/technology/vol1.html (accessed 10.6.20).

Dong, Y., Lin, H., Abolghasemi, V., Gan, L., Zeitler, J.A., Shen, Y.C., 2017. Investigating Intra-Tablet Coating Uniformity With Spectral-Domain Optical Coherence Tomography. J. Pharm. Sci. 106, 546–553. Doi: http://dx.doi.10.1016/j.xphs.2016.09.021.

Kannatey-Asibu Jr., E. 2009. Principles of Laser Materials Processing, John Wiley&Sons.

Edinger, M., Bar-Shalom, D., Sandler, N., Rantanen, J., Genina, N., 2018. QR encoded smart oral dosage forms by inkjet printing. Int. J. Pharm. 536, 138–145. https://doi.org/10.1016/j.ijpharm.2017.11.052.

Elliott, D.J., 1995. Ultraviolet Laser Technology and Applications, Ultraviolet Laser Technology and Applications. Doi: http://dx.doi.10.1016/c2009-0-21234-7.

European Commission, 2015. Regulations Commission Delegated Regulation (EU) 2016/161 of 2 October 2015 supplementing Directive 2001/83/EC of the European Parliament and of the Council by laying down detailed rules for the safety features appearing on the packaging medicinal product. Off. J. Eur. Union. Doi: http://dx.doi.10.1017/CBO9781107415324.004.

European Medicines Agency, 2018a. Human regulatory,Owerview, Public health threats, Falsified medicines [WWW Document]. URL http://www.ema.europa.eu/ema/index.jsp?curl=pages/special_topics/general/general_content_000186.jsp&mid=WC0b01ac058002d4e8 (accessed 5.8.19).

European Medicines Agency, 2018b. Mobile scanning and other technologies in the labelling and package leaflet of centrally authorised medicinal products [WWW Document]. URL https://www.ema.europa.eu/en/documents/regulatory-procedural-guideline/mobile-scanning-other-technologies-labelling-package-leaflet-centrally-authorised-medicinal-products_en.pdf (accessed 1.6.21).

F. Menges, 2020. Spectragryph - optical spectroscopy software, Version1.2.15 2020, http://www.effemm2.de/spectragryph/.

Fittler, A., Vida, R.G., Káplár, M., Botz, L., 2018a. Consumers turning to the internet pharmacy market: Cross-sectional study on the frequency and attitudes of hungarian patients purchasing medications online. J. Med. Internet Res. 20, 1–11. Doi: http://dx.doi.10.2196/11115.

Fittler, A., Vida, R.G., Rádics, V., Botz, L., 2018b. A challenge for healthcare but just another opportunity for illegitimate online sellers: Dubious market of shortage oncology drugs. PLoS One 13, 1–17. https://doi.org/10.1371/journal.pone.0203185.

Fukuchi, K., 2020. Libqrencode - a fast and compact QR Code encoding library, v.4.1.1. [WWW Document]. URL https://github.com/fukuchi/libqrencode (accessed 1.11.21).

Guo, H.X., Heinämäki, J., Yliruusi, J., 2002. Diffusion of a freely water-soluble drug in aqueous enteric-coated pellets. AAPS PharmSciTech 3, 8. https://doi.org/10.1208/pt030216.

Haaser, M., Gordon, K.C., Strachan, C.J., Rades, T., 2013. Terahertz pulsed imaging as an advanced characterisation tool for film coatings - A review. Int. J. Pharm. 457, 510–520. https://doi.org/10.1016/j.ijpharm.2013.03.053.

Han, S., Bae, H.J., Kim, J., Shin, S., Choi, S.E., Lee, S.H., Kwon, S., Park, W., 2012a. Lithographically encoded polymer microtaggant using high-capacity and error-correctable QR Code for anti-counterfeiting of drugs. Adv. Mater. 24, 5924–5929. https://doi.org/10.1002/adma.201201486.

Han, S., Bae, H.J., Kim, J., Shin, S., Kwon, S., Park, W., 2012b. Drug authentication using high capacity and error-correctable encoded microtaggants. In: Proc. 16th Int. Conf. Miniaturized Syst. Chem. Life Sci. MicroTAS, pp. 1429–1431.

Ho, L., Müller, R., Römer, M., Gordon, K.C., Heinämäki, J., Kleinebudde, P., Pepper, M., Rades, T., Shen, Y.C., Strachan, C.J., Taday, P.F., Zeitler, J.A., 2007. Analysis of sustained-release tablet film coats using terahertz pulsed imaging. J. Control. Release 119, 253–261. https://doi.org/10.1016/j.jconrel.2007.03.011.

Lawrence, J. (Ed.), 2010. Advances in Laser Materials Processing Technology, Research and Application, Woodhead Publishing Limited. Woodhead Publishing. Doi: http://dx.doi.10.1163/18750176-90000221.

Ludasi, K., Jójárt-Laczkovich, O., Sovány, T., Hopp, B., Smausz, T., Regdon, G., 2019. Comparison of conventionally and naturally coloured coatings marked by laser technology for unique 2D coding of pharmaceuticals. Int. J. Pharm. 570 https://doi.org/10.1016/j.ijpharm.2019.118665.

Ludasi, K., Sovány, T., Laczkovich, O., Hopp, B., Smausz, T., Regdon, G., 2018. Unique laser coding technology to fight falsified medicines. Eur. J. Pharm. Sci. 123 https://doi.org/10.1016/j.ejps.2018.07.023.

Roth, L., Biggs, K.B., Bempong, D.K., 2019. Substandard and falsified medicine screening technologies. AAPS Open 5. https://doi.org/10.1186/s41120-019-0031-y.

Sacher, S., Wahl, P., Weißensteiner, M., Wolfgang, M., Pokhilchuk, Y., Looser, B., Thies, J., Raffa, A., Khinast, J.G., 2019. Shedding light on coatings: Real-time monitoring of coating quality at industrial scale. Int. J. Pharm. 566, 57–66. https://doi.org/10.1016/j.ijpharm.2019.05.048.

Steen, W., Mazumder, J., 2010. Laser Material Processing, 4th ed. Springer. Doi: http://dx.doi.10.1007/978-1-84996-062-5.

Szatmári, S., 1994. High-brightness ultraviolet excimer lasers. Appl. Phys. B Laser Opt. 58, 211–223. https://doi.org/10.1007/BF01081313.

Szatmári, S., Schäfer, F.P., 1988. Simplified laser system for the generation of 60 fs pulses at 248 nm. Opt. Commun. 68, 196–202. Doi: http://dx.doi.10.1016/0030-4018(88)90184-8.

TeWaTi, 2019. TeraWatt Titan-Sapphire Laser Research Group [WWW Document]. URL www.tewati.eu (accessed 6.11.20).

The European Parlament and the Council of the European Union, 2011. Directive 2011/62/EU of the European Parliament and of the Council of 8 June 2011. Off. J. Eur. Union L 174 (74), 74–87.

Trenfield, S.J., Xian Tan, H., Awad, A., Buanz, A., Gaisford, S., Basit, A.W., Goyanes, A., 2019. Track-and-trace: Novel anti-counterfeit measures for 3D printed personalized drug products using smart material inks. Int. J. Pharm. 567 https://doi.org/10.1016/j.ijpharm.2019.06.034.

Van Overschelde, O., Dinu, S., Guisbiers, G., Monteverde, F., Nouvellon, C., Wautelet, M., 2006. Excimer laser ablation of thin titanium oxide films on glass. Appl. Surf. Sci. 252, 4722–4727.

Viswanathan, P., Muralidaran, Y., Ragavan, G., 2017. Challenges in oral drug delivery: A nano-based strategy to overcome. Nanostruct. Oral Med. 173–201 https://doi.org/10.1016/B978-0-323-47720-8.00008-0.

WHO, 2018. Substandard and falsified medical products [WWW Document]. URL https://www.who.int/en/news-room/fact-sheets/detail/substandard-and-falsified-medical-products (accessed 1.9.21).

WHO, 2017a. WHO Global Surveillance and Monitoring System [WWW Document]. URL http://www.who.int/medicines/regulation/ssffc/publications/gsms-report-sf/en/ (accessed 1.9.21).

WHO, 2017b. Seventieth World Health Assembly Update [WWW Document]. Who. URL http://www.who.int/mediacentre/news/releases/2017/dementia-immunization-refuguees/en/ (accessed 1.9.21).

Wilson, K.E., Crossman, E., 1997. The influence of tablet shape and pan speed on intra-tablet film coating uniformity. Drug Dev. Ind. Pharm. 23, 1239–1243. https://doi.org/10.3109/03639049709146164.

Wolfgang, M., Peter, A., Wahl, P., Markl, D., Zeitler, J.A., Khinast, J.G., 2019. At-line validation of optical coherence tomography as in-line/at-line coating thickness measurement method. Int. J. Pharm. 572, 118766 https://doi.org/10.1016/j.ijpharm.2019.118766.